LBNL-44716


ERNEST ORLANDO LAWRENCE
BERKELEY NATIONAL LABORATORY

# Anion Photoelectron Spectroscopy of Radicals and Clusters

Travis R. Taylor

**Chemical Sciences Division**

December 1999

Ph.D. Thesis



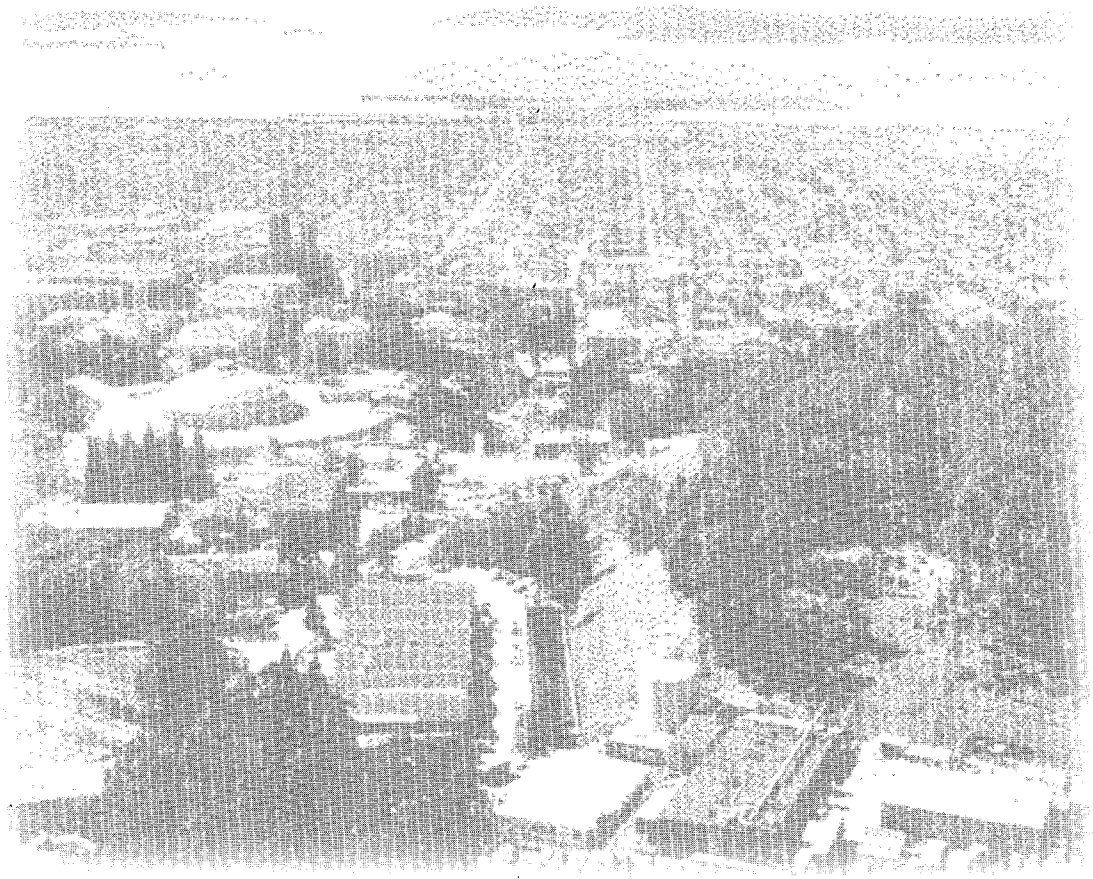

LBNL-44716

# Anion Photoelectron Spectroscopy of Radicals and Clusters

Travis Robert Taylor
Ph.D. Thesis

Department of Chemistry
University of California, Berkeley

and

Chemical Sciences Division
Ernest Orlando Lawrence Berkeley National Laboratory
University of California
Berkeley, CA 94720

December 1999

This work was supported by the Director, Office of Science, Office of Basic Energy Sciences, Chemical Sciences Division, of the U.S. Department of Energy under Contract No. DE-AC03-76SF00098, and by National Science Foundation Grant DMR-9814677.

# Abstract

## Anion Photoelectron Spectroscopy of Radicals and Clusters

by

Travis Robert Taylor

Doctor of Philosophy in Chemistry

University of California, Berkeley

Professor Daniel M. Neumark, Chair

Anion photoelectron spectroscopy is used to study free radicals and clusters. The low-lying $^2\Sigma$ and $^2\Pi$ states of $C_{2n}H$ (n=1-4) have been studied. The anion photoelectron spectra yielded electron affinities, term values, and vibrational frequencies for these combustion and astrophysically relevant species. Photoelectron angular distributions allowed us to correctly assign the electronic symmetry of the ground and first excited states and to assess the degree of vibronic coupling in $C_2H$ and $C_4H$.

Other radicals studied include NCN and $I_3$. We were able to observe the low-lying singlet and triplet states of NCN for the first time. Measurement of the electron affinity of $I_3$ revealed that it has a bound ground state and attachment of an argon atom to this moiety enabled us to resolve the symmetric stretching progression.

Clusters from groups III and V have been studied in an effort to understand how their electronic structure changes as a function of size from discrete molecular states to bulk band structure. Our low-resolution (30 meV) anion photoelectron spectra of 35 $Ga_xP_y^-$ ($x+y \leq 18$) clusters yielded adiabatic and vertical detachment energies. The electron affinities showed an odd/even alternation indicating that they corresponded to

open/closed shell clusters, respectively. A size-dependent trend of the electron affinities for $Ga_xP_x$ (x>6) was observed to extrapolate to the bulk value. A cluster source with a liquid nitrogen cooled channel greatly improved our ability to resolve vibrational structure for GaX, $GaX_2$, $Ga_2X$, and $Ga_2X_3$ (X=P,As). With the aid of Franck-Condon simulations more accurate electron affinities, term energies, and vibrational frequencies are reported.

# Table of contents

# Prologue

## Story of the little birdie

There was a birdie, who didn't even know how to fly yet. One freezing cold morning he tumbles out of his nest and lands on the ground. Well, he starts going peep, peep, peep like crazy because he's damn nearly freezing. Lucky for him, along comes this cow, sees him, and feels sorry for him, so, she lifts her tail and splat, drops this steaming hot cow pie right on him, so the little birdie is nice and warm again but he still ain't happy and he keeps going peep, peep, peep louder than ever. A mean old coyote hears something and comes running. He reaches out a paw and pulls the birdie out of the cow pie, brushes the dirt off him real nice, and then swallows the birdie done in one gulp.

# Chapter 1. Introduction

In anion photoelectron spectroscopy, photons of sufficient energy are used to eject electrons from mass selected anions. Any energy of the photon that is not used in the transition to a neutral state is necessarily reflected in the electron kinetic energy, which is the experimental observable. The intensity and energy of the peaks in the electron kinetic energy distribution provide information about the relative geometry changes and energies between the anion and the neutral states involved. Assuming the anions have no internal energy the spacing between the peaks in the electron kinetic energy distribution reflect the energies between electronic and vibrational states of the neutral. The intensity profiles of vibrational progressions indicate how different the geometries of the neutral states are compared to the initial anion state. Photoelectron energy distributions are plotted in terms of the electron kinetic energy (*eKE*) or electron binding energy (*eBE*) which are energetically related by equation (1)

$$eBE = h\nu - eKE = EA + E^{o}_{\text{int}} \qquad (1)$$

where $h\nu$ is the photon energy, *EA* is the electron affinity, and $E^{o}_{\text{int}}$ is the internal energy of the resultant neutral state with respect to the neutral ground state.

Anion photoelectron spectroscopy offers many advantages over conventional optical techniques. First, the use of anions as a precursor allows us to mass select the anion of choice, ensuring the identity of the signal carrier. The corresponding anion of reactive, short-lived, and radical neutral molecules can be generated by a variety of sources including pulsed electric discharge, laser ablation, and the electron gun. Second, the spin selection rules are more relaxed than in optical spectroscopy where the spin

multiplicity cannot change. For example, starting with a doublet anion state allows the observation both singlet and triplet neutral states, directly yielding their energy splitting. Third, the experimental resolution is high enough to resolve individual vibrational states within an electronic state. In addition to providing valuable vibrational frequencies, often the vibrational structure is essential for the proper identification of the electronic state. Vibrational resolution also allows the measurement of the adiabatic electron affinity, an important fundamental property that can be used in thermodynamic cycles to determine other thermodynamic properties such as bond dissociation energies. Fourth, peaks from electronic states with different photoelectron angular distributions can be distinguished.

The angular dependence of the photodetachment intensity for polarized light and randomly oriented molecules is given by equation (2) below[1]

$$\frac{d\sigma}{d\Omega} = \frac{\sigma_{total}}{4\pi}\left[1 + \frac{\beta(eKE)}{2}(3\cos^2\theta - 1)\right] \qquad (2)$$

where $\theta$ is the angle between the electric vector of the photon and the direction of electron ejection, $\sigma_{total}$ is the total photodetachment cross section and $\beta(eKE)$ is the asymmetry parameter ($-1 \leq \beta \leq 2$). Each electronic state typically has a characteristic asymmetry parameter and can be used to distinguish peaks of overlapping electronic transitions. The asymmetry parameter of a peak can be calculated[2] using equation (3)

$$\beta = \frac{I_{0^o} - I_{90^o}}{\frac{1}{2}I_{0^o} + I_{90^o}} \qquad (3)$$

where $I_{0^o}$ and $I_{90^o}$ are the normalized intensities of the peak taken at the polarization angles $\theta = 0^o$ and $90^o$.

## Chapter 1

The attributes of anion photoelectron spectroscopy discussed above are exploited to provide new and important spectroscopic and structural information about the species studied in this work. This thesis can be divided into two sections pertaining to the types of species studied: radicals and clusters. Chapters 2-4 discuss the spectroscopy of the open shell radicals: $C_{2n}H$ (n=1-4), NCN, and $I_3$. Chapters 5-8 detail the spectroscopy of group III-V clusters in an effort to understand how their molecular properties change as the number of atoms in the cluster is increased. This knowledge will shed light on the bigger picture of how molecular properties evolve into bulk properties. In the remainder of the introduction we demonstrate the ability of our technique to provide important spectroscopic information about the systems studied and further discuss why these systems are relevant to the scientific community.

Chapter 2 investigates the spectroscopy of carbon monohydrides, $C_{2n}H$ (n=1-4) and $C_{2n}D$ (n=1-3). In general the carbon monohydrides, $C_nH$, play an important role in combustion[3] and interstellar chemistry.[3-14] The vibrational and electronic spectroscopy of the $C_{2n}H$ species is complicated by the presence of close-lying $^2\Sigma$ and $^2\Pi$ electronic states. For example, the $\tilde{X}\ ^2\Sigma^+$ ground state of $C_2H$ interacts strongly with the nearby $\tilde{A}\ ^2\Pi$ state. In $C_4H$, the $^2\Sigma$ and $^2\Pi$ states are nearly degenerate. The interaction for these two molecules is strong enough to reveal a breakdown in the Born-Oppenheimer approximation and allow vibronic coupling.

In this chapter we use negative ion photoelectron spectroscopy as a means of probing the electronic and vibrational states of the carbon monohydrides, $C_{2n}H$ (n=1-4) and $C_{2n}D$ (n=1-3). The spectra are recorded at a wavelength of 266 nm (4.657 eV) and yield electron affinities for each species. The spectra are vibrationally resolved, and

some of the vibrational modes in the neutral $C_{2n}H(D)$ radicals are assigned. In addition, photoelectron angular distributions allow one to distinguish between the photodetachment transitions to the $^2\Sigma^+$ and $^2\Pi$ states of the neutrals. The spectra confirm previous work showing that $C_2H$ and $C_4H$ have $^2\Sigma^+$ ground states, while $C_6H$ and $C_8H$ have $^2\Pi$ ground states. In addition, we observe the low-lying $^2\Pi$ or $^2\Sigma^+$ excited states for all four radicals and report term values. The photoelectron angular distributions also serve as a probe of vibronic coupling between the $^2\Sigma^+$ and $^2\Pi$ states. Vibronic coupling is particularly strong in the $C_2H(D)^-$ and $C_4H(D)^-$ spectra.

In chapter 3 we report the anion photoelectron spectrum of the cyanonitrene anion, $NCN^-$, measured at 416 and 266 nm. This radical has been proposed as an intermediate in the combustion of hydrocarbons[15] and nitramine.[16] Ultraviolet emission studies[17] have also suggested that NCN is present in the Comet Brorosen-Metcalf. The NCN radical has a $\tilde{X}\ ^3\Sigma_g^-$ ground state with a molecular orbital configuration[18] of $\ldots 2\sigma_g^{\,2}2\sigma_u^{\,2}1\pi_u^{\,4}1\pi_g^{\,2}$. This configuration also gives rise to two singlet states, the $\tilde{a}\ ^1\Delta_g$ and the $\tilde{b}\ ^1\Sigma_g^+$ states, whose term values with respect to the ground state have been previously unknown. Optical experiments have been limited to independent studies of the triplet[19-21]and singlet[20] manifolds. The 266 nm anion photoelectron spectrum reveals the $\tilde{a}\ ^1\Delta_g$ and the $\tilde{b}\ ^1\Sigma_g^+$ states together with the $\tilde{X}\ ^3\Sigma_g^-$ ground state for the first time. The transitions are nearly vertical indicating that the electron is being removed from a nonbonding orbital i.e. there is no geometry change.

Chapter 4 reports the anion photoelectron spectra of $I_3^-$ and $Ar{\cdot}I_3^-$ at 266 nm. The triiodine radical, $I_3$, has been proposed to play a key role in one of the most fundamental

reactions in gas phase kinetics, the recombination of I atoms to form $I_2$.[22-27] However, in spite of considerable effort,[28] neither $I_3$ nor any other homonuclear trihalogen has ever been spectroscopically identified until now. In fact, the only gas-phase experimental evidence that any of these species is thermodynamically stable comes from the mass-spectrometric observation of $Br_3$ as a photodissociation product from $(Br_2)_2$.[29]

From our spectra we are able to determine the adiabatic electron affinity and use this quantity in a thermodynamic cycle to show that the ground state is thermodynamically stable. Further, we demonstrate that $I_3^-$ can be vibrationally cooled by the addition of an argon atom to form the $Ar{\cdot}I_3^-$ cluster. This cooling results in a clearer analysis of vibrational structure in the photoelectron spectrum of $I_3^-$ than would otherwise be possible; from these features it appears that the ground state of $I_3$ is linear and centrosymmetric.

As previously mentioned, the final four chapters are concerned with understanding the spectroscopic and structural properties of group III-V clusters as a function of size. This knowledge has become increasingly important in the search for technological advances in the fabrication of smaller and faster electronic devices and has motivated the study of semiconductors in several size regimes. Semiconductor nanocrystals, particles typically in the size range of $10^3$ or more atoms, have been the focus of much research in recent years.[30-35] The spectroscopy of these species, particularly quantum confinement effects, can generally be understood in terms of perturbations to the macroscopic material related to their finite size. Molecular clusters in the range of 10-100 atoms present additional challenges, as they are generally too small to be considered as perturbed macroscopic material but too large to treat with the

standard theoretical methods that work so well for small molecules. It is therefore of considerable interest to determine how the structure and spectroscopy of molecular clusters evolve with size.

Chapter 5 surveys the low-resolution anion photoelectron spectra of $Ga_xP_y^-$ clusters with up to 18 atoms taken at a photodetachment wavelength of 266 nm (4.657 eV). We obtain adiabatic electron affinities and vertical detachment energies of the low-lying excited states of the neutral clusters. Photoelectron spectra of clusters with 3-5 atoms are compared to previously reported *ab initio* calculations. Trends in the electron affinities and excitation energies for the larger clusters are discussed.

Our inability to make definitive electronic state assignments prompted the preliminary study of the vibrationally resolved spectra of $GaP_2$, $Ga_2P$, and $Ga_2P_3$ in Chapter 6. However, these spectra proved to be vibrationally hot and cooling the ion beam afforded the vibrationally cold spectra of $GaX_2$, $Ga_2X$, and $Ga_2X_3$ (X=P,As) reported in Chapter 7. Franck-Condon simulations of there data afford much more accurate vibrational frequencies, electron affinities, and term values. From this study we are also able to conclude that these isovalent group III-V clusters have the same electronic structure. The final chapter, Chapter 8, unravels the spin-orbit coupling in the GaP and GaAs diatomics. The ongoing motivation for studying these clusters in our group is to understand how the electronic structure evolves from discrete molecular states to continuum band structure as we increase the cluster size. The current status of this field warrants further discussion.

## Evolution of cluster properties as a function of size

The determination of geometrical and electron structure of gas phase clusters has been approached by several different methods. For systems with only a couple of atoms, rotationally resolved spectra can be used to accurately determine geometries. Dissociation and reactivity studies have yielded indirect information about the geometrical and electronic structure of gas phase clusters. Direct electronic structure information can be obtained via photoelectron ejection experiments such as photoionization and photodetachment spectroscopies. More recently, ion mobility experiments have shown that several geometrical isomers may exist for a given cluster mass. Photoionization experiments have demonstrated the size-dependent trend of the ionization threshold for many transition metal, alkali metal, and group IV clusters. Ion mobility experiments have been performed on metal cluster systems and the group IV elements of carbon, silicon, germanium, and tin. Smalley and coworkers exploited the magnetic bottle anion photoelectron techniques as a means of observing the electronic structure of mass-selected clusters. The group mainly focused on homonuclear clusters such as $C_n^-$, $Si_n^-$, and $Ge_n^-$.[36-38] However they also pioneered the first systematic study of heteronuclear group III-V clusters of gallium arsenide.[39] Homonuclear clusters are simpler theoretically and experimentally than heteronuclear systems. The low mass resolution and low electron kinetic energy resolution prevented them from deriving more than qualitative information from their spectra.

Since then several second-generation magnetic bottle anion photoelectron spectrometers have been built. Wang and coworkers have studied transition metal

clusters with up to 70 atoms[40] and aluminum clusters with up to 162 atoms with impressive energy kinetic energy resolution.[41] Cheshnovsky and coworkers have added a tilted reflectron to their time-of-flight mass spectrometer enabling them to take photoelectron spectra of mercury clusters up to mass ~50,000 amu (n=250).[42]

The mercury system has proven to be an ideal system for demonstrating the evolution of electronic structure. The mercury atom has filled s and d orbitals and unoccupied valence p orbitals. The corresponding anion of a mercury cluster will thus have one electron in a molecular orbital composed of these valence p orbitals. The anion photoelectron spectra show that the valence s and p orbitals combine to form molecular orbitals, which are well separated energetically. As the number of atoms in the cluster increases the energy separation of these molecular orbitals decreases smoothly from 3 to 250 atoms. They have extrapolated the trend to show that this energy gap is closes at 400 ± 30 atoms.[42] This energy gap can be thought of as a band gap. Smaller clusters have a large band gap making them "insulators". Intermediate sized clusters can be thought of as being "semiconductors". Finally, clusters with greater than 400 atoms have no band gap and can be thought of as "metals". This experiment shows the inadequacy of previous experimental and theoretical methods which conclude that the band gap closure occurs at n=80-100. There is clearly much work to be done on both experimental and theoretical fronts to explain the trends in the electronic structure evolution of clusters.

Our group has focused its efforts on homonuclear clusters from group IV elements and heteronuclear clusters from the elements of groups III and V. We have gone to great efforts to understand the electronic and vibrational structure of small clusters from these three groups. In addition, several other research groups have

performed gas phase and matrix experiments revealing the details of the electronic and vibrational structure of III-V molecules: BN,[43-58] AlN,[59] AlP, GaP,[60-62] GaAs,[39,60,63] GaSb,[60] InP,[64-67] InAs,[64] and InSb.[64] The $In_xP_y$ (x,y=1-4) photoelectron spectra taken by Xu *et al.* is the first III-V study published by our group. C.C. (Arnold) Jarrold later revealed the vibrational structure publishing the zero electron kinetic energy (ZEKE) spectra of $In_2P$ and $InP_2$. Two low-resolution studies (30 meV) of $Ga_xP_y^-$ ($x+y\leq 18$) and $In_xP_y^-$ ($x+y\leq 27$) clusters showed a size dependent trend of the electron affinity beginning with stoichiometric clusters having more than 12 atoms. The onset of the size dependent trend coincides with the loss of our ability to resolve electronic structure. For clusters of more than 12 atoms discrete electronic states are no longer observed. The spectra of these two isovalent systems are extremely similar however their bulk properties are quite different. These two studies do not reveal evidence of a band gap at these cluster sizes or photon energies. However, the size dependent trend of the electron affinity extrapolating to the bulk value beginning with just 12 atoms is a very promising sign that the band gap as well as other bulk type properties will be observed.

The above experiments have provided the groundwork for further exciting studies on the III-V systems. Larger clusters and higher energy photons were needed to more effectively probe the evolution of bulk-like properties. We have begun preparations for this, however in the meantime we studied the vibrational and electronic structure of GaX, $GaX_2$, $Ga_2X$, and $Ga_2X_3$ (X=P,As).

We have shown that isovalent III-V species have the same electronic structure and the combination of all these data has lead us to a fuller understanding of the spectroscopy and electronic structure of each individual species. However, at some size range these

similarities must deteriorate to reveal the individual character that these systems exhibit in the bulk.

## References

[1] J. Cooper and R. N. Zare, in *Lectures in Theoretical Physics*, Vol. XI-C, edited by S. Geltman, K. T. Mahanthappa, and W. E. Brittin (Gordon and Breach, New York, 1969), pp. 317-337.

[2] K. M. Ervin and W. C. Lineberger, in *Advances in Gas Phase Ion Chemistry*, Vol. 1 (JAI Press Inc, 1992), pp. .

[3] J. H. Kiefer, S. S. Sidhu, R. D. Kern, K. Xie, H. Chen, and L. B. Harding, Combustion Science and Technology **82,** 101 (1992).

[4] M. Guelin, S. Green, and P. Thaddeus, Astrophysical Journal **224,** L27 (1978).

[5] M. Guelin, J. Cernicharo, S. Navarro, D. R. Woodward, C. A. Gottlieb, and P. Thaddeus, Astronomy and Astrophysics **182,** L37 (1987).

[6] M. Guelin, J. Cernicharo, C. Kahane, J. Gomez-Gonzales, and C. M. Walmsley, Astronomy and Astrophysics **175,** L5 (1987).

[7] W. M. Irvine, M. Ohishi, and N. Kaifu, Icarus **91,** 2 (1991).

[8] C. A. Gottlieb, E. W. Gottlieb, and P. Thaddeus, Astrophysical Journal **264,** 740 (1983).

[9] M. C. McCarthy, M. J. Travers, A. Kovacs, C. A. Gottlieb, and P. Thaddeus, Astronomy and Astrophysics **309,** L31 (1996).

[10] J. C. Pearson, C. A. Gottlieb, D. R. Woodward, and P. Thaddeus, Astronomy and Astrophysics **189,** L13 (1988).

[11] J. Cernicharo and M. Guelin, Astronomy and Astrophysics **309,** L27 (1996).

[12] I. A. Crawford, Monthly Notices of the Royal Astronomical Society **277,** 458 (1995).

[13] J. Fulara, D. Lessen, P. Freivogel, and J. P. Maier, Nature **366,** 439 (1993).

[14] D. A. Kirkwood, M. Tulej, M. V. Pachkov, M. Schnaiter, F. Guthe, M. Grutter, M. Wyss, and J. P. Maier, J. Chem. Phys. **111,** 9280 (1999).

[15] K. R. Jennings and J. W. Linnett, Transactions of the Faraday Society **56,** 1737 (1960).

[16] G. P. Smith, R. A. Copeland, and D. R. Crosley, J. Chem. Phys. **91,** 1987 (1989).

[17] C. R. O'Dell, C. O. Miller, A. L. Cochran, W. D. Cochran, C. B. Opal, and E. S. Barker, Astrophysical Journal **368,** 616 (1991).

[18] Clifford, P. G. Wenthold, W. C. Lineberger, G. A. Petersson, and G. B. Ellison, Journal of Physical Chemistry A **101,** 4338 (1997).

[19] G. Herzberg and D. N. Travis, Can. J. Phys. **42,** 1658 (1964).

[20] H. W. Kroto, T. F. Morgan, and H. H. Sheena, Transactions of the Faraday Society **66,** 2237 (1970).

[21] D. E. Milligan, M. E. Jacox, and A. M. Bass, J. Chem. Phys. **43,** 3149 (1965).

[22] R. M. Noyes and J. Zimmerman, J. Chem. Phys. **18,** 656 (1950).

[23] M. I. Christie, A. J. Harrison, R. G. W. Norrish, and P. G., Proceedings of the Royal Society London **A231,** 446 (1955).

[24] D. L. Bunker and N. Davidson, J. Am. Chem. Soc. **80,** 5090 (1958).

[25] G. Porter, Discussions of the Faraday Society **33,** 198 (1962).

[26] J. A. Blake and G. Burns, J. Chem. Phys. **54,** 1480 (1971).

[27] V. I. Balykin, V. S. Letokhov, V. I. Mishin, and V. A. Semchishen, Chem. Phys. **17,** 111 (1976).

[28] A. L. Kaledin, M. C. Heaven, W. G. Lawrence, Q. Cui, J. E. Stevens, and K. Morokuma, J. Chem. Phys. **108,** 2771 (1998).

[29] M. W. Sigrist, D. J. Krjnovich, F. Huisken, Z. J. Zhang, Y. T. Lee, and Y. R. Shen, Helvitica Chimica Acta **53,** 289 (1980).

[30] A. Henglein, Chem. Rev. **89,** 1861 (1989).

[31] A. D. Yoffe, Adv. Phys. **42,** 173 (1993).

[32] L. Brus, Appl. Phys. **53,** 465 (1991).

[33] H. Weller, Angew. Chem. Int. Ed. Engl. **32,** 41 (1993).

[34] Y. Wang and N. Herron, J. Phys. Chem. **95,** 525 (1991).

[35] A. P. Alivisatos, J. Phys. Chem. **100,** 13226 (1996).

[36] S. H. Yang, C. L. Pettiette, J. Conceicao, O. Cheshnovsky, and R. E. Smalley, Chem. Phys. Lett. **139,** 233 (1987).

[37] S. Yang, K. J. Taylor, M. J. Craycraft, J. Conceicao, C. L. Pettiette, O. Cheshnovsky, and R. E. Smalley, Chem. Phys. Lett. **144,** 431 (1988).

[38] O. Cheshnovsky, S. H. Yang, C. L. Pettiette, M. J. Craycraft, Y. Liu, and R. E. Smalley, Chem. Phys. Lett. **138,** 119 (1987).

[39] C. Jin, K. J. Taylor, J. Conceicao, and R. E. Smalley, Chem. Phys. Lett. **175,** 17 (1990).

[40] L. S. Wang and H. Wu, in *Advances in Metal and Semiconductor Clusters*, Vol. 4, edited by M. A. Duncan (1997), pp. .

[41] X. Li, H. B. Wu, X. B. Wang, and L. S. Wang, Phys. Rev. Lett. **81,** 1909 (1998).

[42] R. Busani, M. Folkers, and O. Cheshnovsky, Phys. Rev. Lett. **81,** 3836 (1998).

[43] B. A. Thrush, Nature **186,** 1044 (1960).

[44] A. E. Douglas and G. Herzberg, Canadian Journal of Research A **18,** 179 (1940).

[45] O. A. Mosher and R. P. Frosch, J. Chem. Phys. **52,** 5781 (1970).

[46] H. Bredohl, I. Dubois, Y. Houbrechts, and P. Nzohabonayo, J. Phys. B: At. Mol. Phys. **17,** 95 (1984).

[47] H. Bredohl, I. Dubois, Y. Houbrechts, and P. Nzohabonayo, Journal of Molecular Spectroscopy **112,** 430 (1985).

[48] R. D. Verma, J. Phys. B **22,** 3689 (1989).

[49] M. Lorenz, J. Agreiter, A. M. Smith, and V. E. Bondybey, J. Chem. Phys. **104,** 3143 (1996).

[50] R. S. Ram and P. F. Bernath, Journal of Molecular Spectroscopy **180,** 414 (1996).

[51] K. R. Asmis, T. R. Taylor, and D. M. Neumark, Chem. Phys. Lett. **295,** 75 (1998).

[52] K. R. Asmis, T. R. Taylor, and D. M. Neumark, J. Chem. Phys. **111** (1999).

[53] K. R. Asmis, T. R. Taylor, and D. M. Neumark, J. Chem. Phys. **111,** in press (1999).

[54] K. R. Asmis, T. R. Taylor, and D. M. Neumark, The European Physical Journal D **9,** In Press (2000).

[55] L. B. Knight, D. W. Hill, T. J. Kirk, and C. A. Arrington, J. Phys. Chem. **96,** 555 (1992).

[56] L. Andrews, P. Hassanzadeh, T. R. Burkholder, and J. M. L. Martin, J. Chem. Phys. **98,** 922 (1993).

[57] C. A. Thompson, L. Andrews, J. M. L. Martin, and J. El-Yazal, J. Phys. Chem. **99,** 13839 (1995).

[58] C. A. Thompson and L. Andrews, J. Am. Chem. Soc. **117,** 10125 (1995).

[59] M. Ebben and J. J. ter Meulen, Chem. Phys. Lett. **177,** 229 (1991).

[60] S. Li, R. J. Van Zee, and W. Weltner, J. Phys. Chem. **97,** 11393 (1993).

[61] T. R. Taylor, K. R. Asmis, C. Xu, and D. M. Neumark, Chem. Phys. Lett. **297,** 133 (1998).

[62] T. R. Taylor, K. R. Asmis, H. Gomez, and D. M. Neumark, The European Physical Journal D **9,** In Press (2000).

[63] G. W. Lemire, G. A. Bishea, S. A. Heidicke, and M. D. Morse, J. Chem. Phys. **92,** 121 (1990).

[64] S. Li, R. J. Van Zee, and W. Weltner Jr., J. Phys. Chem. **97,** 11393 (1993).

[65] C. Xu, E. Debeer, D. W. Arnold, C. C. Arnold, and D. M. Neumark, J. Chem. Phys. **101,** 5406 (1994).

[66] K. R. Asmis, T. R. Taylor, and D. M. Neumark, Chem. Phys. Lett. **308,** 347 (1999).

[67] C. C. Arnold and D. M. Neumark, Can. J. Phys. **72,** 1322 (1994).

# Chapter 2. Photoelectron Spectra of the $C_{2n}H^-$ (n=1-4) and $C_{2n}D^-$ (n=1-3) Anions


## Abstract

Anion photoelectron spectra of the carbon monohydrides, $C_{2n}H^-$ for n=1-4 and $C_{2n}D^-$ for n=1-3 have been measured. The spectra were recorded at a wavelength of 266 nm (4.657 eV) and yield electron affinities for each species. The spectra are vibrationally resolved, and some of the vibrational modes in the neutral $C_nH(D)$ radicals are assigned. In addition, photoelectron angular distributions allow one to distinguish between photodetachment transitions to the $^2\Sigma^+$ and $^2\Pi$ states of the neutrals. The spectra confirm previous work showing that $C_2H$ and $C_4H$ have $^2\Sigma^+$ ground states, while $C_6H$ and $C_8H$ have $^2\Pi$ ground states. In addition, we observe the low-lying $^2\Pi$ or $^2\Sigma^+$ excited states for all four radicals. The photoelectron angular distributions also serve as a probe of vibronic coupling between the $^2\Sigma^+$ and $^2\Pi$ states. These effects are particularly prominent in the $C_2H^-$ and $C_4H^-$ spectra.


## I. Introduction

Bare carbon clusters, $C_n$, have been extensively studied over the past decade using experiment[1-18] and theory.[19-29] The related carbon monohydrides, $C_nH$, which play and important role in combustion[30] and interstellar chemistry, have received somewhat less attention. Several $C_nH$ chains [31-36] have been observed in the interstellar medium. In addition, $C_nH$ radicals are candidates for the diffuse interstellar bands.[37] Through microwave spectroscopy the ground vibrational and electronic states have been well-

characterized and several of these species have been identified in the interstellar medium.[38-40] However, the vibrational and electronic spectroscopy of these open shell species is complicated by the presence of close-lying $^2\Sigma$ and $^2\Pi$ electronic states. For example, the $\tilde{X}\ ^2\Sigma^+$ state ground state of $C_2H$ interacts strongly with the nearby $\tilde{A}\ ^2\Pi$ state. In $C_4H$, the $^2\Sigma$ and $^2\Pi$ states are nearly degenerate. In $C_6H$ and $C_8H$ the $^2\Pi$ state is the ground state; a low-lying $^2\Sigma$ state is expected in each case but its term value is unknown. In this paper we use negative ion photoelectron spectroscopy of the carbon monohydride anions $C_{2n}H^-$ (n=1-4) and $C_{2n}D^-$ (n=1-3) as a means of probing the electronic and vibrational spectroscopy of the neutral species. Our experiments provide new insight concerning the energetics and interactions of the $^2\Sigma$ and $^2\Pi$ states, and represent the first measurements of the electron affinities for $C_4H$, $C_6H$, and $C_8H$.

The ethynyl radical, $C_2H$, is the most thoroughly studied of the $C_nH$ species. Experimental techniques applied to this radical include electron spin resonance (ESR),[41-43] laser magnetic resonance,[44,45] microwave and millimeter-wave spectroscopy,[46-49] matrix isolation infrared spectroscopy [50-54], color center and diode laser spectroscopy,[55-64] Fourier transform infrared (FTIR) emission spectroscopy,[65] laser-induced fluorescence (LIF),[65-67] and photoelectron spectroscopy of the $C_2H^-$ anion.[68] Extensive theoretical work on the spectroscopy of $C_2H$ has also been carried out.[69-71] These investigations have focused primarily on the infrared region, which probes the vibrational transitions within the $\tilde{X}\ ^2\Sigma^+$ state as well as electronic transitions to the low-lying $\tilde{A}\ ^2\Pi$ state, for which $T_0 \approx$ 3600-3700 $cm^{-1}$. Further information comes from photodissociation experiments[72-77]on $C_2H_2$ in which the $H+C_2H$ translational energy distribution reveals vibrational progressions in both states of $C_2H$. Even though several of these spectra are of sufficient

resolution to fully resolve rotational and fine structure, assignment of the observed bands has been far from straightforward due to strong vibronic coupling between the $\tilde{X}\ ^2\Sigma^+$ and $\tilde{A}\ ^2\Pi$ states as well as Fermi resonance interactions within the $\tilde{X}\ ^2\Sigma^+$ state. Thus, for example, no single band corresponding to the $\tilde{A}$ - $\tilde{X}$ vibrational origin has been observed, because the $\tilde{A}$ (000) vibrational ground state is strongly coupled to several nearby vibrationally excited levels of the $\tilde{X}$ state.

In the first spectroscopic observation of $C_4H$, its optical, infrared, and ESR spectra were obtained via matrix isolation spectroscopy.[78] It was later identified in the interstellar medium through its millimeter-wave spectrum.[31] Subsequently, several laboratory microwave spectroscopy studies have been performed,[38,79-81] and an FTIR study in a rare gas matrix[82] yielded a more complete set of vibrational frequencies for the ground state. Several *ab initio* studies have been carried out on $C_4H$ in which geometries, vibrational frequencies, and electronic term values were calculated.[30,81,83-87] The experiments indicate that $C_4H$ has a $^2\Sigma^+$ ground state, but the *ab initio* calculations indicate that the lowest $^2\Sigma^+$ and $^2\Pi$ states are nearly degenerate. Most of the calculations[81,85,86] agree with the experimental assignment of the $^2\Sigma$ state as the ground state but place the $^2\Pi$ state within 100 $cm^{-1}$, although two calculations[84,87] predict the $^2\Pi$ state to be the ground state. As previously mentioned the $\tilde{X}\ ^2\Sigma^+$ and $\tilde{A}\ ^2\Pi$ states are nearly degenerate, increasing the opportunity for vibronic coupling between the two electronic states. Perturbed rotation lines in the millimeter wave spectra[33,79] provide evidence of the vibronic interaction. Recent LIF results[88] on the $\tilde{B}\ ^2\Pi \leftarrow \tilde{X}\ ^2\Sigma^+$ transition can only be explained by invoking vibronic coupling between the $\tilde{X}\ ^2\Sigma^+$ and

$\tilde{A}\ ^2\Pi$ states. In this work we directly observe the $\tilde{A}\ ^2\Pi$ state and the effects of its coupling with the ground state.

A millimeter-wave spectrum assigned to the $C_6H$ radical was first observed in the envelope of a carbon star;[32] this assignment was subsequently confirmed in laboratory measurements.[39] Both studies indicated that $C_6H$ has a $^2\Pi$ ground state. The only other laboratory measurements have been in cryogenic matrices by Graham and coworkers[89] using FTIR spectroscopy and by Maier and coworkers[13,15] using electronic absorption. Several *ab initio* studies have also been carried out in which geometries, vibrational frequencies, term values, and various thermodynamic quantities were calculated. [30,83-85,87,90-93] The calculations predict a low-lying $^2\Sigma^+$ state which has not been observed experimentally.

The $C_8H$ radical is the least studied of the species considered here. As with $C_6H$, it was also first seen in the envelope of a carbon star[36] with its assignment confirmed by laboratory measurements.[40] An electronic absorption band in the visible region was seen by Maier and coworkers.[15] Electronic excitation energies have been calculated.[83,87]

Here we report vibrationally-resolved photoelectron spectra of $C_{2n}H^-$ (n=1-4) and $C_{2n}D^-$ (n=1-3). The anions are closed-shell $^1\Sigma$ species, and in all cases the lowest $^2\Sigma$ and $^2\Pi$ neutral states are accessible by anion photodetachment. We also obtain photoelectron angular distributions, which can be used to distinguish between transitions to the two neutral states. This is particularly useful in analyzing the $C_2H^-$ and $C_4H^-$ spectra in which the two bands are strongly overlapped.

## II. Experimental

The anion photoelectron spectrometer used in this study has been described in detail previously.[94,95] In the work presented here, a mixture of 4% $C_2H_2$ and 1% $CO_2$ at 40 psi is expanded through a pulsed piezoelectric valve at a backing pressure of 40 psi. The resulting molecular beam passes through a pulsed electric discharge assembly,[96] and $C_nH^-$ anions are formed by firing the discharge during the molecular beam pulse. The negative ions pass through a skimmer into a differentially pumped region. They are extracted perpendicular to their flow direction by a pulsed electric field and injected into a linear reflectron time-of-flight (TOF) mass spectrometer,[97,98] affording a mass resolution $m/\Delta m$ of 2000. The ions of interest are selectively photodetached with the fourth harmonic of a pulsed Nd:YAG laser(266 nm, hν=4.657 eV). The electron kinetic energy (eKE) distribution is determined by TOF analysis. The energy resolution is 8 meV at 0.65 eKE and degrades as $(eKE)^{3/2}$ at higher eKE. The laser polarization can be rotated by means of a half-wave plate, and each photoelectron spectrum is measured at least two polarization angles θ, defined with respect to the electron detection axis, in order to characterize the photoelectron angular distribution. Secondary electrons initiated by scattered photons necessitate the collection and subtraction of background spectra.

## III. Results

Figure 1 shows the photoelectron spectra of the carbon monohydride anions $C_{2n}H^-$ (n=1-4) taken at the polarization angles of $\theta=0^\circ$ and $90^\circ$ with a photon energy of 4.67 eV. The photoelectron spectra of $C_2H(D)^-$ and $C_4H(D)^-$ are presented in more detail in Figures 2 and 3, respectively.

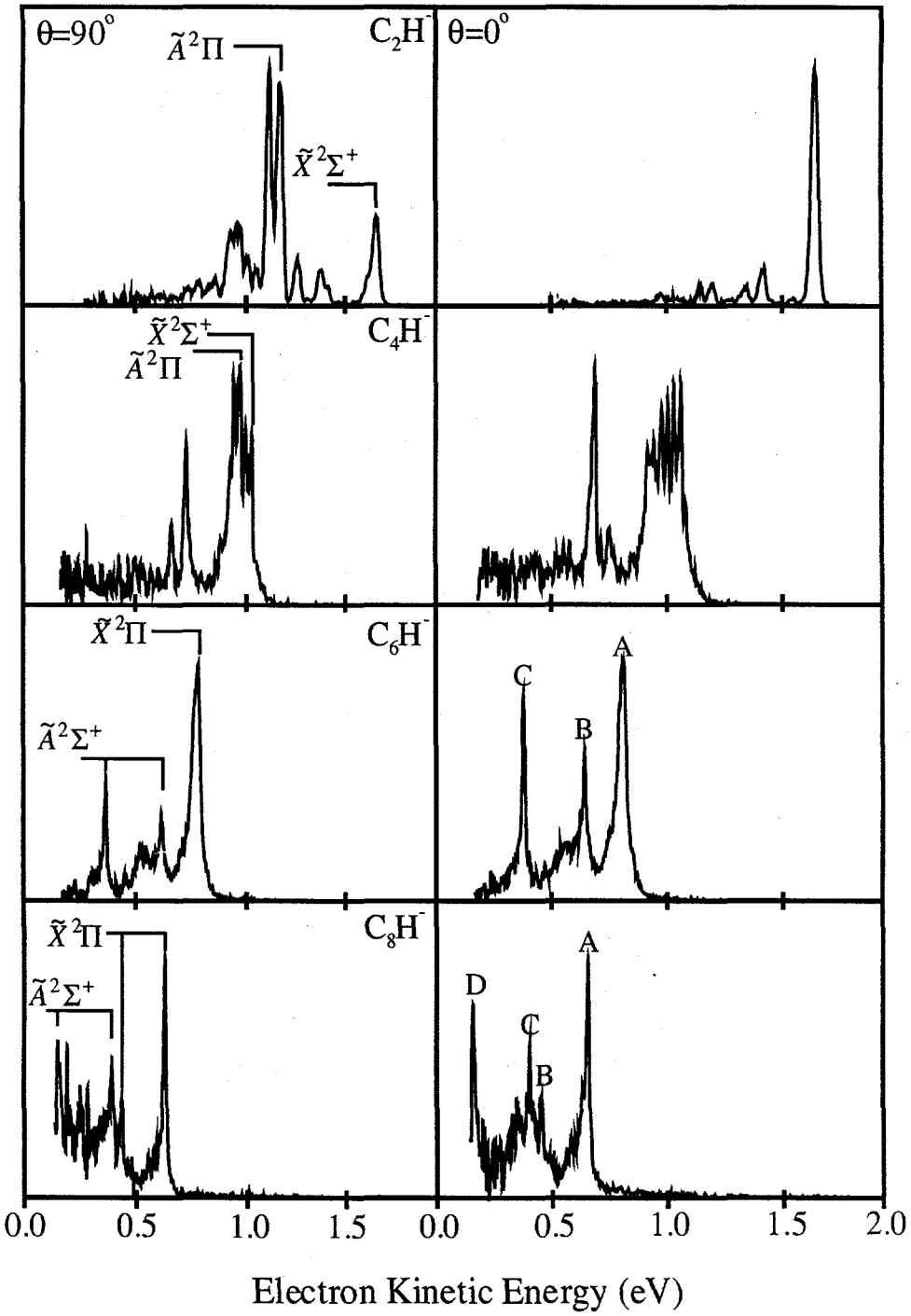


Fig. 1. Photoelectron spectra of $C_{2n}H^-$ for n=1-4 taken at the photodetachment wavelength of 266 nm (4.657 eV). Laser polarization angles are θ=0° and 90° with respect to the direction of electron collection.

In these and all other photoelectron spectra the electron kinetic energy, eKE, is related to the internal energy of the neutral and anion by:

$$eKE = h\nu - EA - E^{o} + E^{-}. \qquad (1)$$

Here, $h\nu$ is the photon energy, $EA$ is the adiabatic electron affinity, $E^{o}$ is the internal energy of the neutral, and $E^{-}$ is the internal energy of the anion. Rotational energy contributions are neglected. As indicated by Eq. (1) the peaks occurring at lowest eKE in the photoelectron spectrum correspond to the highest internal energy states of the neutral.

The photoelectron differential cross section[99] is given in Eq.(2)

$$\frac{d\sigma}{d\Omega} = \frac{\sigma_{total}}{4\pi}\left[1 + \frac{\beta(E)}{2}\left(3\cos^{2}\theta - 1\right)\right] \qquad (2)$$

The polarization angle, θ, is the angle between the electric vector of the photon and the axis along which the electrons are detected. The differential cross section is parameterized in terms of the anisotropy parameter, β, for which $-1 \leq \beta \leq 2$. The anisotropy parameter for a particular peak is obtained from the relative peak intensities taken at different polarization angles. Peaks with differing values of β generally result from transitions to different neutral electronic states, so this is a useful means of assigning electronic states and distinguishing contributions from overlapping electronic bands. Values of β for all spectra are listed in Tables I-IV.

As *n* increases for the $C_{2n}H$ species the spectral features shift to lower eKE, indicating an increase in electron affinity. The relative intensities of the peaks in the $\theta=90^{\circ}$ and $\theta=0^{\circ}$ spectra of all anions change dramatically, indicating the presence of transitions to at least two electronic states.

Figure 2 shows the photoelectron spectra of $C_2H(D)^-$ at 4.657 eV taken at laser polarization angles $\theta=90^{\circ}$ and $\theta=0^{\circ}$. Peaks A1-C were observed at higher resolution in the photoelectron spectrum taken by Ervin *et al.*[68] at 3.531 eV, but the higher photon energy used in our experiment yields many more peaks. The spectra in Fig. 2 show resolved vibrational structure. Peaks A1-B2 at high eKE have strongly positive $\beta$ parameters, while $\beta<0$ for peaks C-K. This generally indicates the presence of transitions to two electronic states of the neutral, a result expected for $C_2H$ with its close-lying $^2\Sigma^+$ and $^2\Pi$ states. The energy shifts upon isotopic substitution are sufficiently small so that one can easily correlate peaks in the $C_2D^-$ and $C_2H^-$ spectra. The intensity distribution of the peaks in the $C_2D^-$ spectra differs substantially from the $C_2H^-$ spectra. Peak F is considerably larger in the $C_2D^-$ spectra and the relative intensities of peaks C, D, E, G1, and J are significantly lower. On the other hand, peak M appears in the $C_2D^-$ $\theta=0^{\circ}$ spectrum but not in the $C_2H^-$ spectra.

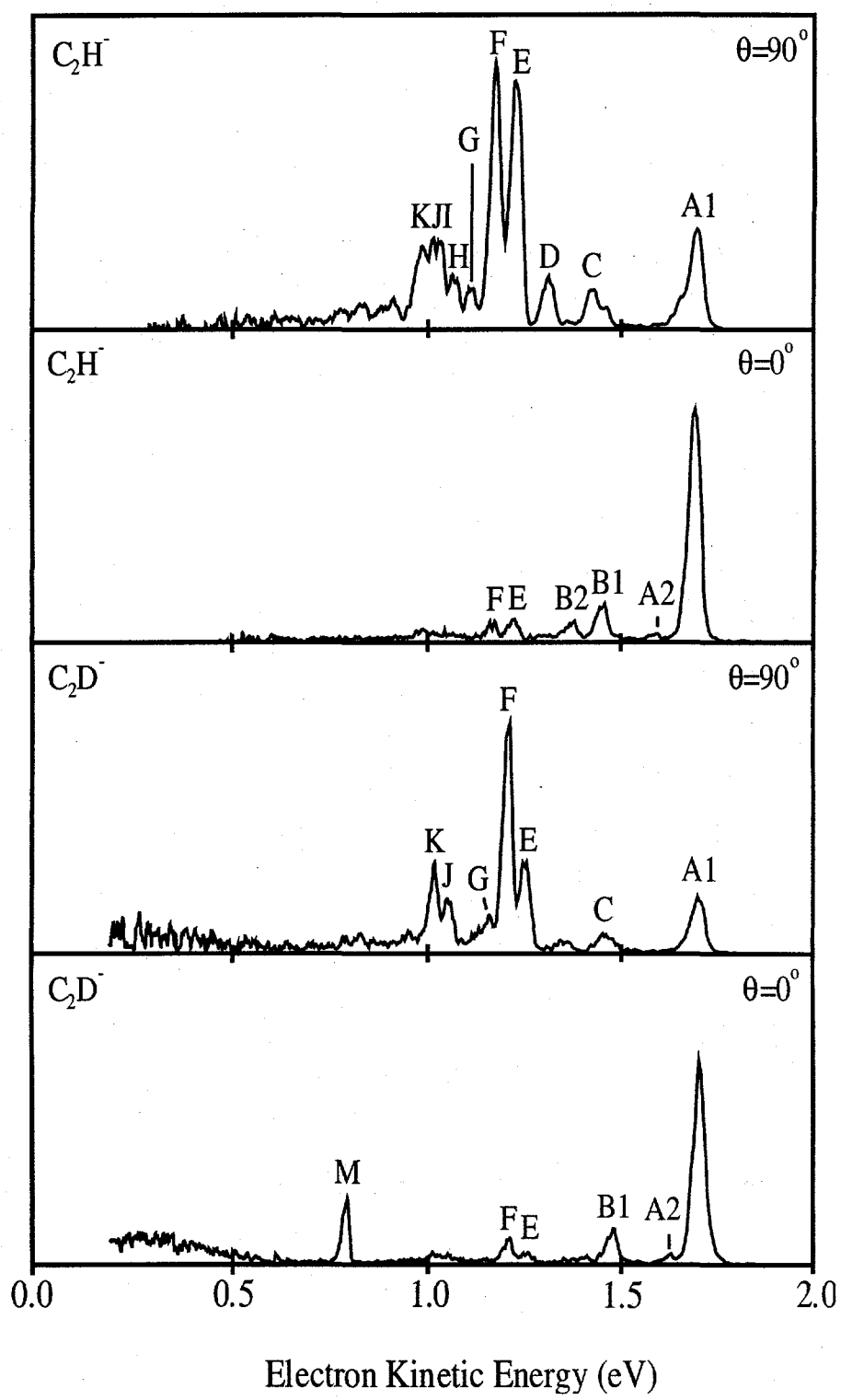


Fig. 2. Photoelectron spectra of $C_2H(D)^-$ taken at the photodetachment wavelength of 266 nm (4.657 eV). Laser polarization angles are $\theta=0^\circ$ and $90^\circ$ with respect to the direction of electron collection.

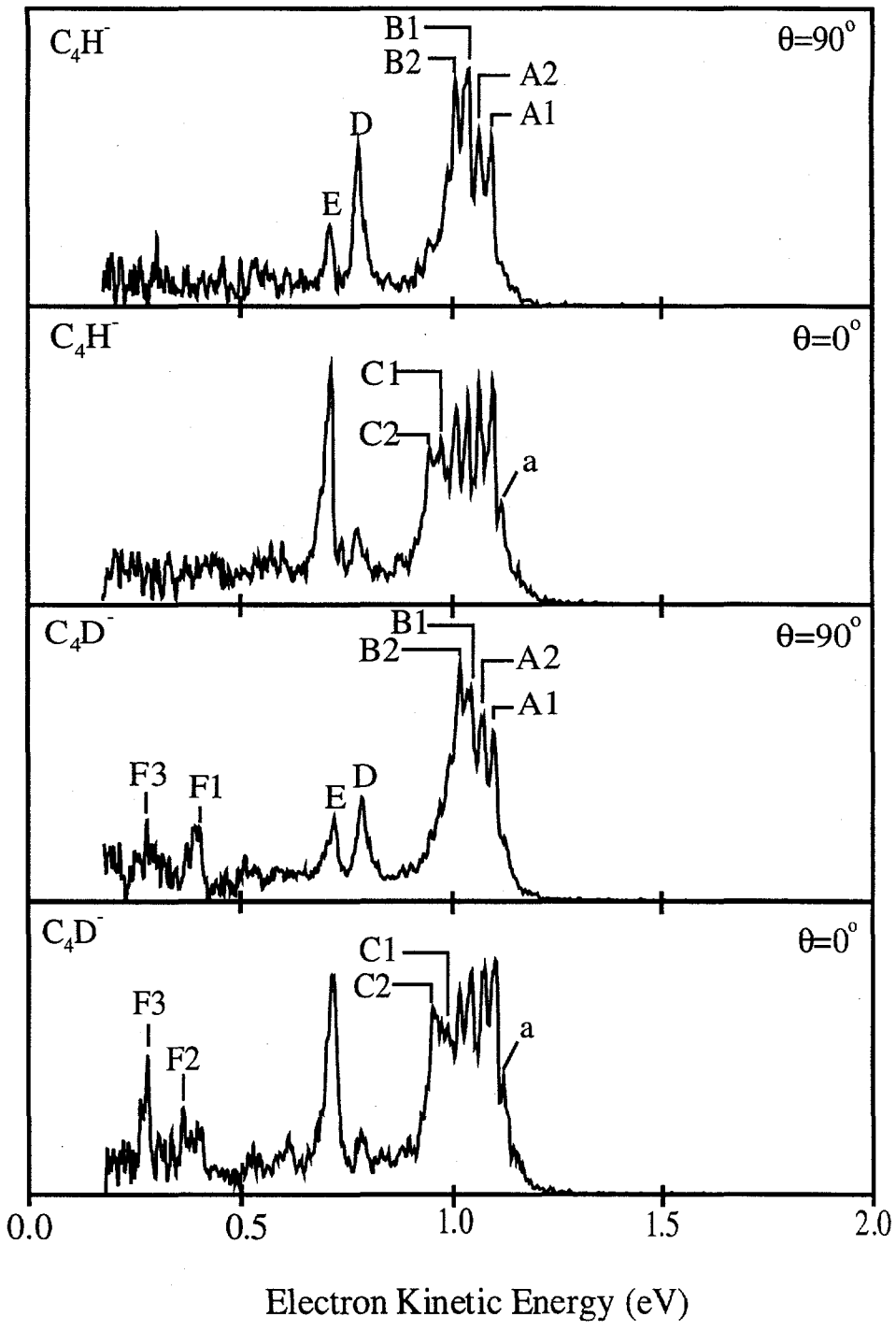


Fig. 3. Photoelectron spectra of $C_4H(D)^-$ taken at the photodetachment wavelength of 266 nm (4.657 eV). Laser polarization angles are $\theta=0^\circ$ and $90^\circ$ with respect to the direction of electron collection.

The $C_4H^-$ and $C_4D^-$ spectra in Figures 1 and 3 consist of a partially-resolved group of at least six peaks around eKE=1.0 eV (peaks A1-C2), and two more isolated features, peaks D and E, at lower eKE. The $C_4H^-$ and $C_4D^-$ are similar, except for some small peaks below 0.5 eV that appear only in the $C_4D^-$ spectrum. As with $C_2H(D)^-$, the relative peak intensities vary strongly with laser polarization, particularly in the group of peaks around 1.0 eV, indicating the presence of at least two overlapping electronic states. The spectral features in Figure 3 can be classified into three groups according to their $\beta$ parameter and energy. Peaks A1-A2, C1-C3, and E have $\beta>0$ and are most prominent at $\theta=0°$. Peaks B1-B2 and D have $\beta\leq 0$ and peaks F1-F3 have $\beta>0$ and lie at a much higher energy than the first group.

The $C_6H^-$ and $C_8H^-$ spectra each show several distinct peaks superimposed on broad underlying signal. The peak positions and anisotropy parameters are listed in Table IV. The photoelectron angular distributions indicate that transitions to two electronic states contribute to each spectrum. In the $C_6H^-$ spectra, peak A decreases in intensity relative to peaks B and C as the laser polarization is rotated from 90° to 0°. In the $C_8H^-$ spectra, a similar trend is seen for peaks A and B relative to peaks C and D.

## IV. Analysis and Discussion

### A. General Considerations

The analyses for most photoelectron spectra are valid within the Franck-Condon (FC) approximation, which relies on the assumption that the electronic and vibrational wavefunctions are separable. The transition intensity, I, is governed by

$$I \propto |\tau_e|^2 \left|\langle \psi_{v''}^- | \psi_{v'}^o \rangle\right|^2. \qquad (3)$$

Here $\tau_e$ is the electronic transition dipole moment and $\left|\langle \psi_{v''}^- | \psi_{v'}^o \rangle\right|^2$ is the Franck-Condon factor for the vibrational wavefunctions of the negative ion and corresponding neutral. If the anion and neutral are linear, one therefore expects vibrational progressions in the totally symmetric stretching modes. Transitions involving even changes of bending quanta can also be observed if there is a sufficiently large change in the vibrational frequency of a bending mode upon photodetachment. The photoelectron spectra of linear $C_n^-$ clusters are explained within the FC approximation as discussed by Arnold *et al.*[3]

However, the previous photoelectron spectrum[68] of $C_2H^-$ showed activity in the $C_2H$ bending mode ($\nu_2$), including transitions in which $\Delta v$ is odd, even though the anion and neutral are linear. In addition, many transitions in the infrared spectra of $C_2H$ which are nominally between two vibrational levels of the $\tilde{X}\ ^2\Sigma^+$ state show a significant spin-orbit splitting in the upper state.[100] Both observations are attributed to strong vibronic coupling effects because of the close-lying $\tilde{X}\ ^2\Sigma^+$ and $\tilde{A}\ ^2\Pi$ states in $C_2H$, resulting in nonseparability of the electronic and vibrational wavefunctions. The nature of the vibronic coupling in $C_2H$, a combination of Renner-Teller coupling within the $\tilde{A}\ ^2\Pi$ state and Herzberg-Teller coupling between the $\tilde{X}\ ^2\Sigma^+$ and $\tilde{A}\ ^2\Pi$ states, has been explored in a series of theoretical papers by Peric *et al.*[69-71] It is unusually strong in $C_2H$ because of a low-energy intersection between the $^2\Sigma^+$ and $^2\Pi$ states for linear geometries.

Although the resolution of anion photoelectron spectroscopy is not nearly as high as many of the other techniques used to investigate $C_2H$, the photoelectron angular distributions provide insight into the vibronic coupling between the $\tilde{X}\ ^2\Sigma^+$ and $\tilde{A}\ ^2\Pi$

states that is generally not available elsewhere. This connection was demonstrated in the original photoelectron spectrum[68] and is further amplified in the spectra presented here at higher photon energy. Since the larger $C_{2n}H$ radicals studied here also have close-lying $^2\Sigma^+$ and $^2\Pi$ states, one expects vibronic coupling to play a role in the photoelectron spectra of the corresponding $C_{2n}H^-$ anions. An understanding of vibronic coupling in the $C_2H^-$ spectra can therefore be used to interpret similar effects in the spectra of the larger anions.

## B. $C_2H(D)$

The $C_2H^-$ anion is linear with a $(...4\sigma^2 1\pi^4 5\sigma^2)$ $^1\Sigma^+$ ground state. One-electron detachment from the ground state anion can produce the ground $\tilde{X}$ $^2\Sigma^+$ $(...4\sigma^2 1\pi^4 5\sigma^1)$ and first excited $\tilde{A}$ $^2\Pi$ $(...4\sigma^2 1\pi^3 5\sigma^2)$ neutral states, so transitions to both states of $C_2H$ should be observable in the photoelectron spectra. In the absence of vibronic coupling, one therefore would expect to see two sets of peaks, possibly with differing $\beta$ values, that correspond to transitions to vibrational levels of the two electronic states. The discussion below shows that the situation is considerably more complex.

As a result of the considerable spectroscopic work already carried out on $C_2H$ and $C_2D$, many of the peaks seen in the photoelectron spectrum can be correlated with previously observed and assigned peaks. These correspondences are shown in Tables I and II. The two most prominent peaks are A1 and F, which correspond to transitions to the (000) level of the $\tilde{X}$ $^2\Sigma^+$ state and the $(01^-0)$ level of the $\tilde{A}$ $^2\Pi$ state, respectively. The two peaks have very different angular distributions, with $\beta \cong 1$ for peak A1 and $\beta \cong -1$ for peak F. The $\tilde{A}(01^-0)$ level has $\Sigma^-$ vibronic symmetry (K=0) but pure $\Pi$

electronic character; it is not vibronically coupled to the $\tilde{X}\ ^2\Sigma^+$state.[42] We can therefore associate positive values of β with peaks that have largely Σ electronic character and negative values of β with transitions to states with significant Π character, or which are allowed only because of vibronic coupling to the $\tilde{A}\ ^2\Pi$ state.

Peaks A1, A2, B1, and B2 are the only peaks in the $C_2H^-$ spectrum with β>0. This is consistent with the assignments in Table I, which show them all to be fully allowed transitions to $\tilde{X}$ state vibrational levels. On the other hand, peaks C and D are each assigned as a pair of overlapped transitions to the $\tilde{X}$ (011)/ $\tilde{X}$ (050) and $\tilde{X}$ (031)/ $\tilde{X}$ (070) levels, respectively. These transitions are only allowed through vibronic coupling to an $\tilde{A}$ state level with the same (Π) vibronic symmetry, and this is consistent with the negative β values observed for these peaks.

Next to peak F, peak E is the most intense of the peaks with β<0. It lies 3750 $cm^{-1}$ from peak A1, which is in the vicinity of the estimated origin of 3772 $cm^{-1}$ for the $\tilde{A}$ - $\tilde{X}$ transition.[60] Comparison with high resolution data indicates that Peak E is composed of several features; three previously observed vibrational bands at 3600 $cm^{-1}$, 3692 $cm^{-1}$, and 3786 $cm^{-1}$ all lie within the envelope of peak E (275 $cm^{-1}$).[56,58,63,100] The observation of multiple bands results from strong mixing of the $\tilde{A}$(000) level with nearby $\tilde{X}$ state levels of the appropriate symmetry.

Similar effects are seen in this energy range in the $C_2D^-$ spectra. Peaks A1, A2, and B2 have positive values of β, as expected from their assignments, whereas β<0 for peaks C and E. Peak C is assigned to the $\tilde{X}$ (011) transition, and is therefore allowed only by vibronic coupling. Just as is the $C_2H^-$ spectra, peak E at 3594 $cm^{-1}$ lies in the

range of the estimated $\tilde{A}$ state origin, 3697 $cm^{-1}$.[60] Stephens *et al.*[60] observed a band in $C_2D$ at 3513 $cm^{-1}$. Although Peric[101] assigns this band to the $\tilde{A}$(000) origin, it is clear that $\tilde{X}$ state levels are mixed in because the spin-orbit coupling constant in the upper state (-6.3 $cm^{-1}$) is considerably less than it would be for a pure $\tilde{A}$ state (~-25 $cm^{-1}$). In any case, the 100 $cm^{-1}$ offset of peak E relative to the 3513 $cm^{-1}$ band suggests that it results from an overlapped transition. It is not clear what this might be because no transitions between 3600 and 3700 $cm^{-1}$ (originating from the $\tilde{X}$ (000) level) have been seen in either gas phase or matrix absorption[53] experiments.

For both isotopes, $\beta<0$ for all peaks with lower electron energy than peak F (except peak M in $C_2D^-$). As shown in Tables I and II, many of these peaks correspond to transitions that have been seen previously in either gas phase or matrix experiments and assigned to particular $\tilde{X}$ or $\tilde{A}$ state transitions. Implicit in these assignments is the notion that virtually all of these states are vibronically coupled to various $\tilde{A}$ state levels; this is supported by the theoretical work of Peric *et al.*[70,71,101] Our photoelectron angular distributions explicitly show that all of the transitions in this energy region correspond to neutral states with significant $\tilde{A}$ state character, and that this mixing with the $\tilde{A}$ state accounts for essentially all of the intensity in the photoelectron spectrum. Given the overlapped appearance of the many of the peaks in this energy range, it is difficult to make more definitive assignments than those already listed in Tables I and II.

**Table I.** Peak positions and spectral assignments for the $C_2H$ photoelectron spectra.

| Peak | Assignment | Position | Splitting from peak A1 ($cm^{-1}$)[a] | β[b] | Previous observations[c] | Ref. |
|---|---|---|---|---|---|---|
| A1 | $\tilde{X}$ (000) | 1.699 | 0 | 1.04 | 0 | |
| A2 | $\tilde{X}$ (020) | 1.602 | 783 | 0.98 | 760 | 67 |
| B1 | $\tilde{X}$ (001) | 1.468 | 1866 | 0.87 | 1841 | 61 |
| C | $\tilde{X}$ (011), $\tilde{X}$ (050) | 1.435 | 2136 | -0.58 | 2091, 2166 | 63, 67 |
| B2 | $\tilde{X}$ (021) | 1.389 | 2505 | 1.29 | 2550 | 68 |
| D | $\tilde{X}$ (031), $\tilde{X}$ (070) | 1.319 | 3064 | -0.99 | 2928, 3101 | 100, 67 |
| E | $\tilde{X}$ (051), $\tilde{A}$ ($00^{0}0$) | 1.236 | 3740 | -0.95 | 3786, 3686[d] | 67, 56 |
| F | $\tilde{A}$ ($01^{1}0$) | 1.184 | 4155 | -0.96 | 4143 | 56 |
| G | $\tilde{X}$ (071), $\tilde{A}$ ($02^{2}0$) | 1.123 | 4651 | -0.73 | 4697 | 103 |
| H | $\tilde{X}$ (*011*0) | 1.077 | 5017 | -0.76 | 5005, 4987 | 103, 103 |
| I | $\tilde{A}$ ($01^{+}0$) | 1.044 | 5287 | -1.02 | 5083[d] | 53 |
| J | $\tilde{X}$ (*012*0) | 1.024 | 5445 | -0.91 | 5403 | 77, 65, 60 |
| K | $\tilde{A}$ (091) | 0.999 | 5649 | -0.88 | 5602[d] | 53 |

[a] Error ± 50 $cm^{-1}$
[b] Average error ± 0.25.
[c] All values rounded to the nearest whole number.
[d] Neon matrix value as noted, all other values are gas phase.

**Table II.** Peak positions and spectral assignments for the $C_2D^-$ photoelectron spectra.

| Peak | Assignment | Position | Splitting from peak A1 ($cm^{-1}$)[a] | β[b] | Gas phase[c] | Ref. |
|---|---|---|---|---|---|---|
| A1 | $\tilde{X}$ (000) | 1.701 | 0 | 1.51 | | |
| A2 | $\tilde{X}$ (020) | 1.627 | 598 | 1.45 | 605 | 68 |
| B1 | $\tilde{X}$ (001) | 1.481 | 1774 | 1.37 | 1743 | 62 |
| C | $\tilde{X}$ (011) | 1.463 | 1920 | 0.28 | 2015 | 68 |
| E | $\tilde{A}$ ($00^{0}0$) | 1.256 | 3594 | -0.46 | 3513 | 60 |
| F | $\tilde{A}$ ($01^{1}0$) | 1.213 | 3940 | -0.58 | 3999 | 60 |
| G | $\tilde{A}$ ($02^{2}0$) | 1.162 | 4345 | -0.56 | 4384[d] | 53 |
| J | | 1.059 | 5179 | -0.3 | 5206 | 60 |
| K | | 1.023 | 5469 | -0.54 | 5460 | 60 |
| M | | 0.797 | 7295 | 1.59 | | |

[a] Error ± 50 $cm^{-1}$.
[b] Average error ± 0.25.
[c] All values are rounded to the nearest whole number.
[d] Neon matrix value as noted, all other values are gas phase.

## C. $C_4H(D)$

The $C_4H^-$ and $C_4D^-$ spectra each exhibit a partially-resolved group of at least six peaks, A1-C2 around eKE=1.0 eV. Peaks A1-B2 are approximately evenly spaced with an average spacing of 223 $cm^{-1}$, and peaks C1 and C2 are separated by 226 $cm^{-1}$. This spacing is close to calculated frequencies by Kiefer *et al.*[30] for the $\nu_7$ bend mode in the $^2\Sigma^+$ and $^2\Pi$ states of $C_4H$. All other calculated frequencies are considerably higher. Thus, independently of the detailed peak assignments, it is clear that we observe strong $\Delta v=1$ transitions in a non-totally symmetric bending mode even though the anion and relevant neutral states are linear. As in the $C_2H^-$ photoelectron spectra, this is a signature of a breakdown in the Franck-Condon approximation caused by vibronic coupling between nearby $\Sigma$ and $\Pi$ electronic states.

$C_4H^-$ is a $^1\Sigma^+$ species with molecular orbital configuration...$1\pi^4 2\pi^4 9\sigma^2$. The lowest neutral $^2\Sigma^+$ and $^2\Pi$ states are formed by photodetachment from the $9\sigma$ and $2\pi$ orbitals, respectively. As mentioned in the Introduction, these states are believed to be nearly degenerate, with the $^2\Sigma^+$ state lying slightly lower in energy, so one might expect transitions to these electronic states to overlap in the photoelectron spectrum. In our spectra, the anisotropy parameters for peaks A1-C2 imply that this group of peaks indeed consists of overlapped electronic transitions; we find $\beta>0$ for peaks A1, A2, C1, and C2, whereas $\beta\cong0$ for peaks B1 and B2. By analogy with the $C_2H^-$ photoelectron angular distributions, we assign the peaks with $\beta>0$ to transitions to the $^2\Sigma^+$ state, and peaks B1 and B2 to transitions to the $^2\Pi$ state. Given that this group of peaks most likely consists of overlapped vibrational progressions in the two electronic states, these assignments represent the dominant rather than the sole electronic character of the neutral level.

We now consider the peak assignments in more detail. The assignment of peaks A1 and A2 to the $^2\Sigma^+$ state implies that this is the ground electronic state of $C_4H$, a result consistent with previous experiments and most calculations. Peak A1 is assigned to the vibrational origin of the $\tilde{X}\ ^2\Sigma^+$ state, yielding electron affinities of 3.558±0.015 eV and 3.552±0.015 eV in $C_4H$ and $C_4D$, respectively. The electron affinity of $C_4H$ is in reasonable agreement with the value of 3.46±0.07 eV calculated by Natterer and Koch.[84] The signal at higher electron energies than peak A1 is most likely due to anion hot bands. We tentatively assign peak a to the $\tilde{X}\ ^2\Sigma^+(\nu_7'=0) \leftarrow \tilde{X}\ ^1\Sigma^+ (\nu_7''=1)$ hot band affording a $\nu_7$ frequency in the anion of 210 $cm^{-1}$ and 169 $cm^{-1}$ in $C_4H(D)$, respectively.

Peaks A1 and A2 are separated by 226 $cm^{-1}$ and 210 $cm^{-1}$ in $C_4H(D)$, respectively. They represent the beginning of the $\nu_7$ bending progression in the $^2\Sigma^+$ ground state. Peaks B1 and B2 belong to the $\tilde{A}\ ^2\Pi$ excited electronic state and are separated by 210 $cm^{-1}$ and 185 $cm^{-1}$ in $C_4H(D)$, respectively, indicating the beginning of a second $\nu_7$ bending progression. The appearance of the $C_4H^-$ spectra suggests that peak B1 is the origin of the $\tilde{A}$ state, yielding an $\tilde{A}$ - $\tilde{X}$ splitting of 468 $cm^{-1}$. However, peaks A2 and B1 are separated by 242 $cm^{-1}$ and 258 $cm^{-1}$ in the $C_4H^-$ and $C_4D^-$ spectra, respectively. This is not significantly different from the bending frequencies in both states, so it is possible that the $\tilde{A}$ state origin lies under peak A2 or even A1. In any case the two electronic states are approximately separated energetically by some integral value of the bending frequency. Endo and coworkers[102] have estimated the $\tilde{A}$ - $\tilde{X}$ splitting in dispersed fluorescence spectra to be 159 $cm^{-1}$ and 149 $cm^{-1}$ in $C_4H(D)$, respectively. They did not observe the $\tilde{A}$ state origin directly but make their estimation by

extrapolating vibrational progressions in the $\tilde{A}$ state to its origin. Their analysis, if correct, is consistent with the $\tilde{A}$ state origin lying under peak A2.

Peaks C1 and C2 have β parameters indicating that they are from the $\tilde{X}\ ^2\Sigma^+$ state. The spacing between peaks A1 and C1 is 960 $cm^{-1}$ and 895 $cm^{-1}$ in $C_4H(D)$, respectively. This is close to the calculated frequency of 910 $cm^{-1}$ for the $\nu_4$ stretching mode, [30] (lowest frequency C-C stretch) so peaks C1 and C2 are tentatively assigned to the $4_0^1$ and $4_0^1 7_0^1$ transitions. Making assignments in this region is difficult because these peaks are overlapped with pure bending progressions from the $\tilde{X}$ and $\tilde{A}$ states; this is particularly problematic in the $C_4D^-$ spectrum where the individual peaks are less obvious.

Peak D has a β parameter associating it with the $\tilde{A}\ ^2\Pi$ state. It is located 2081 $cm^{-1}$ and 2073 $cm^{-1}$ from peak B1 in the $C_4H(D)^-$ spectrum, respectively. This is in excellent agreement with the calculated value[30] for the $\nu_2$ frequency (C≡C stretch) of the $C_4H$ $\tilde{A}\ ^2\Pi$ state, 2139 $cm^{-1}$. The negligible isotopic shift is consistent with the matrix spectroscopy study of Shen *et al.*[82] that showed a very small isotopic shift for the analogous $\nu_2$ mode in the $\tilde{X}\ ^2\Sigma^+$. Peak D is therefore assigned to the $2_0^1$ transition to the $\tilde{A}\ ^2\Pi$ state. If peak A2 were the $\tilde{A}$ state origin, the same assignment for peak D yields 2323 $cm^{-1}$ for the $\nu_2$ frequency in the $\tilde{A}$ state, which is still close to the calculated value.

The positive β parameter for peak E suggests it is a transition to a vibrational level of the $\tilde{X}\ ^2\Sigma^+$ state. It lies 3065 $cm^{-1}$ and 3097 $cm^{-1}$ in $C_4H(D)$, respectively, from peak A1. While this in the range of a C-H stretch, it is considerably lower than the $\nu_1$ frequency of 3307 $cm^{-1}$ observed by Shen *et al.*[82] Moreover no isotopic shift is observed.

Based on the calculated frequencies,[30] the $2_0^1 4_0^1$ combination band should occur at 3193 $cm^{-1}$, close to the observed energy, and a negligible isotope shift is expected for this transition since both modes are carbon-carbon stretches. However, we do not observe the $2_0^1$ transition, which should lie about 2100 $cm^{-1}$ from peak A1.[30,82] The next excited electronic state, the $B\ ^2\Pi$ state, lies 3.2 eV above the $\tilde{X}\ ^2\Sigma^+$ state,[78,86,87], so this is not a reasonable assignment for peak E. Assignment to the $2_0^1 4_0^1$ combination band is the most reasonable option but this is clearly problematic.

The peak assignments and energetics for the $C_4H^-$ and $C_4D^-$ spectra are summarized in Tables III and V. Overall, the $C_4H(D)^-$ photoelectron spectra are the most complex of those reported here. The spectra yield an accurate electron affinity and represent the first published observation and characterization of the low-lying $\tilde{A}\ ^2\Pi$ state. They show that this state lies at most only 468 $cm^{-1}$ above the $\tilde{X}\ ^2\Sigma^+$ state. We obtain bending and stretching vibrational frequencies for both electronic states. However, the assignments of several features are not definitive. We hope that the vibronic coupling effects that complicate these spectra will receive more experimental and theoretical attention in the near future.

**Table III.** Peak positions and assignments for the $C_4H(D)^-$ photoelectron spectra.

| Peak | Assignment | Position ($C_4H$) | Splitting from A1 ($cm^{-1}$)[a] | $\beta$[b] | Position ($C_4D$) | Splitting from A1 ($cm^{-1}$)[a] | $\beta$[b] |
|---|---|---|---|---|---|---|---|
| a | $\tilde{X}\,7_1^0$ | 1.125 | -210 | | 1.126 | -169 | |
| A1 | $\tilde{X}\,0_0^0$ | 1.099 | 0 | 0.29 | 1.105 | 0 | 0.41 |
| A2 | $\tilde{X}\,7_0^1$ | 1.071 | 226 | 0.29 | 1.079 | 210 | 0.34 |
| B1 | $\tilde{A}\,7_0^n$ | 1.041 | 468 | 0.00 | 1.047 | 468 | 0.22 |
| B2 | $\tilde{A}\,7_0^{n+1}$ | 1.016 | 669 | -0.01 | 1.024 | 653 | 0.10 |
| C1 | $\tilde{X}\,4_0^1$ | 0.980 | 960 | 0.62 | 0.994 | 895 | 0.37 |
| C2 | $\tilde{X}\,4_0^1 7_0^1$ | 0.952 | 1186 | 0.81 | 0.959 | 1178 | 0.83 |
| D | $\tilde{A}\,2_0^1$ | 0.783 | 2549 | -0.37 | 0.790 | 2541 | -0.17 |
| E | $\tilde{X}\,2_0^1 4_0^1$ | 0.715 | 3065 | 0.99 | 0.721 | 3097 | 0.77 |
| F1 | | | | | 0.404 | 5654 | 0.69 |
| F2 | | | | | 0.367 | 5952 | 0.91 |
| F3 | | | | | 0.280 | 6654 | 0.52 |

[a] Error is ±50 $cm^{-1}$.
[b] Average error ± 0.25.

## D. $C_6H$

The $C_6H^-$ spectra show a different polarization dependence than the $C_2H^-$ and $C_4H^-$ spectra, in that $\beta$ is *smaller* for peak A, the peak at highest eKE, than for peaks B and C at lower eKE. This suggests that the energy ordering of the two neutral electronic states contributing to this spectrum is reversed, and that the ground state of $C_6H$ is a $^2\Pi$ state, consistent with the earlier microwave spectra[39] and *ab initio* calculations.[83-85,87,91-93] We take peak A to be the vibrational origin of the transition to the $\tilde{X}\,^2\Pi$ state, yielding an electron affinity of 3.809±0.015 eV and 3.805±0.015 eV for $C_6H(D)$, respectively.

This is in reasonable agreement with values calculated by Feher[93] (3.6 eV) and Natterer[92] (3.69±0.05 eV). No other peaks can be definitively assigned to the $\tilde{X}\ ^2\Pi$ state.

Peaks B and C are assigned to the $\tilde{A}\ ^2\Sigma^+$ first excited state. Peak B is the origin this state, giving a term value of 0.181 eV. This lies between the values calculated by Sobolewski[87] (0.25 eV) and Woon[85] (0.11 eV). Peak C appears to belong to the $\tilde{A}\ ^2\Sigma^+$ state and we assign it to a vibrational transition with a frequency of 2202 $cm^{-1}$ and 2202 $cm^{-1}$ in $C_6H(D)$, respectively. No *ab initio* calculations or experimental values are available for the $\tilde{A}\ ^2\Sigma^+$ state. However, comparison with calculations[89,90] performed on the ground state suggest that a frequency of 2202 $cm^{-1}$ corresponds to the largest C≡C stretching frequency, the $\nu_2$ mode, which corresponds to the triple bond nearest to the H atom. The relative simplicity of these spectra compared to those for $C_2H^-$ and $C_4H^-$ suggests that vibronic coupling plays a significantly smaller role. Peak assignments and energetics for $C_6H^-$ and $C_6D^-$ are summarized in Tables IV and V.

**Table IV.** Peak positions and assignments for $C_6H(D)^-$[a] and $C_8H^-$ photoelectron spectra.

| Molecule | Peak | Assignment | Position | Splitting from peak A ($cm^{-1}$)[b] | β[c] |
|---|---|---|---|---|---|
| $C_6H$ | A | $\tilde{X}\ ^2\Pi$ origin | 0.848 (0.852) | 0 (0) | 0.22 (0.11) |
| | B | $\tilde{A}\ ^2\Sigma^+$ | 0.667 (0.672) | 1460 (1452) | 0.48 (0.46) |
| | C | $\tilde{A}\,2_0^1$ | 0.394 (0.399) | 3662 (3654) | 0.48 (0.45) |
| $C_8H$ | A | $\tilde{X}\ ^2\Pi$ origin | 0.691 | 0 | -0.24 |
| | B | $\tilde{X}\,4_0^1$ or $5_0^1$ | 0.485 | 1661 | -0.29 |
| | C | $\tilde{A}\ ^2\Sigma^+$ | 0.438 | 2041 | -0.11 |
| | D | $\tilde{A}\,2_0^1$ or $3_0^1$ | 0.188 | 4057 | -0.04 |

[a] Values in parenthesis are for $C_6D$.
[b] Error ± 50 $cm^{-1}$.
[c] Average error ± 0.25.

## E. $C_8H$

The polarization dependence of the peaks in the $C_8H^-$ spectra is similar to that in the $C_6H^-$ spectra in that the peaks at largest eKE have the smallest values of β. We therefore assign peaks A and B to transitions to the ground $\tilde{X}\ ^2\Pi$ state of $C_8H$ and peaks C and D to transitions to the low-lying $\tilde{A}\ ^2\Sigma^+$ state. This is consistent with the calculations by Pauzat[83] and Adamowicz[87] that predict a $^2\Pi$ ground state. The position of peak A yields an electron affinity of 3.966±0.010 eV. Peak C is assigned to the origin of the $\tilde{A}\ ^2\Sigma^+$ state, yielding a term value of 0.253 eV, noticeably lower than the value of 0.52 eV calculated by Adamowicz.[87]

Peaks B and D correspond to transitions to vibrationally excited levels of the $\tilde{X}\ ^2\Pi$ and $\tilde{A}\ ^2\Sigma^+$ states, respectively. The separation between peaks A and B is 1661 $cm^{-1}$. This most likely corresponds to the frequency of modes $\nu_4$ or $\nu_5$, C≡C stretching modes near the carbon terminus. Peak D is located 2016 $cm^{-1}$ above peak C and corresponds to a high frequency C≡C stretching mode, most likely $\nu_2$ or $\nu_3$. Peak assignments and energetics are summarized in Tables IV and V. No experimental or theoretical values are available for comparison.

**Table V.** Electron Affinities for $C_{2n}H(D)$.

| Molecule | Present Work | Other exp. | Ab initio |
|---|---|---|---|
| $C_2H$ | 2.956±0.020 | 2.969±0.006[a] | 2.961±0.015[b] |
| | | | 2.964[c] |
| | | | 3.09[d] |
| $C_2D$ | 2.954±0.020 | 2.973±0.006[a] | |
| $C_4H$ | 3.558±0.015 | | 3.46±0.07[e] |
| $C_4D$ | 3.552±0.015 | | |
| $C_6H$ | 3.809±0.015 | | 3.6[f] |
| | | | 3.69±0.05[g] |
| $C_6D$ | 3.805±0.015 | | |
| $C_8H$ | 3.966±0.010 | | |

[a] Reference [68].
[b] Reference [104].
[c] Reference [85].
[d] Reference [105].
[e] Reference [84].
[f] Reference [93].
[g] References [84,92].

## V. Conclusions

The anion photoelectron spectra presented here yield electron affinities for several $C_{2n}H$ radicals and provide information on the vibrational and electronic spectroscopy of these species, including vibrational frequencies and term values for low-lying excited states. All the spectra presented here consist of transitions to two close-lying electronic states of the neutral radical; these transitions can be distinguished and assigned based on the photoelectron angular distributions.

Salient features of the spectra are as follows. The $C_2H(D)^-$ photoelectron spectra were taken at a higher photon energy than in previous work. We observe transitions to several levels of the $C_2H$ $\tilde{X}\ ^2\Sigma^+$ state that lie below the $\tilde{A}\ ^2\Pi$ state, some of which are allowed only by vibronic coupling with the $\tilde{A}\ ^2\Pi$ state. Transitions to levels above the $\tilde{A}\ ^2\Pi$ state origin appear to have considerable $\tilde{A}\ ^2\Pi$ state character even though many of them have previously been assigned to excited vibrational levels of the $\tilde{X}\ ^2\Sigma^+$state. It thus appears that vibronic coupling between the two states is very strong above the $\tilde{A}\ ^2\Pi$ state origin.

In the $C_4H(D)^-$ photoelectron spectra, transitions to the $\tilde{X}\ ^2\Sigma^+$ and $\tilde{A}\ ^2\Pi$ states of $C_4H(D)$ are even more strongly overlapped than in the $C_2H(D)^-$ spectra; the term value for the $\tilde{A}\ ^2\Pi$ state is no larger than 468 $\pm$50 $cm^{-1}$. Extended bending progressions in both states provide evidence of strong vibronic coupling. Such coupling renders a standard Franck-Condon analysis of the spectra virtually useless, and several of the vibrational assignments must be considered as tentative.

The $C_6H^-$ and $C_8H^-$ spectra are simpler than the $C_4H^-$ spectrum, most likely reflecting the larger separation between the ground and first excited states. The photoelectron angular distributions indicate that the ordering of these two electronic states is reversed from the smaller radicals; they have $^2\Pi$ ground states and $^2\Sigma^+$ excited states. Our spectra represent the first experimental observation of the $^2\Sigma^+$ state in both cases. Overall, our spectra confirm trends that have been predicted in previous *ab initio* calculations, namely that the $^2\Pi$ state becomes progressively lower in energy relative to the $^2\Sigma^+$ state as the carbon chain length increases from 2-8.

## Acknowledgements

This work is supported by the National Science Foundation under Grant No. DMR-9521805. The authors would also like to thank Dr. Kennosuke Hoshina and Prof. Yasuki Endo for providing us with unpublished results on $C_4H(D)$ and Dr. Gordon R. Burton for early contributions to this project.

## References

[1] W. Weltner and R. Van Zee, Chem. Rev. **89,** 1713 (1989).

[2] S. L. Yang, C. L. Pettiette, Conceicao, O. Cheshnovsky, and R. E. Smalley, Chem. Phys. Lett. **139,** 233 (1987).

[3] D. W. Arnold, S. E. Bradforth, T. N. Kitsopoulos, and D. M. Neumark, J. Chem. Phys. **95,** 8753 (1991).

[4] N. Moazzen-Ahmadi, A. R. W. McKellar, and T. Amano, J. Chem. Phys. **91,** 2140 (1989).

[5] N. Moazzen-Ahmadi, A. R. W. McKellar, and T. Amano, Chem. Phys. Lett. **157,** 1 (1989).

[6] P. F. Bernath, K. H. Hinkle, and J. J. Keady, Science **244,** 562 (1989).

[7] J. R. Heath and R. J. Saykally, J. Chem. Phys. **94,** 3271 (1991).

[8] J. R. Heath and R. J. Saykally, in *On clusters and clustering, from atoms to fractals*, edited by P. J. Reynolds (Elsevier, Amsterdam, 1993), pp. 7-21.

[9] H. J. Hwang, A. Van Orden, K. Tanaka, E. W. Kuo, J. R. Heath, and R. J. Saykally, Mol. Phys. **79,** 769 (1993).

[10] T. F. Giesen, A. Van Orden, H. J. Hwang, R. S. Fellers, R. A. Provencal, and R. J. Saykally, Science **265,** 756 (1994).

[11] C. C. Arnold, Y. X. Zhao, T. N. Kitsopoulos, and D. M. Neumark, J. Chem. Phys. **97,** 6121 (1992).

[12] C. C. Arnold and D. M. Neumark, J. Chem. Phys. **99,** 1442 (1993).

[13] D. Forney, J. Fulara, P. Freivogel, M. Jakobi, D. Lessen, and J. P. Maier, J. Chem. Phys. **103,** 48 (1995).

[14] D. Forney, P. Freivogel, M. Grutter, and J. P. Maier, J. Chem. Phys. **104,** 4954 (1996).

[15] P. Freivogel, J. Fulara, M. Jakobi, D. Forney, and J. P. Maier, J. Chem. Phys. **103,** 54 (1995).

[16] G. von Helden, M. T. Hsu, N. Gotts, and M. T. Bowers, J. Phys. Chem. **97,** 8182 (1992).

[17] K. A. Gingerich, H. C. Finkbeiner, and R. W. Schmude, J. Am. Chem. Soc. **116,** 3884 (1994).

[18] H. Handschuh, G. Gantefor, B. Kessler, P. S. Bechthold, and W. Eberhardt, Phys. Rev. Lett. **74,** 1095 (1995).

[19] K. Raghavachari and J. S. Binkley, J. Chem. Phys. **87,** 2191 (1987).

[20] D. H. Magers, R. J. Harrison, and R. J. Bartlett, J. Chem. Phys. **84,** 3284 (1986).

[21] C. Liang and H. F. Schaefer, III, Chem. Phys. Lett. **169,** 150 (1990).

[22] V. Parasuk and J. Almlöf, J. Chem. Phys. **94,** 8172 (1991).

[23] G. Pacchioni and J. Koutecký, J. Chem. Phys. **88,** 1066 (1988).

[24] L. Adamowicz, Chem. Phys. Lett. **182,** 45 (1991).

[25] V. Parasuk and J. Almlöf, J. Chem. Phys. **91,** 1137 (1989).

[26] R. F. Liu and X. F. Zhou, J. Chem. Phys. **99,** 1440 (1993).

[27] S. Schmatz and P. Botschwina, Inter. J. Mass. Spec. and Ion. Proc. **150,** 621 (1995).

[28] S. Schmatz and P. Botschwina, Chem. Phys. Lett. **235,** 5 (1995).

[29] J. M. L. Martin, J. P. Francois, and R. Gijbels, J. Chem. Phys. **93,** 8850 (1990).

[30] J. H. Kiefer, S. S. Sidhu, R. D. Kern, K. Xie, H. Chen, and L. B. Harding, Combust. Sci. Technol. **82,** 101 (1992).

[31] M. Guelin, S. Green, and P. Thaddeus, Astrophys. J. **224,** L27 (1978).

[32] M. Guelin, J. Cernicharo, C. Kahane, J. Gomez-Gonzales, and C. M. Walmsley, Astron. Astrophys. **175,** L5 (1987).

[33] M. Guelin, J. Cernicharo, S. Navarro, D. R. Woodward, C. A. Gottlieb, and P. Thaddeus, Astron. Astrophys. **182,** L37 (1987).

[34] W. M. Irvine, M. Ohishi, and N. Kaifu, Icarus **91,** 2 (1991).

[35] I. A. Crawford, Monthly Notices of the Royal Astronomical Society **277,** 458 (1995).

[36] J. Cernicharo and M. Guelin, Astron. Astrophys. **309,** L27 (1996).

[37] J. Fulara, D. Lessen, P. Freivogel, and J. P. Maier, Nature **366,** 439 (1993).

[38] C. A. Gottlieb, E. W. Gottlieb, P. Thaddeus, and H. Kawamura, Astrophys. J. **275,** 916 (1983).

[39] J. C. Pearson, C. A. Gottlieb, D. R. Woodward, and P. Thaddeus, Astron. Astrophys. **189,** L13 (1988).

[40] M. C. McCarthy, M. J. Travers, A. Kovacs, C. A. Gottlieb, and P. Thaddeus, Astron. Astrophys. **309,** L31 (1996).

[41] E. L. Cochran, F. J. Adrian, and V. A. Bowers, J. Chem. Phys. **40,** 213 (1965).

[42] W. R. M. Graham, K. I. Dismuke, and W. Weltner, Jr., J. Chem. Phys. **60,** 3817 (1974).

[43] M. Jinguji, C. A. McDowell, and K. Shimokoshi, J. Mol. Struct. **130,** 317 (1985).

[44] R. J. Saykally, L. Veseth, and K. M. Evenson, J. Chem. Phys. **80,** 2247 (1984).

[45] J. M. Brown and K. M. Evenson, J. Mol. Spectrosc. **131,** 161 (1988).

[46] K. V. L. N. Sastry, P. Helminger, A. Charo, E. Herbst, and F. C. de Lucia, Astrophys. J. **251,** L119 (1981).

[47] C. A. Gottlieb, E. W. Gottlieb, and P. Thaddeus, Astrophys. J. **264,** 740 (1983).

[48] M. Bogey, C. Demuynck, and J. L. Destombes, Astron. Astrophys. **144,** L15 (1985).

[49] Y. Endo, H. Kanamori, and E. Hirota, Chem. Phys. Lett. **160,** 280 (1989).

[50] D. E. Milligan, M. E. Jacox, and L. Abouaf-Marguin, J. Chem. Phys. **46,** 4562 (1967).

[51] M. E. Jacox, Chem. Phys. **7,** 424 (1975).

[52] M. E. Jacox and W. B. Olson, J. Chem. Phys. **86,** 3134 (1987).

[53] D. Forney, M. E. Jacox, and W. E. Thompson, J. Mol. Spectrosc. **170,** 178 (1995).

[54] R. A. Shepherd and W. R. M. Graham, J. Chem. Phys. **86,** 2600 (1987).

[55] P. G. Carrick, A. J. Merer, and R. F. Curl, Jr., J. Chem. Phys. **78,** 3652 (1983).

[56] R. F. Curl, P. G. Carrick, and A. J. Merer, J. Chem. Phys. **82,** 3479 (1985).

[57] R. F. Curl, P. G. Carrick, and A. J. Merer, J. Chem. Phys. **83,** 4278 (1985).

[58] W. B. Yan, C. B. Dane, D. Zeitz, J. L. Hall, and R. F. Curl, J. Mol. Spectrosc. **123,** 486 (1987).

[59] W. B. Yan, J. L. Hall, J. W. Stephens, M. L. Richnow, and R. F. Curl, J. Chem. Phys. **86,** 1657 (1987).

[60] J. W. Stephens, Y. Wen-bin, M. L. Richnow, H. Solka, and R. F. Curl, J. Mol. Struct. **190,** 41 (1988).

[61] H. Kanamori, K. Seki, and E. Hirota, J. Chem. Phys. **87,** 73 (1987).

[62] H. Kanamori and E. Hirota, J. Chem. Phys. **88,** 6699 (1988).

[63] H. Kanamori and E. Hirota, J. Chem. Phys. **89,** 3962 (1988).

[64] K. Kawaguchi, T. Amano, and E. Hirota, J. Mol. Spectrosc. **131,** 58 (1988).

[65] M. Vervloet and M. Herman, Chem. Phys. Lett. **144,** 48 (1988).

[66] Y. C. Hsu, J. J. M. Lin, D. Papousek, and J. J. Tsai, J. Chem. Phys. **98,** 6690 (1993).

[67] Y. C. Hsu, Y. J. Shiu, and C. M. Lin, J. Chem. Phys. **103,** 5919 (1995).

[68] K. M. Ervin and W. C. Lineberger, J. Phys. Chem. **95,** 1167 (1991).

[69] M. Peric, R. J. Buenker, and S. D. Peyerimhoff, Mol. Phys. **71,** 673 (1990).

[70] M. Peric, S. D. Peyerimhoff, and R. J. Buenker, Mol. Phys. **71,** 693 (1990).

[71] M. Peric, S. D. Peyerimhoff, and R. J. Buenker, Z. Phys. D **24,** 177 (1992).

[72] J. Zhang, C. W. Riehn, M. Dulligan, and C. Wittig, J. Chem. Phys. **103,** 6815 (1995).

[73] S. H. S. Wilson, C. L. Reed, D. H. Mordaunt, M. N. R. Ashfold, and M. Kawasaki, Bull. Chem. Soc. Japan **69,** 71 (1996).

[74] J.-H. Wang, Y.-T. Hsu, and K. Liu, J. Phys. Chem. A **101,** 6593 (1997).

[75] D. H. Mordaunt, M. N. R. Ashfold, R. N. Dixon, P. Loffler, L. Schnieder, and K. H. Welge, J. Chem. Phys. **108,** 519 (1998).

[76] Y. C. Hsu, F. T. Chen, L. C. Chou, and Y. J. Shiu, J. Chem. Phys. **105,** 9153 (1996).

[77] T. R. Fletcher and S. R. Leone, J. Chem. Phys. **90,** 871 (1989).

[78] K. I. Dismuke, W. R. M. Graham, and W. Weltner, Jr., J. Mol. Spectrosc. **57,** 127 (1975).

[79] S. Yamamoto, S. Saito, M. Guelin, J. Cernicharo, H. Suzuki, and M. Ohishi, Astrophys. J. **323,** 149 (1987).

[80] W. Chen, S. E. Novick, M. C. McCarthy, C. A. Gottlieb, and P. Thaddeus, J. Chem. Phys. **103,** 7828 (1995).

[81] M. C. McCarthy, C. A. Gottlieb, P. Thaddeus, M. Horn, and P. Botschwina, J. Chem. Phys. **103,** 7820 (1995).

[82] L. N. Shen, T. J. Doyle, and W. R. M. Graham, J. Chem. Phys. **93,** 1597 (1990).

[83] F. Pauzat, Y. Ellinger, and A. D. McLean, Astrophys. J. **369,** L13 (1991).

[84] J. Natterer and W. Koch, Mol. Phys. **84,** 691 (1995).

[85] D. E. Woon, Chem. Phys. Lett. **244,** 45 (1995).

[86] M. Kolbuszewski, Astrophys. J. **432,** L63 (1994).

[87] A. L. Sobolewski and L. Adamowicz, J. Chem. Phys. **102,** 394 (1995).

[88] K. Hoshina, H. Kohguchi, Y. Ohshima, and Y. Endo, J. Chem. Phys. **108,** 3465 (1998).

[89] T. J. Doyle, L. N. Shen, C. M. L. Rittby, and W. R. M. Graham, J. Chem. Phys. **95,** 6224 (1991).

[90] R. F. Liu, X. F. Zhou, and P. Pulay, J. Chem. Phys. **97,** 1602 (1992).

[91] A. Murakami, K. Kawaguchi, and S. Saito, Publ. Astron. Soc. Japan **39,** 189 (1987).

[92] J. Natterer, W. Koch, D. Schroder, N. Goldberg, and H. Schwarz, Chem. Phys. Lett. **229,** 429 (1994).

[93] M. Feher and J. P. Maier, Chem. Phys. Lett. **227,** 371 (1994).

[94] R. B. Metz, A. Weaver, S. E. Bradforth, T. N. Kitsopoulos, and D. M. Neumark, J. Phys. Chem. **94,** 1377 (1990).

[95] C. Xu, G. R. Burton, T. R. Taylor, and D. M. Neumark, J. Chem. Phys. **107,** 3428 (1997).

[96] D. L. Osborn, D. J. Leahy, D. R. Cyr, and D. M. Neumark, J. Chem. Phys. **104,** 5026 (1996).

[97] G. Markovich, R. Giniger, M. Levin, and O. Cheshnovsky, J. Chem. Phys. **95,** 9416 (1991).

[98] B. A. Mamyrin and D. V. Shmikk, JETP **76,** 1500 (1979).

[99] J. Cooper and R. N. Zare, in *Lectures in Theoretical Physics*, Vol. XI-C, edited by S. Geltman, K. T. Mahanthappa, and W. E. Brittin (Gordon and Breach, New York, 1969), pp. 317-337.

[100] W. B. Yan and T. Amano, J. Chem. Phys. **99,** 4312 (1993).

[101] M. Peric, S. D. Peyerimhoff, and R. J. Buenker, J. Mol. Spectrosc. **148,** 180 (1991).

[102] K. Hoshina and Y. Endo, Personal communication (1996).

[103] F. T. Chen, L. C. Chou, and Y. C. Hsu, in *The 22nd International Symposium of Free Radicals,* (Doorwerth, The Netherlands., 1993).

[104] J. A. Montgomery and G. A. Petersson, Chem. Phys. Lett. **168,** 75 (1990).

[105] W. I. Sou and W. K. Li, J. Chem. Res.-S , 464 (1995).

# Chapter 3. The Singlet-Triplet Splittings of NCN


## Abstract

The photoelectron spectrum of the cyanonitrene anion, $NCN^-$, has been measured at 416 and 266 nm. The 266 nm spectrum reveals the $\tilde{a}\ ^1\Delta_g$ and the $\tilde{b}\ ^1\Sigma_g^+$ states together with the $\tilde{X}\ ^3\Sigma_g^-$ ground state for the first time. These low-lying singlet states are separated from the triplet ground state by $1.010 \pm 0.010$ and $1.629 \pm 0.010$ eV, respectively. We find a vibrational frequency of $1120 \pm 50$ $cm^{-1}$ for the $\upsilon_1$ mode of the $\tilde{b}\ ^1\Sigma_g^+$ state. The ions were produced in a new source particularly suitable for anion precursors with low vapor pressure.


## I. Introduction

The cyanonitrene radical, NCN, has been proposed as an intermediate in the combustion of hydrocarbons[1] and nitramine.[2] Ultraviolet emission studies[3] have also suggested that NCN is present in the Comet Brorosen-Metcalf. The NCN radical has a $\tilde{X}\ ^3\Sigma_g^-$ ground state with a molecular orbital configuration[4] of $...2\sigma_g^2 2\sigma_u^2 1\pi_u^4 1\pi_g^2$. This configuration also gives rise to two singlet states, the $\tilde{a}\ ^1\Delta_g$ and the $\tilde{b}\ ^1\Sigma_g^+$ states, whose term values with respect to the ground state have been previously unknown. Many studies have been carried out to characterize cyanonitrene theoretically[4-9] and experimentally.[1,2,4,10-22] Optical experiments have been limited to independent studies of the triplet[11,14,15] and singlet[14] manifolds. Photodissociation experiments involving excitation in both manifolds have recently been carried out in our laboratories,[23] but no transitions between the manifolds were observed. By measuring the photoelectron

spectrum of the anion, $NCN^-$, we can access both the triplet and singlet states through detachment of a single electron from the anion $^2\Pi$ ground state. Hence for the first time we are able to obtain the singlet-triplet splittings for the low-lying electronic states of NCN.

Recently, Ellison and coworkers[4] have measured the anion photoelectron spectrum of $NCN^-$ at a photon energy of 3.531 eV. They reported an electron affinity of $2.484 \pm 0.006$ eV for NCN. At this energy only the transition to the $\tilde{X}\ ^3\Sigma_g^-$ ground state of the neutral is accessible; the $\tilde{a}\ ^1\Delta_g$ state was calculated to lie 1.249 eV above the ground state.[4] In this paper we report the anion photoelectron spectra of $NCN^-$ taken at photon energies of 2.977 eV (416nm) and 4.657 eV (266 nm). At 266 nm, transitions to the $\tilde{a}\ ^1\Delta_g$ and the $\tilde{b}\ ^1\Sigma_g^+$ states are observed and we report their term energies.

## II. Experimental

As shown by Ellison, $NCN^-$ is readily produced from cyanamide ($H_2NCN$). The low vapor pressure of this precursor (estimated to be ~4 mtorr at 298K) necessitated development of a new configuration of our pulsed discharge ion source,[24] shown in Figure 1. The stainless steel reservoir was filled with cyanamide and placed between a pulsed molecular beam valve and the pulsed discharge assembly. This enables the cyanamide to be entrained in the pulsed molecular beam prior to passing through the discharge. Teflon spacers prevent thermal contact with the pulsed valve and electric discharge plates, allowing the reservoir to be heated without affecting the pulsed valve, although heating was not necessary in this case. Analysis of our photodissociation

spectroscopy measurements[23] indicate that this source produces $NCN^-$ ions with vibrational and rotational temperatures of ~200 K and ~50 K, respectively.

The anion photoelectron spectrometer used in this study has been described in detail previously.[25,26] In the work presented here, $O_2$ at a backing pressure of ~3 atm was expanded through the reservoir/pulsed discharge source containing the precursor cyanamide ($H_2NCN$). The resultant flow supersonically expands into the source vacuum chamber and passes through a skimmer. The negative ions are extracted perpendicular to their flow direction by a pulsed electric field and injected into a linear reflectron time-of-flight (TOF) mass spectrometer,[27,28] affording a mass resolution $m/\Delta m$ of 2000. The ions of interest are selectively photodetached with photons having wavelengths of 266 nm (4.657 eV) and 416 nm (2.977 eV). The photon wavelength of 266 nm was obtained by frequency quadrupling the fundamental of a pulsed Nd:YAG laser. To generate light at 416 nm the Nd:YAG third harmonic at 355 nm was passed through a Raman cell filled with hydrogen at high pressure (325 psig). The electron kinetic energy (eKE) distribution is determined by TOF analysis in a 1 m field-free flight tube. The energy resolution is 8 meV at 0.65 eKE and degrades as $(eKE)^{3/2}$ at higher eKE. All spectra reported were taken at a laser polarization angle $\theta = 90^\circ$, which was found to correspond to the maximum of the photoelectron angular distribution.

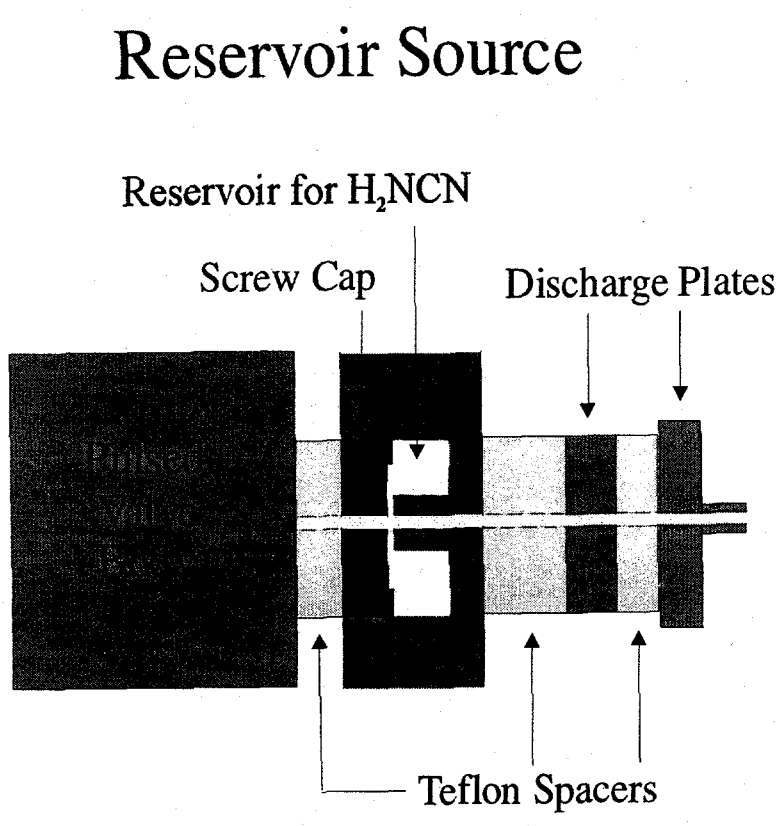


Fig. 1. Schematic of the reservoir/pulsed discharge source. The drawing is not to scale.

## III. Results/Discussion

Figure 2 shows the anion photoelectron spectra taken at 266 nm and 416 nm (see inset). The photoelectron spectra are reported in electron binding energy, eBE, which is defined as $eBE = h\nu - eKE$. The inset shows the transition to the $\tilde{X}\ ^3\Sigma_g^-$ ground state of

the neutral, a single feature labeled as peak X. This peak is located at eKE=0.496 eV eKE affording an electron affinity of 2.481 ± 0.008 eV, in excellent agreement with the value reported by Ellison and coworkers.[4] The structure extending to higher eKE as part of peak X indicates that the $^2\Pi$ anion electronic ground state is internally excited. This is at least partly due to detachment from the two spin-orbit levels of the anion, which are split by only 77 $cm^{-1}$.

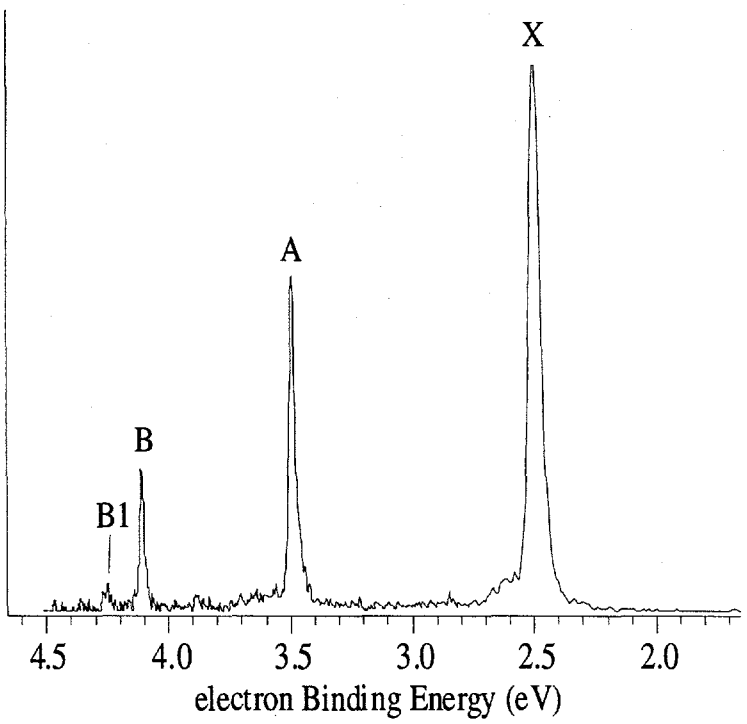


Figure 2. Photoelectron spectrum of $NCN^-$ taken at 266 and 416 nm (see inset). Both spectra were taken at a laser polarization angle of $\theta=90^\circ$ with respect to the direction of electron detection.

The main spectrum in Figure 2 shows the 266 nm spectrum with peaks labeled X, A, B, and B1. Peak X is the ground state as previously discussed. Peaks A and B are represent transitions to two excited electronic states. From Hund's rules and the state ordering of the isoelectronic species CCO,[29] CNN,[30] $N_3^+$,[31] and $NCO^+$,[32] these peaks are assigned to the $\tilde{a}\ ^1\Delta_g$ and the $\tilde{b}\ ^1\Sigma_g^+$ states located at $1.010 \pm 0.010$ and $1.629 \pm 0.010$ eV above the ground state, respectively. These spacings are referenced to the peak centers; no attempt was made to fit the peak shapes. Peak B1 is $1120 \pm 50$ $cm^{-1}$ from peak B and we assign this transition to the $\upsilon_1$=1 level of the $\tilde{b}\ ^1\Sigma_g^+$ state, in accord with the known $\upsilon_1$ fundamentals of the other electronic states.[2,14,16] Like the ground state, these electronic transitions are nearly vertical, and the peaks exhibit the same asymmetry towards higher electron kinetic energy.

The results obtained here allow a full characterization of the low-lying electronic states of NCN, as shown in Fig. 3. Herzberg and Travis[11] identified the first electronic transition from the ground state as the $\tilde{B}\ ^3\Sigma_u^- \leftarrow \tilde{X}\ ^3\Sigma_g^-$ transition having an energy of 4.154 eV. Kroto and coworkers[14] observed another transition within the triplet manifold, the $\tilde{A}\ ^3\Pi_u \leftarrow \tilde{X}\ ^3\Sigma_g^-$ band, with an energy of 3.767 eV. They also observed two transitions within the singlet manifold assigned as the $\tilde{c}\ ^1\Pi_u \leftarrow \tilde{a}\ ^1\Delta_g$ and $\tilde{d}\ ^1\Delta_u \leftarrow \tilde{a}\ ^1\Delta_g$ transitions with energies of 3.725 and 4.385 eV, respectively. With our measurement of the $\tilde{a}\ ^1\Delta_g$ and the $\tilde{b}\ ^1\Sigma_g^+$ term energies we can now properly reference the excited singlet electronic states to the ground state, as shown in Figure 3.

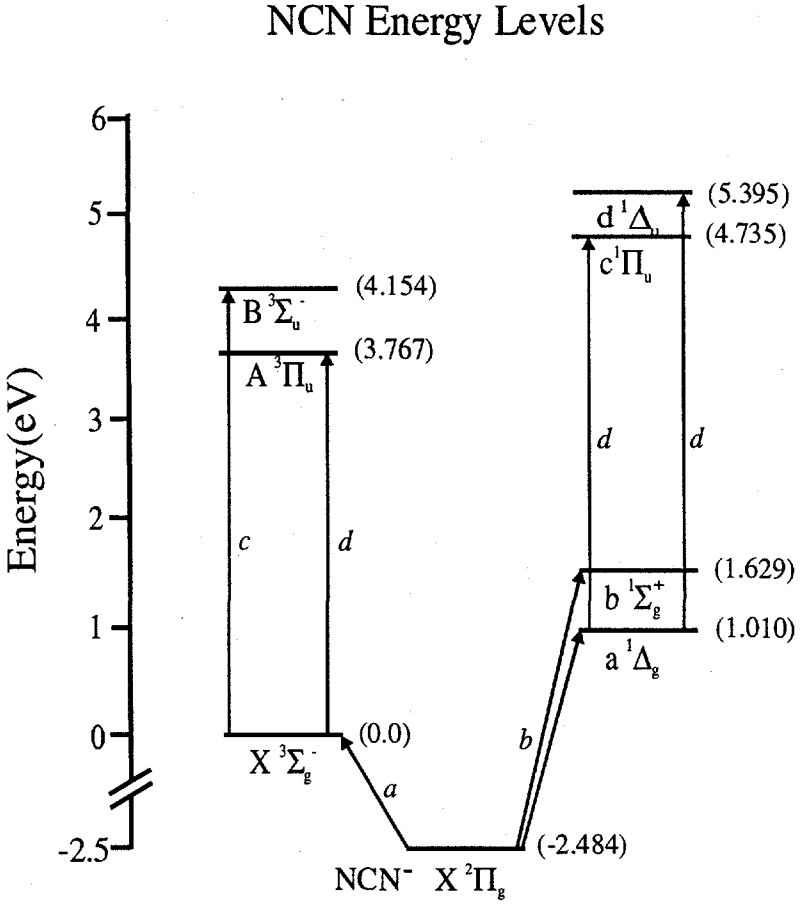


Fig. 3. Energy level diagram of the singlet and triplet manifolds of NCN. Labeled transitions are from the following papers: a) Ref. 4 b) This work c) Ref. 11 d) Ref. 14.

## Acknowledgements

This research is supported by the Air Force Office of Scientific Research under Grant No. F49620-97-1-0018. The authors would also like to acknowledge Leo Lehr and Rainer Weinkauf for their contributions to the source design and manufacture.

## References

[1] K. R. Jennings and J. W. Linnett, Trans. Faraday Soc. **56,** 1737 (1960).

[2] G. P. Smith, R. A. Copeland, and D. R. Crosley, J. Chem. Phys. **91,** 1987 (1989).

[3] C. R. O'Dell, C. O. Miller, A. L. Cochran, W. D. Cochran, C. B. Opal, and E. S. Barker, Astrophys. J. **368,** 616 (1991).

[4] Clifford, P. G. Wenthold, W. C. Lineberger, G. A. Petersson, and G. B. Ellison, J. Phys. Chem. A **101,** 4338 (1997).

[5] G. Berthier and L. Kurdi, Comptes Rendus de l'Academie des Sciences, Serie II (Mecanique, Physique, Chimie, Sciences de l'Univers, Sciences de la Terre) **299,** 1171 (1984).

[6] H. U. Suter, M. B. Huang, and B. Engels, J. Chem. Phys. **101,** 7686 (1994).

[7] C. Thomson, J. Chem. Phys. **58,** 841 (1973).

[8] G. R. Williams, Chem. Phys. Lett. **25,** 602 (1974).

[9] J. M. L. Martin, P. R. Taylor, J. P. Francois, and R. Gijbels, Chem. Phys. Lett. **226,** 475 (1994).

[10] G. P. Smith, R. A. Copeland, and D. R. Crosley, AIP Conf. Proc. , 659 (1988).

[11] G. Herzberg and D. N. Travis, Can. J. Phys. **42,** 1658 (1964).

[12] H. W. Kroto, J. Chem. Phys. **44,** 831 (1966).

[13] H. W. Kroto, Can. J. Phys. **45,** 1439 (1967).

[14] H. W. Kroto, T. F. Morgan, and H. H. Sheena, Trans. Faraday Soc. **66,** 2237 (1970).

[15] D. E. Milligan, M. E. Jacox, and A. M. Bass, J. Chem. Phys. **43,** 3149 (1965).

[16] D. E. Milligan and M. E. Jacox, J. Chem. Phys. **45,** 1387 (1966).

[17] S. A. Beaten, Y. Ito, and J. M. Brown, J. Mol. Spectrosc. **178,** 99 (1996).

[18] S. A. Beaton and J. M. Brown, J. Mol. Spectrosc. **183,** 347 (1997).

[19] K. D. Hensel and J. M. Brown, J. Mol. Spectrosc. **180,** 170 (1996).

[20] M. Wienkoop, W. Urban, and J. M. Brown, J. Mol. Spectrosc. **185,** 185 (1997).

[21] J. M. Fluornoy and L. Y. Nelson, Chem. Phys. Lett. **6,** 521 (1970).

[22] D. McNaughton, G. F. Metha, and R. Tay, Chem. Phys. **198,** 107 (1995).

[23] R. T. Bise, H. Choi, and D. M. Neumark, J. Chem. Phys. **111,** 4923 (1999).

[24] D. L. Osborn, D. J. Leahy, D. R. Cyr, and D. M. Neumark, J. Chem. Phys. **104,** 5026 (1996).

[25] C. Xu, G. R. Burton, T. R. Taylor, and D. M. Neumark, J. Chem. Phys. **107,** 3428 (1997).

[26] R. B. Metz, A. Weaver, S. E. Bradforth, T. N. Kitsopoulos, and D. M. Neumark, J. Phys. Chem. **94,** 1377 (1990).

[27] B. A. Mamyrin and D. V. Shmikk, Sov. Phys. JETP **49,** 762 (1979).

[28] G. Markovich, R. Giniger, M. Levin, and O. Cheshnovsky, J. Chem. Phys. **95,** 9416 (1991).

[29] V. Zengin, B. J. Persson, K. M. Strong, and R. E. Continetti, J. Chem. Phys. **105,** 9740 (1996).

[30] E. P. Clifford, P. G. Wenthold, W. C. Lineberger, G. A. Petersson, K. M. Broadus, S. R. Kass, S. Kato, C. H. DePuy, V. M. Bierbaum, and G. B. Ellison, J. Phys. Chem. A **102,** 7100 (1998).

[31] J. M. Dyke, N. B. H. Jonathan, A. E. Lewis, and A. Morris, Mol. Phys. **47,** 1231 (1982).

[32] J. M. Dyke, N. Jonathan, A. E. Lewis, J. D. Mills, and A. Morris, Mol. Phys. **50,** 77 (1983).

# Chapter 4. Characterization of the $I_3$ radical by anion photoelectron spectroscopy


## Abstract

The ground and first excited states of the $I_3$ radical are characterized by photoelectron spectroscopy of $I_3^-$ and $Ar{\cdot}I_3^-$ at 266 nm. The electron affinity of $I_3$ is 4.226 $\pm$ 0.013 eV. Based on the recently determined bond dissociation energy of $I_3^-$, the $I_3$ ground state is bound by 0.143 $\pm$ 0.06 eV. The first excited state of $I_3$ lies 0.27 eV above the ground state. A vibrational progression is seen in the ground state band of the $I_3^-$ photoelectron spectrum. The addition of an argon atom to $I_3^-$ vibrationally cools the anion, facilitating the interpretation of this vibrational structure. Simulations indicate that the $I_3$ ground state is linear with a symmetric stretch frequency of 115 $\pm$ 5 $cm^{-1}$ and is likely to be centrosymmetric.


## I. Introduction

The triiodine radical, $I_3$, has been proposed to play a key role in one of the most fundamental reactions in gas phase kinetics, the recombination of I atoms to form $I_2$, via the following mechanism:[1-6]

$$\begin{aligned} I + I_2 &\rightarrow I_3 \\ I + I_3 &\rightarrow 2I_2 \end{aligned} \qquad (1)$$

However, in spite of considerable effort,[7] neither $I_3$ nor any other homonuclear trihalogen ($X_3$) has ever been spectroscopically identified. In fact, the only gas-phase experimental

evidence that any of these species is thermodynamically stable comes from the mass-spectrometric observation of $Br_3$ as a photodissociation product from $(Br_2)_2$.[8]

In this Communication we use anion photoelectron spectroscopy of $I_3^-$ to show that $I_3$ is a covalently bound molecule and probe its vibrational spectroscopy. Further, we demonstrate that $I_3^-$ can be vibrationally cooled by the addition of an argon atom to form the $Ar{\cdot}I_3^-$ cluster. This cooling results in a clearer analysis of vibrational structure in the photoelectron spectrum of $I_3^-$ than would otherwise be possible; from these features it appears that the ground state of $I_3$ is linear and centrosymmetric.

Several other studies have indirectly estimated the thermodynamic stability of triiodine.[3-5] Because iodine is the least electronegative halogen, $I_3$ should be the most stable trihalogen and is the most likely to be linear.[9,10] There are no high level *ab initio* calculations available for $I_3$, however, calculations by Morokuma and coworkers[7] on isovalent $Cl_3$ show its ground state to be a highly asymmetric $Cl{\cdot}Cl_2$ van der Waals complex with a low-lying linear, centrosymmetric excited state.

The triiodide anion is considerably better characterized than the $I_3$ radical. $I_3^-$ is a hypervalent 22 electron triatomic violating the Lewis octet rule. In Walsh's 1953 paper,[9] $I_3^-$ was predicted to be linear and all subsequent *ab initio* calculations have shown that it is both linear and centrosymmetric.[11-19] While many experimental studies of $I_3^-$ have been performed, nearly all of these have been limited to the solid and solution phases. In the gas phase, Do *et al.*[20] recently carried out collision induced dissociation experiments in which they determined the $I^- + I_2$ binding energy to be $1.31 \pm 0.06$ eV. Time-resolved studies of $I_3^-$ photodissociation in the gas phase have recently been carried out in our laboratory;[21] in that work, a low-resolution photoelectron spectrum of $I_3^-$ was presented.

The higher resolution work presented here offers a much more detailed picture of the energetics and spectroscopy of $I_3$.

## II. Experimental

The anion photoelectron spectrometer used in this study has been described in detail previously.[22,23] In the work presented here, argon carrier gas (2 psig) is passed over crystalline $I_2$ and supersonically expanded through a pulsed piezoelectric valve. Anions are generated by crossing a 1 keV electron beam with the molecular beam. The negative ions pass through a skimmer into a differentially pumped region. They are extracted perpendicular to their flow direction by a pulsed electric field and injected into a linear reflectron time-of-flight (TOF) mass spectrometer,[24,25] affording a mass resolution $m/\Delta m$ of 2000. The ions of interest are selectively photodetached with the fourth harmonic of a pulsed Nd:YAG laser(266 nm, hν=4.657 eV). The electron kinetic energy (eKE) distribution is determined by TOF analysis. The energy resolution is 8 meV at 0.65 eKE and degrades as $(eKE)^{3/2}$ at higher eKE. The laser polarization can be rotated by means of a half-wave plate, defining a polarization angle θ as the angle between the electric vector of the photon and the direction of electron detection.

## III. Results

Figure 1 shows the anion photoelectron spectra of $I_3^-$ (top) and $Ar{\cdot}I_3^-$ (bottom) taken at 266 nm (4.657 eV) and a polarization angle of θ=90°. In these photoelectron spectra the electron kinetic energy, eKE, is related to the internal energy of the neutral and anion by $eKE = h\nu - EA - E^o + E^-$. Here $h\nu$ is the photon energy, $EA$ is the adiabatic

electron affinity, $E^o$ is the internal energy of the neutral, and $E^-$ is the internal energy of the anion.

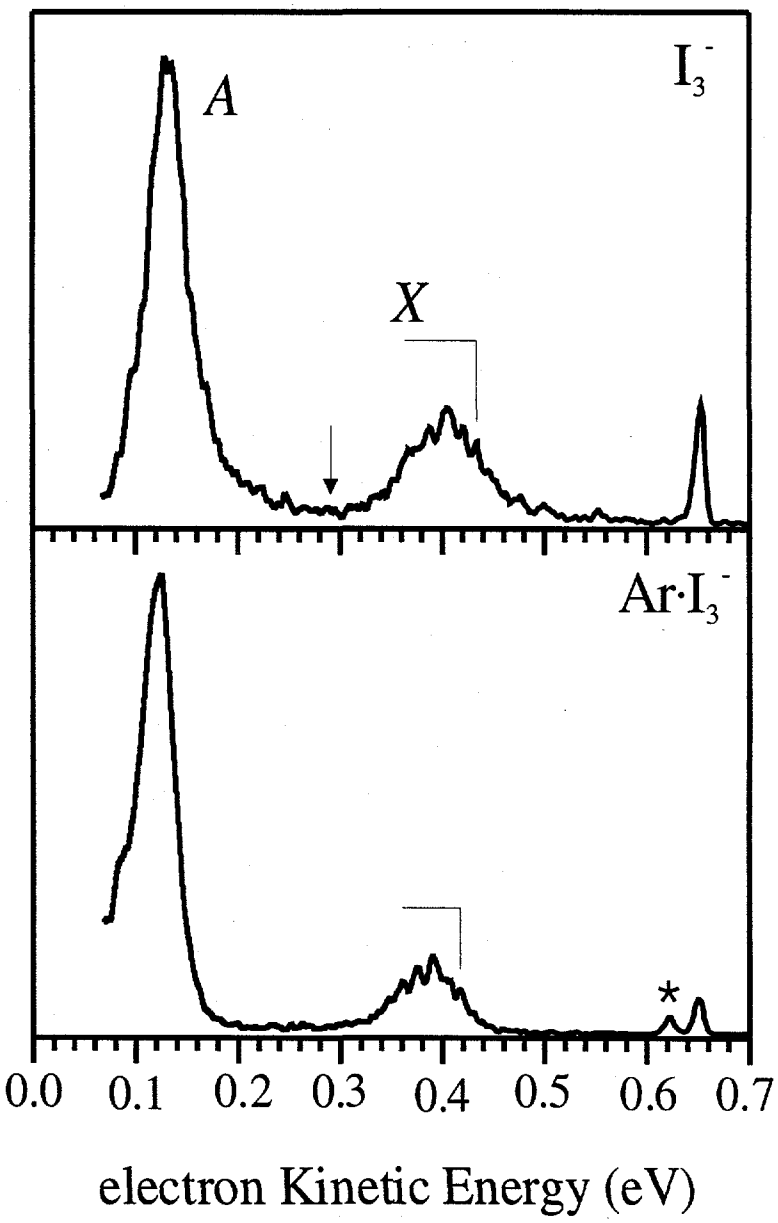


Fig. 1. Photoelectron spectrum of $I_3^-$ (top) and $Ar \cdot I_3^-$ (bottom) taken at the photodetachment wavelength of 266 nm (4.657 eV). Laser polarization angle is 90° with respect to the direction of electron collection.

The three features observed in the photoelectron spectrum of $I_3^-$ are centered at 0.652, 0.402, and 0.132 eV eKE. The highest energy feature is due to a two-photon process, photodissociation of $I_3^-$ to form $I^- + I_2$ followed by photodetachment to the $^2P_{1/2}$ spin-orbit state of atomic iodine (photodetachment to the $^2P_{3/2}$ state is observed but not shown in Fig. 1). Features X and A at lower eKE correspond to detachment to the ground and first excited states of $I_3$, respectively. We estimate the energy separation between features X and A to be 0.27 eV by taking the difference in the vertical detachment energies. Feature X is 60 meV wide showing a partially resolved vibrational progression with a frequency of ~14 meV. Feature A is 40 meV wide and shows no vibrational structure. Comparison with the photoelectron spectrum taken at $\theta=0°$ yields anisotropy parameters $\beta$ of 0.24 and –0.21 for features X and A, respectively.[26]

The bottom panel of Figure 1 shows the anion photoelectron spectrum of the $Ar{\cdot}I_3^-$ cluster. In this cluster, the internal energy of the $I_3^-$ moiety must be less than the dissociation energy, or predissociation to $Ar + I_3^-$ will occur. As a result, features X and A are narrower, the baseline between them is flatter, and the vibrational structure in feature X is more regular and somewhat better-resolved. These effects are all attributed to a vibrationally colder $I_3^-$ chromophore; similar results were seen in the photoelectron spectrum of $Ar{\cdot}I_2^-$.[27] due to stronger binding of the argon in the anion than in the neutral, features X and A are centered at slightly lower eKEs, 0.385 eV and 0.121 eV, respectively.

In addition to the three features seen in the $I_3^-$ spectrum, the $Ar{\cdot}I_3^-$ spectrum shows a peak 28 meV below the $I\ ^2P_{1/2}$ two-photon feature labeled with an (*). This peak is from detachment of $Ar{\cdot}I^-$, which is known to have an electron affinity 26.7 meV higher

than that of $I^-$.[28] Hence, both $Ar{\cdot}I^-$ and $I^-$ result from photodissociation of $Ar{\cdot}I_3^-$ at 266 nm in about a 1:2 ratio.

## IV. Discussion

First we show that the ground state of $I_3$ is bound with respect to dissociation. Any feature in the photoelectron spectrum at a higher electron kinetic energy than $eKE_{min} = h\nu - D_o(I_2{\cdot\cdot}I^-) - EA(I)$ corresponds to a transition to a state of $I_3$ that lies below the $I + I_2$ asymptote. From the $I_3^-$ dissociation energy of 1.31±0.06 eV measured by Do *et al.*[20] and the electron affinity of atomic iodine, 3.059038 eV,[29] we find $eKE_{min} = 0.288 \pm 0.06$ eV. This energy is indicated with an arrow in the top panel of Figure 1. Feature X lies entirely above this value, so the ground state of $I_3$ is thermodynamically stable.

The vibrational structure in feature X of the $I_3^-$ spectrum is somewhat irregular, and it is not obvious where the origin lies. Contributions from vibrational hot bands are considerably reduced in the $Ar{\cdot}I_3^-$ spectrum, so the intensity should fall off more rapidly to the high eKE side of the origin in the $Ar{\cdot}I_3^-$ spectrum than in the $I_3^-$ spectrum. Based on this expectation and the fairly clear correspondence between several vibrational features in the two spectra, the vibrational origins are assigned as shown in Fig. 1.

Feature X in the $Ar{\cdot}I_3^-$ spectrum shows a vibrational progression of 115 $cm^{-1}$. No experimental or theoretical frequencies of $I_3$ are available for the purpose of assigning this progression. A recent calculation of the $I_3^-$ vibrational frequencies at the CCSD(T) level of theory[18] yields $\omega_1$=107.8 $cm^{-1}$, $\omega_2$=58.2 $cm^{-1}$, and $\omega_3$=129.3 $cm^{-1}$, suggesting that the active $I_3$ mode is a stretching mode rather than the bending mode. This indicates that the neutral is linear, since the anion is linear. If $I_3$ were linear but highly asymmetric,

such as the $Cl \cdot Cl_2$ van der Waals complex predicted to be the ground state for $Cl_3$,[7] then one would expect an extended progression in the $I_2$ stretch with a frequency comparable to that of diatomic $I_2$, 214 $cm^{-1}$, which is clearly too high. On the other hand, if $I_3$ were linear and centrosymmetric, the dominant progression would be in the symmetric stretching mode. This is the most reasonable interpretation of the observed 115 $cm^{-1}$ progression, although a small barrier at the centrosymmetric geometry cannot entirely be ruled out.

Figure 2 shows a Franck-Condon simulation of the $Ar \cdot I_3^-$ spectrum superimposed on the experimental data. Only the symmetric stretch was considered; the gas phase value of 112 $cm^{-1}$ for $I_3^-$ was used here.[21] The simulation yields a neutral frequency of $115 \pm 5$ $cm^{-1}$, a vibrational temperature of 95K, and an electron affinity of $4.239 \pm 0.010$ eV for $Ar \cdot I_3$.

The best simulation of the $I_3^-$ spectrum (using a single vibrational mode) was obtained by shifting the origin by $+13 \pm 3$ meV and increasing the vibrational temperature to 205K. However, agreement with experiment was not nearly as good as in the $Ar \cdot I_3^-$ spectrum, presumably because of increased contributions from sequence bands involving excited bending and antisymmetric stretching modes in the anion. Nonetheless, on the basis of the origin shift we find the electron affinity of $I_3$ to be 4.226 $\pm$ 0.013 eV. The electron affinity has been experimentally estimated by Do *et al.*[20] to be $4.15 \pm 0.12$ eV and theoretically estimated to be 3.6 eV at the $X_\alpha$ DVM level by Gutsev.[15] With our measurement of the electron affinity the dissociation energy $D_o$ for $I_3 \rightarrow I_2 + I$ is $0.143 \pm 0.06$ eV. This value can be compared with the experimental estimates of 0.23 and 0.24 eV by Blake *et al.*[5] and Bunker *et al.*,[3] respectively.

The increase in electron affinity of $I_3$ upon addition of an Ar atom, 13 meV, is considerably less than the increases for I and $I_2$, which are 26.7 and 24 meV, respectively.[27,28] These shifts are related to the difference in the neutral and anion solvation energies via

$$EA(Ar \cdot I_p) - EA(I_p) = SE(Ar \cdot I_p^-) - SE(Ar \cdot I_p), p = 1-3 \qquad (2)$$

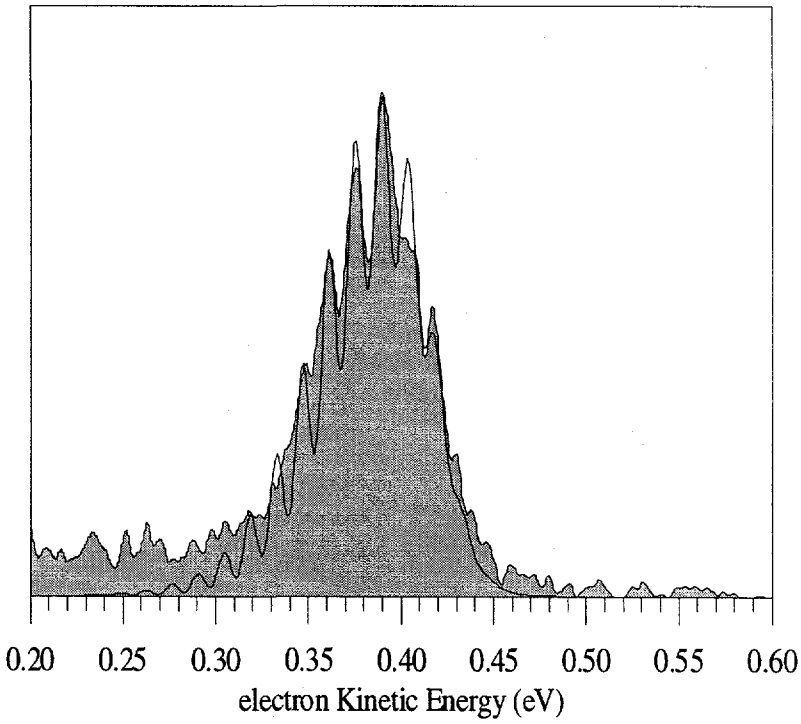


Fig 2. Simulation of $Ar \cdot I_3^-$ the photoelectron spectrum (solid line) superimposed on the experimental data (gray filled area).

where $SE(Ar \cdot I_p^-)$ and $SE(Ar \cdot I_p)$ are defined as the Ar binding energies in the anion and neutral complexes, respectively, and $p$ indicates the number of iodine atoms. The anomalously small shift for $Ar \cdot I_3$ suggests that the anion solvation energy is considerably lower than for the smaller species. In $Ar \cdot I^-$ and $Ar \cdot I_2^-$, the Ar atom is adjacent to all I atoms in the anion ($Ar \cdot I_2^-$ is T-shaped) and can interact strongly with all charge centers. However, the HOMO in $I_3^-$ is a non-bonding $\pi_u$ orbital with a node at the central I atom.[30] Thus, regardless of whether the Ar atom is bonded to the central I atom or one of the end atoms, its overall interaction with the excess charge on the $I_3^-$ should be weaker than in $Ar \cdot I^-$ or $Ar \cdot I_2^-$, consistent with the experimental results.

In this Communication we have shown that the ground state of $I_3$ is stable and have characterized its vibrational spectroscopy, dissociation energy, and electron affinity via photoelectron spectroscopy of $I_3^-$. Furthermore, we have shown that the addition of an argon atom significantly cools the $I_3^-$ chromophore, resulting in better-resolved vibrational structure in the photoelectron spectrum. This may prove invaluable in investigating the photoelectron spectroscopy of other anions in which progressions in low-frequency vibrations occur.

## Acknowledgements

This research is supported by the Air Force Office of Scientific Research under Grant No. F49620-97-1-0018.

## References


1 R. M. Noyes and J. Zimmerman, J. Chem. Phys. **18,** 656 (1950).

2 M. I. Christie, A. J. Harrison, R. G. W. Norrish, and P. G., Proc. Roy. Soc. (London) **A231,** 446 (1955).

3 D. L. Bunker and N. Davidson, J. Am. Chem. Soc. **80,** 5090 (1958).

4 G. Porter, Disc. Faraday Soc. **33,** 198 (1962).

5 J. A. Blake and G. Burns, J. Chem. Phys. **54,** 1480 (1971).

6 V. I. Balykin, V. S. Letokhov, V. I. Mishin, and V. A. Semchishen, Chem. Phys. **17,** 111 (1976).

7 A. L. Kaledin, M. C. Heaven, W. G. Lawrence, Q. Cui, J. E. Stevens, and K. Morokuma, J. Chem. Phys. **108,** 2771 (1998).

8 M. W. Sigrist, D. J. Krajnovich, F. Huisken, Z. J. Zhang, Y. T. Lee, and Y. R. Shen, Helvitica Physica Acta **53,** 289 (1980).

9 A. D. Walsh, J. Chem. Soc. , 2266 (1953).

10 Y. T. Lee, P. R. LeBreton, J. D. McDonald, and D. R. Herschbach, J. Chem. Phys. **51,** 455 (1969).

11 P. W. Tasker, Mol. Phys. **33,** 511 (1977).

12 T. Okada and J. Hata, Mol. Phys. **43,** 1151 (1981).

13 P. Pyykko and L. L. Lohr, Inorg. Chem. **20,** 1950 (1981).

14 J. J. Novoa, F. Mota, and S. Alvarez, J. Phys. Chem. **92,** 6561 (1988).

15 G. L. Gutsev, Russian J. Struct. Chem. **30,** 733 (1989).

16 Z. Y. Lin and M. B. Hall, Polyhedron **12,** 1499 (1993).

17 D. Danovich, J. Hrusak, and S. Shaik, Chem. Phys. Lett. **233,** 249 (1995).

18 S. B. Sharp and G. I. Gellene, J. Phys. Chem. A **101,** 2192 (1997).

19 Y. Ogawa, O. Takahashi, and O. Kikuchi, J. Mol. Struct. (Theochem) **424,** 285 (1998).

20 K. Do, T. P. Klein, C. A. Pommerening, and L. S. Sunderlin, J. Am. Soc. Mass Spectrom. **8,** 688 (1997).

21 M. T. Zanni, B. J. Greenblatt, A. V. Davis, and D. M. Neumark, Laser Techniques for State-Selective and State-to-State Chemistry IV, Proc. SPIE **3271,** 196 (1998).

22 C. Xu, G. R. Burton, T. R. Taylor, and D. M. Neumark, J. Chem. Phys. **107,** 3428 (1997).

23 R. B. Metz, A. Weaver, S. E. Bradforth, T. N. Kitsopoulos, and D. M. Neumark, J. Phys. Chem. **94,** 1377 (1990).

24 B. A. Mamyrin and D. V. Shmikk, Sov. Phys. JETP **49,** 762 (1979).

25 G. Markovich, R. Giniger, M. Levin, and O. Cheshnovsky, J. Chem. Phys. **95,** 9416 (1991).

26 J. Cooper and R. N. Zare, J. Chem. Phys. **48,** 942 (1968).

27 K. R. Asmis, T. R. Taylor, C. Xu, and D. M. Neumark, J. Chem. Phys. **109,** 4389 (1998).

28 Y. X. Zhao, I. Yourshaw, G. Reiser, C. C. Arnold, and D. M. Neumark, J. Chem. Phys. **101,** 6538 (1994).

29 D. Hanstorp and M. Gustafsson, J. Phys. B: At. Mol. Opt. Phys. **25,** 1773 (1992).

30 H. Isci and W. R. Mason, Inorg. Chem. **24,** 271 (1985).

# Chapter 5. Evolution of Electronic Structure as a Function of Size in Gallium Phosphide Semiconductor Clusters


## Abstract

Anion photoelectron spectra have been taken of $Ga_xP_y^-$ clusters at a photodetachment wavelength of 266 nm (4.657 eV). Clusters of varying stoichiometry with up to 18 atoms have been investigated. We obtain electron affinities and vertical detachment energies to the ground and low-lying excited states of the neutral clusters. Photoelectron spectra of clusters with 3-5 atoms are compared to previously reported *ab initio* calculations. Trends in the electron affinities and excitation energies for the larger clusters are discussed.


## I. Introduction

Understanding the spectroscopic and thermodynamic properties of semiconducting particles as a function of size has become increasingly important in the search for technological advances in the fabrication of smaller and faster electronic devices. This has motivated the study of semiconductors in several size regimes. Semiconductor nanocrystals, particles typically in the size range of $10^3$ or more atoms, have been the focus of much research in recent years.[1-6] The spectroscopy of these species, particularly quantum confinement effects, can generally be understood in terms of perturbations to the macroscopic material related to their finite size. Molecular clusters in the range of 10-100 atoms present additional challenges, as they are generally too small to be considered as perturbed macroscopic material but too large to treat with

the standard spectroscopic and theoretical methods that work so well for small molecules. It is therefore of considerable interest to determine how the structure and spectroscopy of molecular clusters evolve with size. In this paper we address this issue for gallium phosphide clusters by photoelectron spectroscopy of size-selected cluster anions of various stoichiometries with up to 18 atoms.

Photoelectron spectroscopy of anions has been an important tool for studying size-dependent properties of clusters, as it combines mass-selectivity with moderate spectral resolution. The photoelectron spectra of homonuclear semiconductor clusters such as $Si_n^-$ [7-11] and $Ge_n^-$ [8,12] are well-characterized. Heteronuclear clusters present additional complexity since both size and stoichiometry can be varied. The first systematic study of heteronuclear semiconductor clusters was performed on $Ga_xAs_y^-$ clusters by Smalley and co-workers.[13,14] Wang[15] and Kaya[11] have measured photoelectron spectra of $Si_xO_y^-$ and $Si_xC_y^-$ clusters, respectively.

We have previously reported photoelectron and zero electron kinetic energy (ZEKE) spectra of small $In_xP_y^-$ clusters ($x,y \leq 4$).[16,17] This work and the photodissociation studies by Mandich and co-workers[18] on neutral InP clusters have shown that the spacing between the ground and first excited electronic states in the neutral clusters was close to the bulk InP band gap of 1.344 (300 K). InP is a direct gap semiconductor, while GaP has an indirect band gap of 2.272 eV (300 K). If these significant differences in the bulk electronic structure are reflected in the molecular cluster size regime, one would expect rather different photoelectron spectra for small GaP and InP clusters; this was a major motivation for the work presented here. More generally, we wish to compare our results

to previous experimental and theoretical investigations in the hope of understanding the electronic structure of these clusters and how they extrapolate to the bulk properties.

Only four experimental studies of gallium phosphide clusters in any size range have been published. Nozik[19] and coworkers have taken the optical absorption spectra of passivated nanocrystals in the 20-30 Å size regime. Stucky and coworkers[20] measured spectra of GaP clusters in a similar size range produced in the cavities of zeolite Y. Both observed quantum confinement effects, but found that the optical spectra anomalously extended to the red of the indirect gap in bulk GaP. In the small molecule regime, Weltner and coworkers[21] have recorded the IR absorption spectrum of GaP, $Ga_2P$, and $GaP_2$ trapped in a 4 K argon matrix. From these spectra they were able to obtain isotope specific vibrational fundamentals for these species. Huang *et al.*[22] have measured mass spectra of GaP cluster anions produced by laser ablation and observed a tendency for the clusters to have more gallium than phosphorous atoms.

Theoretical investigations of GaP clusters have been carried out by Andreoni,[23] Ramakrishna,[24,25] and Balasubramanian.[26-29] Andreoni used the Car-Parrinello molecular dynamics method to study the structures, stability, and melting of small stoichiometric GaAs, GaP, and AlAs clusters. Ramakrishna has used an empirical pseudopotential method to investigate the electronic states of GaP nanocrystals ranging from 5-100 Å in radius. These calculations predict the nanocrystals to change from an indirect to a direct band gap semiconductor for clusters smaller than about 20 Å, a prediction which has yet to be confirmed experimentally. Balasubramanian and Feng have performed *ab initio* calculations on a series of $Ga_xP_y$ clusters with five or fewer atoms.[26-29] They calculated ground and excited state geometries and energies at the complete active space self-

consistent field (CASSCF) and multi-reference singles-doubles configuration interaction (MRSDCI) levels of theory.

The spectra reported here represent the first study of the electronic structure of gallium phosphide in the molecular cluster size regime. We obtain electron affinities and vertical detachment energies to the ground and low-lying electronic states of the neutral clusters. In general, the photoelectron spectra of $Ga_xP_y^-$ clusters are quite similar to those of $In_xP_y^-$ clusters.[17,30] Photoelectron spectra of the smallest clusters can be directly compared to the *ab initio* calculations of Balasubramanian in order to assign the observed electronic transitions. Trends in the larger clusters are also discussed; the most notable of these is that the electron affinities of stoichiometric (x=y) clusters with ten or more atoms appear to extrapolate smoothly to the bulk value.

## II. Experimental

The anion photoelectron spectrometer used in this study has been described in detail previously.[31,32] Cluster anions were generated in a laser ablation/pulsed molecular beam source. A rotating and translating single crystal disc of GaP (Crystallode Inc.) was ablated with second harmonic (532 nm) of a pulsed Nd:YAG laser. The laser pulses were typically 5.0-7.5 mJ/pulse before focussing on the target with a 1 m lens. Any ablated material is caught up in a supersonic beam of argon expanded through a pulsed piezoelectric valve at a backing pressure of 20 psig. The negative ions pass through a skimmer into a differentially pumped region. They are extracted perpendicular to their flow direction by a pulsed electric field and injected into a linear reflectron time-of-flight (TOF) mass spectrometer,[33,34] affording a mass resolution $m/\Delta m$ of 2000. The ions of

interest are selectively photodetached with the fourth harmonic of a pulsed Nd:YAG laser(266 nm, hν=4.657 eV). The electron kinetic energy (eKE) distribution is determined by TOF analysis in a field-free flight tube. For these experiments an electron flight tube length of 30 cm was used in order to increase the signal collection over our previous 100 cm long flight tube. The energy resolution is 30 meV at 0.65 eKE and degrades as $(eKE)^{3/2}$ at higher eKE. The laser polarization can be rotated by means of a half-wave plate. Secondary electrons initiated by scattered photons necessitate the collection and subtraction of background spectra in the spectra taken at high laser power.

## III. Results

Figure 1 shows the mass spectrum of $Ga_xP_y^-$ cluster anions produced by the laser ablation source; it represents a composite of three different mass spectra, each taken under different source conditions to optimize a particular mass range. The spectrum is composed of bunches of peaks separated in mass by a gallium atom. Each bunch of peaks is composed of 2-3 different cluster stoichiometries, as shown in the inset. Each cluster stoichiometry is represented by several peaks due to the natural isotope abundance of gallium ($Ga^{69}$:$Ga^{71}$, 100.0:66.4) which increases the complexity of the spectrum as the number of gallium atoms increases. The stoichiometries and intensities of the clusters are very sensitive to the laser power and the angle at which the laser beam impinges the disc. Although the ion intensities are very dependent on the source conditions, all of the mass spectra show that the most intense peaks are always of the stoichiometry, $Ga_xP_{1-4}$. In general higher laser ablation pulse energies produce more gallium rich clusters.

The masses that were photodetached are marked with an asterisk. The mass value and the stoichiometry of each cluster can be found in Table I. The most intense peak in the isotope distribution was always detached for any given cluster stoichiometry. The stoichiometric (x=y) clusters $Ga_1P_1$, $Ga_8P_8$, $Ga_9P_7$, and $Ga_9P_9$ are not marked in the figure due to their very low intensity.

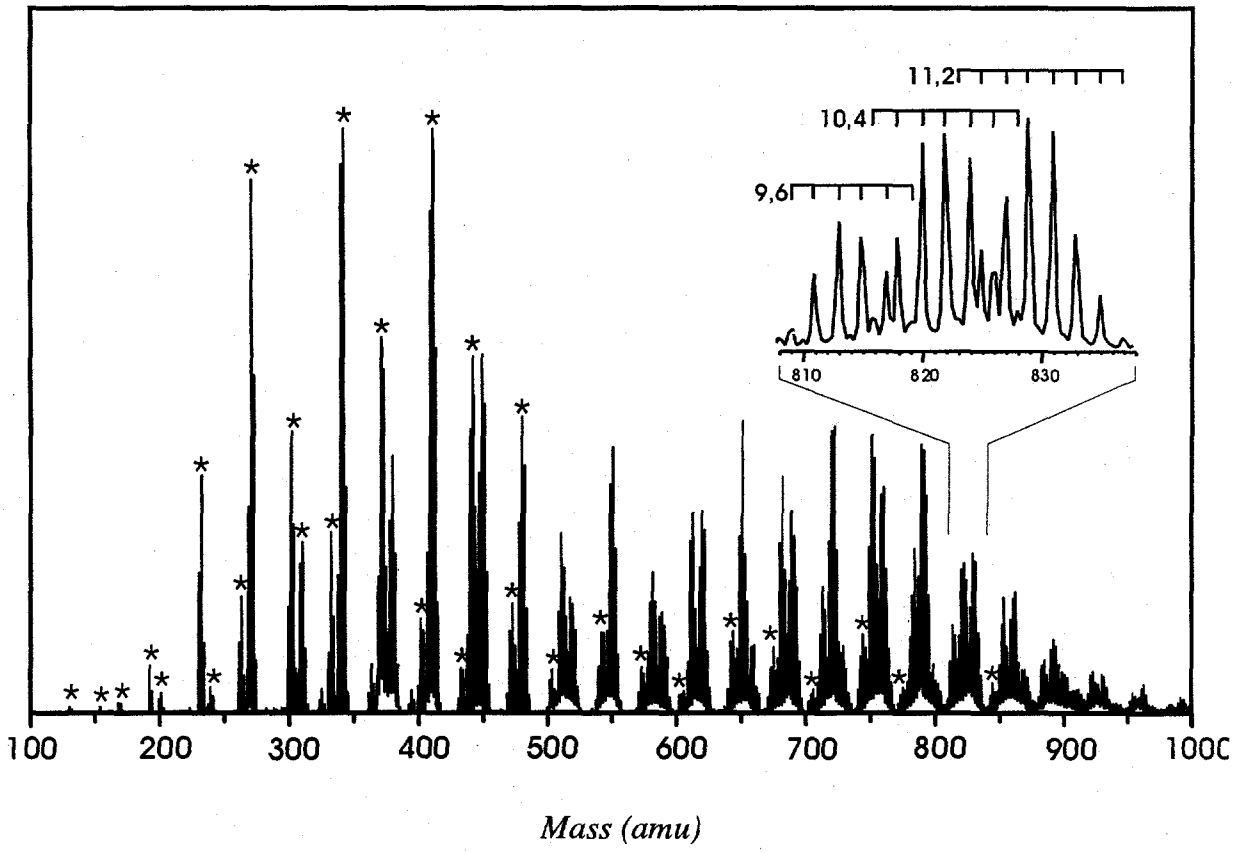


Figure 1. Mass spectrum of $Ga_xP_y^-$ clusters. This is a composite of three spectra obtained under different source conditions. Asterisks (*) mark the peaks that were photodetached. The inset shows the individual mass peaks comprising the bunch around 820 amu.

Figures 2 and 3 show 35 photoelectron spectra of $Ga_xP_y^-$ taken at a photon energy of 4.657 eV. In these spectra the electron kinetic energy, eKE, is related to the internal energy of the neutral and anion by the following equation, $eKE = h\nu - EA - E^o + E^-$. Here, $h\nu$ is the photon energy, $EA$ is the adiabatic electron affinity, $E^o$ is the internal energy of the neutral, and $E^-$ is the internal energy of the anion. The spectra show peaks corresponding to different electronic states of the neutral cluster, with the lowest-lying state occurring at the highest eKE. The only state for which vibrational structure is resolved is at lowest eKE in the $GaP_2^-$ spectrum. All of the spectra shown in Figure 2 were taken at a laser polarization of $\theta$=55°, the "magic angle," with respect to the electron detector; we obtained spectra at other laser polarization angles for selected clusters but observed little or no effect on the peak intensities.

Photoelectron spectra of the stoichiometric clusters $Ga_1P_1$-$Ga_9P_9$, $Ga_9P_7$, and $Ga_9P_8$ were taken at a laser fluence of 2.5 mJ/cm$^2$·pulse. Spectra of the other clusters were taken at a fluence ten times higher, and many of these show a common feature marked with an asterisk. The absence of this feature at lower laser fluence suggests that it results from a two-photon process involving photodissociation and subsequent photodetachment of a common daughter ion, and we do not consider it further in the assignments discussed below.

The spectra directly yield vertical detachment energies (VDEs) for each neutral electronic state, using $VDE = h\nu - eKE(\max)$, where $eKE(\max)$ is the electron kinetic energy at the band maximum for the state in question. Where possible, these maxima are marked by dots in Fig. 1, and the corresponding VDEs are given in Table I. For each

cluster, the peaks are labeled X, A, B, C, etc. in order of increasing VDE. The adiabatic electron affinity (EA), i.e. the energy needed to form the ground electronic and vibrational state of the neutral from the anion ground state, is also of interest. Determination of the EA is complicated by absence of vibrational structure. The arrows in each spectrum indicate our best estimate of the ground state origins; these are generally taken to lie at the point of inflection at highest eKE. The resulting EAs are tabulated in Table I.

## IV. Analysis and Discussion

### A. Smaller Clusters

Assignment of electronic features in the gallium phosphide photoelectron spectra for clusters with 3-5 atoms is possible through comparison with the calculations of Balasubramanian and co-workers at the CASSCF and MRSDCI levels of theory. For $GaP_2$ Balasubramanian finds a $^2B_2$ ground state with $C_{2v}$ symmetry and a $\angle$P-Ga-P bond angle of 43.9°, indicating strong P-P bonding. The low-lying $^2A_1$ and $^2B_1$ excited states, also with $C_{2v}$ symmetry, are predicted to have term energies of 1.07 eV and 2.33 eV, respectively, and considerably larger bond angles of 56.0° and 55.8°, respectively. In the $GaP_2^-$ photoelectron spectrum, the difference in the VDEs for peaks X and A is 0.99 eV, and that for peaks X and B is 2.34 eV. Based on the agreement with theory, we assign peaks X, A, and B to transitions to the $^2B_2$, $^2A_1$, and $^2B_1$ states of $GaP_2$. Higher resolution studies of this and other small GaP clusters are currently in progress, and a discussion of the vibrational structure in peak B will be deferred until this work is complete.

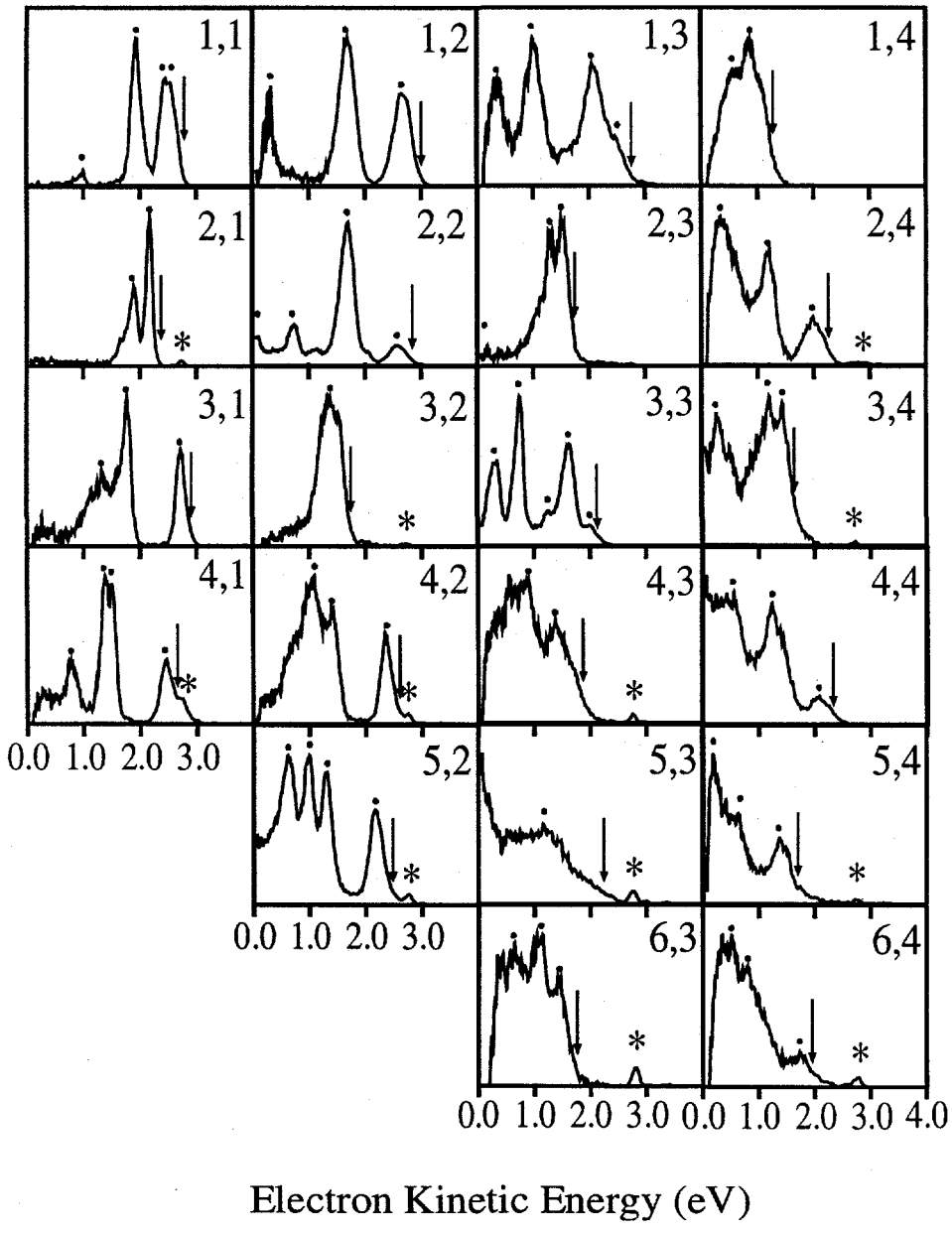


Figure 2. Photoelectron spectra of the smaller $Ga_xP_y^-$ clusters taken at 266 nm (4.657 eV). All spectra were taken at a laser polarization of $\theta$=54.7° with respect to the direction of electron collection.

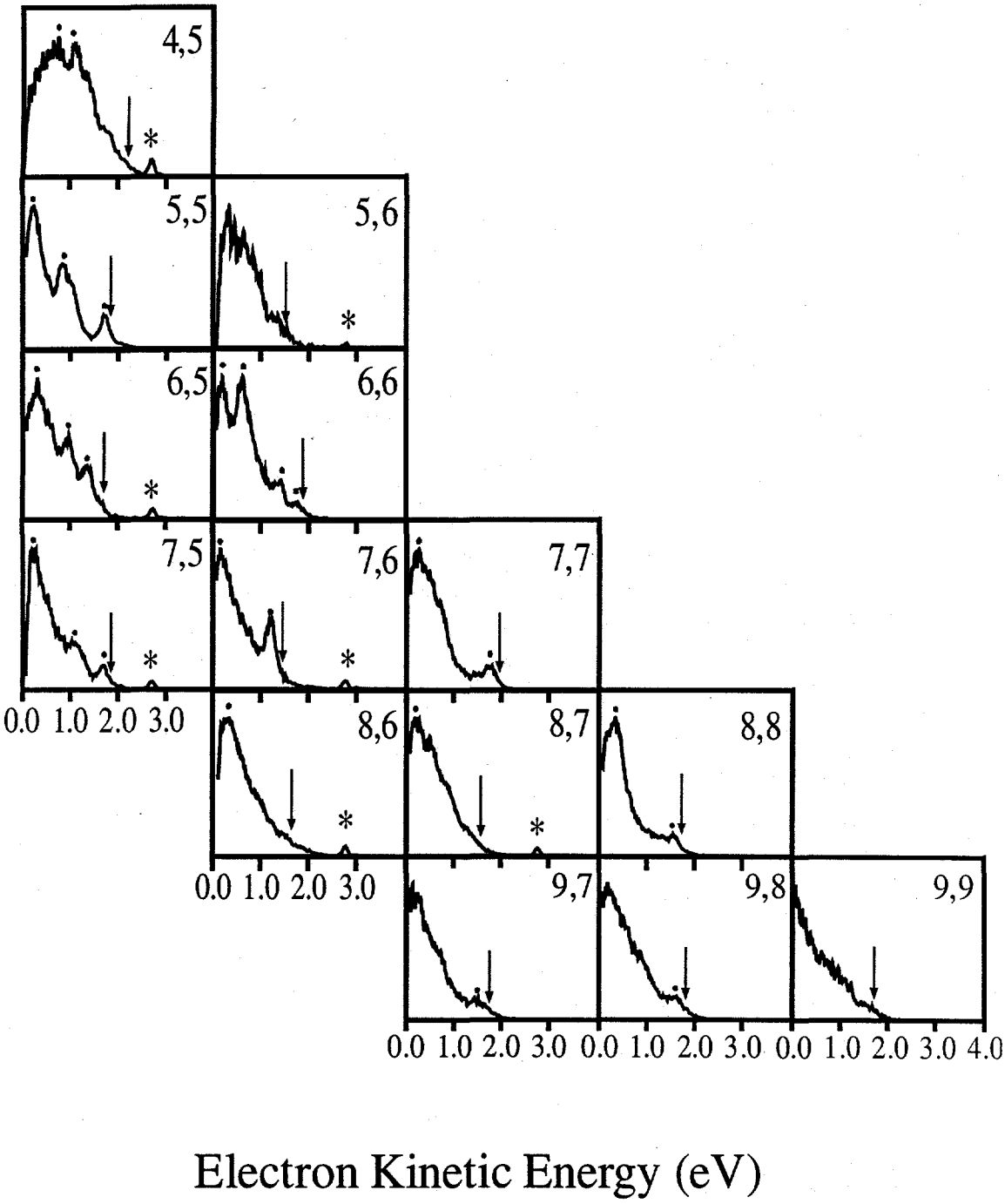


Figure 3. Photoelectron spectra of the larger $Ga_xP_y^-$ clusters taken at 266 nm (4.657 eV). All spectra were taken at a laser polarization of $\theta$=54.7° with respect to the direction of electron collection.

$Ga_2P$ is calculated to have a $^2B_1$ electronic ground state ($C_{2v}$) with a bond angle of 111°. In our photoelectron spectrum the transition to the ground state is narrow (100 meV FWHM) and intense indicating very similar geometries in the neutral and anion, in particular that the anion is also strongly bent. Peak A is also a relatively sharp feature indicating that $Ga_2P$ is bent in this electronic state as well. It is located 0.27 eV above the ground state as calculated by the difference in VDEs. In Balasubramanian's calculation the next excited state, the $^2B_2$ state, lies 0.09 eV above the ground state with a bond angle of 93°. Two additional linear states, the $^2\Pi_u$ and $^2\Sigma_u$ states, are calculated to lie 0.16 and 0.34 eV above the ground state. While any of these three excited states is a candidate for peak A based on energies alone, detachment to the two linear states would yield very extended progressions, rather than the sharp peak A seen in our spectrum. Therefore we assign peak A to the $^2B_2$ state.

The $Ga_2P_2^-$ photoelectron spectrum shows four distinct peaks, with peak A considerably more intense than the other three. Peaks X and A have similar widths, while peak B is narrower. Based on differences in the vertical detachment energies, peaks X and A are separated by 0.90 eV, while peaks X and B are separated by 1.85 eV. These results can be compared to *ab initio* calculations on $Ga_2P_2$, which is predicted to be a rhombus having $D_{2h}$ symmetry with a closed shell $^1A_g$ ground state. At the MRSDCI level of theory, the lowest lying excited states and their energies are $^3A_u$ (1.182 eV), $^1A_u$(1.376 eV), $^3B_{2g}$ (1.527 eV), and $^1B_{2g}$ (1.789 eV). The leading configuration of the $^1A_g$ ground state is $\ldots 1b_{2u}^2 1b_{1u}^2 2b_{1u}^2 1b_{3g}^2 1b_{3u}^2 1b_{1g}^0$, so assuming the anion is formed by addition of an electron to the $1b_{1g}$ orbital, all of these excited states are accessible via one-electron detachment. Our previous study of $Si_4^-$ showed that transitions to triplet and

singlet open shell states with the same molecular orbital configuration (the $^3A_u$ and $^1A_u$ states, for example) should have similar intensities. The assignment most consistent with the calculations is that peak A is an overlapping transition to the $^3A_u$ and $^1A_u$ states, and that peaks B and C are transitions to the $^3B_{2g}$ and $^1B_{2g}$ states, respectively. This assignment is somewhat problematic as it implies the $^3A_u$ /$^1A_u$ splitting is smaller than calculated, while the $^3B_{2g}$ /$^1B_{2g}$ splitting is considerably larger. Moreover, at the same level of theory, the calculated state ordering for $In_2P_2$ is quite different from $Ga_2P_2$, with the $^3B_{2g}$ and $^1B_{2g}$ states lying below the $^3A_u$ and $^1A_u$ states,[35] even though the anion photoelectron spectra are very similar.

The $Ga_3P^-$ photoelectron spectrum shows well-separated transitions to the ground and first excited states of $Ga_3P$; the difference in VDEs is 0.96 eV. The excited state peak appears to consist of overlapped transitions to at least two electronic states. This qualitatively agrees with the *ab initio* calculations which predict $Ga_3P$ to have a $^1A_1$ ground state and a cluster of three excited states, the $^3A_2$, $^3A_1$, and $^1E$ states starting at $T_e$= 2.14 eV. However, the calculated excitation energies are clearly much larger than in the experimental spectrum. Agreement with theory is better for $GaP_3$. The peak in the $GaP_3^-$ spectrum at highest electron energy shows transitions to two overlapping states with VDE differences of 0.38 eV; the next peak lies 1.46 eV above the ground state. Balasubramanian predicts $GaP_3$ to have a $^3A_2$ ground state with $^1E$ and $^3E$ excited states lying 0.36 and 1.07 eV, respectively, above the $^3A_2$ state, with all states having $C_{3v}$ symmetry. The overall agreement supports this calculated ordering of electronic states.

The photoelectron spectra of $Ga_2P_3^-$ and $Ga_3P_2^-$ show that the neutral clusters have essentially the same electron affinity, 3.03 eV. The ground and first excited states of

$Ga_2P_3$ are separated by only 0.21 eV. While only a single large peak is seen in the $Ga_3P_2^-$ spectrum, its irregular shape suggests it represents transitions to at least two overlapped electronic transitions. The experimental spectra are consistent with calculations that predict that the ground and first excited states are nearly degenerate for both neutral clusters. For $Ga_2P_3$, the trigonal bipyramidal ($D_{3h}$) $^2A_2$" state is calculated to lie only 0.05 eV above the distorted trigonal bipyramidal $^2B_1$ state, resulting from Jahn-Teller distortion of a $^2E$" state. In $Ga_3P_2$, the two lowest lying states are the distorted trigonal bipyramidal $^2A_1$ state and the edge-capped tetrahedral $^2B_1$ states, with the $^2A_1$ state lying 0.08 eV below the $^2B_1$ state; these states result from Jahn-Teller distortion of the $D_{3h}$ trigonal bipyramidal $^2E$' and $^2E$" states, respectively.

## B. Larger Clusters

Figure 4 shows a plot of electron affinity *vs.* the number of atoms for clusters with various stoichiometries. The electron affinities are plotted as a function of $N^{-1/3}$, where N is the total number of atoms. Clusters with an even number of atoms are shown with solid shapes and odd clusters are represented by open shapes. In general, for a particular stoichiometry $Ga_xP_{x+y}$, the electron affinity increases with *x*. Moreover, for clusters with approximately the same number of atoms, odd clusters have higher electron affinities than even clusters, consistent with our previous work on InP and GaAs clusters.[17] This trend arises because the odd neutral clusters are open-shell species with an odd number of electrons, so that addition of an electron fills an orbital, resulting in a high detachment

energy. In contrast, the even neutral clusters are expected to be closed shell species with lower electron affinities.

The overall trend of electron affinity with cluster size is of interest. Photoelectron spectroscopy of metal, semiconductor, and weakly bound clusters have generally shown that above a certain size, the electron affinity smoothly increases and extrapolates to the bulk value. We can estimate the electron affinity of bulk GaP according to the relationship $EA_{bulk} = E_i - E_g$, where $E_i(=6.01\pm0.030\ eV)$ is the bulk ionization energy and $E_g$=2.272 is the (indirect) band gap at 300 K, yielding $EA_{bulk}$=3.74 eV. A linear fit to the average electron affinity of the five largest stoichiometric clusters appears to extrapolate to the bulk value. This agrees well with our most recent study of $In_xP_y^-$ clusters in a similar size range,[30] although the trend is clearer for indium phosphide clusters. Planned experiments on larger GaP clusters should clarify this trend in the electron affinities. Another important trend is the presence or absence of a "gap" between the transition to the ground state and the first excited state of the neutral cluster. Such a gap is generally present in the even clusters and absent in the odd clusters, particularly for similar stoichiometries. The largest clusters exhibiting this pattern are$Ga_7P_7$, $Ga_8P_7$, and $Ga_9P_7$. The origin of this trend, which was also seen in InP clusters, is related to the even-odd alternation of electron affinities. Addition of an electron to an even, closed-shell cluster results in a single electron in what was formerly the LUMO of the neutral cluster, and the gap in the resulting anion photoelectron spectrum represents the HOMO-LUMO spacing in the neutral cluster. Odd clusters generally do not show this pattern as the additional electron generally fills a singly occupied orbital in the neutral cluster.

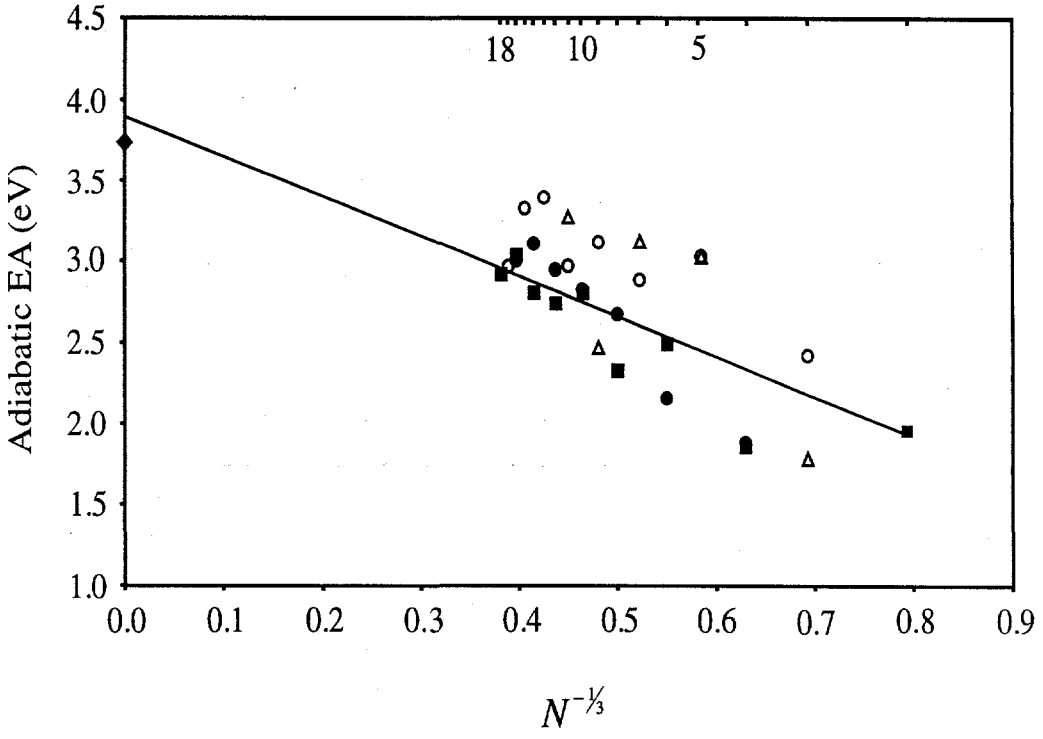


Figure 4. Plot of the adiabatic electron affinities versus $N^{-1/3}$, where N is the number of atoms in the cluster. The different stoichiometries are represented by the following symbols: ■ $Ga_xP_x$, ● $Ga_{x+2}P_x$, ○ $Ga_{x+1}P_x$, Δ $Ga_xP_{x+1}$, and ◆ bulk electron affinity.

**Table I.** Estimated adiabatic electron affinities and vertical detachment energies for $Ga_xP_y^-$.

| Cluster Ga,P | Mass | Adiabatic EA | Vertical Detachment Energy (VDE) | | | | |
|---|---|---|---|---|---|---|---|
| | | | X | A | B | C | D |
| 1,1‡ | 100 | 1.96 | 2.11 | 2.20 | 2.72 | 3.66 | |
| 1,2‡ | 131 | 1.78 | 1.98 | 2.97 | 4.32 | | |
| 1,3‡ | 162 | 1.95 | 2.19 | 2.57 | 3.65 | 4.30 | |
| 1,4‡ | 193 | 3.48 | 3.80 | 4.03 | | | |
| 2,1‡ | 171 | 2.42 | 2.50 | 2.77 | | | |
| 2,2‡ | 202 | 1.86 | 2.08 | 2.98 | 3.93 | 4.66 | |
| 2,3‡ | 233 | 3.03 | 3.14 | 3.35 | 4.66 | | |
| 2,4‡ | 264 | 2.40 | 2.67 | 3.48 | 4.27 | | |
| 3,1‡ | 240 | 1.88 | 1.93 | 2.89 | 3.34 | | |
| 3,2‡ | 271 | 3.03 | 3.27 | | | | |
| 3,3‡ | 302 | 2.50 | 2.67 | 3.04 | 3.39 | 3.91 | 4.35 |
| 3,4‡ | 333 | 3.12 | 3.23 | 3.46 | 4.40 | | |
| 4,1‡ | 309 | 2.09 | 2.20 | 3.16 | 3.29 | 3.87 | |
| 4,2‡ | 340 | 2.16 | 2.29 | 3.27 | 3.58 | | |
| 4,3‡ | 371 | 2.88 | 3.28 | 3.75 | | | |
| 4,4 | 402 | 2.33 | 2.59 | 3.42 | 4.10 | | |
| 4,5 | 433 | 2.47 | 3.52 | 3.86 | | | |
| 5,2‡ | 411 | 2.37 | 2.48 | 3.37 | 3.68 | 4.04 | |
| 5,3 | 442 | 2.67 | 3.42 | | | | |
| 5,4 | 473 | 3.11 | 3.28 | 4.03 | 4.48 | | |
| 5,5‡ | 504 | 2.81 | 2.93 | 3.80 | 4.42 | | |
| 5,6 | 535 | 3.27 | | | | | |
| 6,3‡ | 511 | 3.05 | 3.22 | 3.53 | 4.03 | | |
| 6,4 | 542 | 2.83 | 2.93 | 3.86 | 4.14 | | |
| 6,5 | 573 | 2.97 | 3.32 | 3.72 | 4.35 | | |
| 6,6 | 604 | 2.74 | 2.93 | 3.27 | 4.03 | 4.46 | |
| 7,5‡ | 644 | 2.95 | 2.96 | 3.60 | 4.39 | | |
| 7,6 | 675 | 3.39 | 3.48 | 4.50 | | | |
| 7,7 | 706 | 2.81 | 2.93 | 4.40 | | | |
| 8,6 | 744 | 3.11 | 4.38 | | | | |
| 8,7 | 775 | 3.33 | 4.46 | | | | |
| 8,8 | 806 | 3.04 | 3.13 | 4.32 | | | |
| 9,7 | 844 | 3.00 | 3.23 | | | | |
| 9,8 | 875 | 2.97 | 3.21 | | | | |
| 9,9 | 906 | 2.92 | | | | | |

‡ These EAs have and uncertainty of ±75 meV. All others are ±150 meV.

Two further comments regarding the HOMO-LUMO gap are warranted. Previous photoelectron spectra and photodissociation spectra of InP clusters showed that the HOMO-LUMO gap in these clusters was close to the bulk InP band gap of 1.4 eV. However, photoelectron spectra of GaP cluster anions in the same size range are very similar to those of InP clusters, while the band gap of bulk GaP is much larger than that of InP. This indicates that the similarity between the bulk band gap to the HOMO-LUMO gap in small InP clusters is coincidental rather than reflective of some signature of the bulk electronic structure in these very small clusters.

Finally, it appears that clusters with an excess of gallium atoms tend to deviate from the even-odd HOMO-LUMO pattern. Specifically, the photoelectron spectra of $Ga_3P^-$, $Ga_4P^-$, $Ga_4P_2^-$, and $Ga_5P_2^-$ are all similar, with the transition to the electronic ground state of the neutral well separated from transitions to a series of excited electronic states. It appears that the addition of a Ga atom to either $Ga_3P$ or $Ga_4P_2$ results in little change in the electronic structure of the neutral cluster. It would clearly be of interest to perform *ab initio* calculations on this series of clusters in order to better understand this observation.

## Acknowledgements

This research is supported by the National Science Foundation under Grant No. DMR-9521805. K. R. A. gratefully acknowledges a postdoctoral fellowship from the Swiss National Science Foundation.

## References

1 A. Henglein, Chem. Rev. **89,** 1861 (1989).

2 A. D. Yoffe, Adv. Phys. **42,** 173 (1993).

3 L. Brus, Appl. Phys. **53,** 465 (1991).

4 H. Weller, Angew. Chem. Int. Ed. Engl. **32,** 41 (1993).

5 Y. Wang and N. Herron, J. Phys. Chem. **95,** 525 (1991).

6 A. P. Alivisatos, J. Phys. Chem. **100,** 13226 (1996).

7 C. Xu, T. R. Taylor, G. R. Burton, and D. M. Neumark, J. Chem. Phys. **108,** 1395 (1998).

8 O. Cheshnovsky, S. H. Yang, C. L. Pettiette, M. J. Craycraft, Y. Liu, and R. E. Smalley, Chem. Phys. Lett. **138,** 119 (1987).

9 G. S. Ickingkonert, H. Handschuh, P. S. Bechthold, G. Gantefor, B. Kessler, and W. Eberhardt, Surf. Rev. Lett. **3,** 483 (1996).

10 H. Kawamata, Y. Negishi, R. Kishi, S. Iwata, A. Nakajima, and K. Kaya, J. Chem. Phys. **105,** 5369 (1996).

11 A. Nakajima, T. Taguwa, K. Nakao, M. Gomei, R. Kishi, S. Iwata, and K. Kaya, J. Chem. Phys. **103,** 2050 (1995).

12 G. R. Burton, C. Xu, C. C. Arnold, and D. M. Neumark, J. Chem. Phys. **104,** 2757 (1996).

13 Y. Liu, Q. L. Zhang, F. K. Tittel, R. F. Curl, and R. E. Smalley, J. Chem. Phys. **85,** 7434 (1986).

14 C. Jin, K. J. Taylor, J. Conceicao, and R. E. Smalley, Chem. Phys. Lett. **175,** 17 (1990).

15 L. S. Wang, H. B. Wu, S. R. Desai, J. W. Fan, and S. D. Colson, J. Phys. Chem. **100,** 8697 (1996).

16 C. C. Arnold and D. M. Neumark, Can. J. Phys. **72,** 1322 (1994).

17 C. Xu, E. Debeer, D. W. Arnold, C. C. Arnold, and D. M. Neumark, J. Chem. Phys. **101,** 5406 (1994).

18 D. D. Kolenbrander and M. L. Mandich, J. Chem. Phys. **92,** 4759 (1990).

19 O. I. Micic, J. R. Sprague, C. J. Curtis, K. M. Jones, J. L. Machol, A. J. Nozik, H. Giessen, B. Fluegel, G. Mohs, and N. Peyghambarian, J. Phys. Chem. **99,** 7754 (1995).

20 J. E. Mac Dougall, H. Eckert, G. D. Stucky, N. Herron, Y. Wang, K. Moller, T. Bein, and D. Cox, J. Am. Chem. Soc. **111,** 8006 (1989).

21 S. Li, R. J. Van Zee, and W. Weltner, J. Phys. Chem. **97,** 11393 (1993).

22 R. B. Huang, P. Zhang, W. Y. Li, and L. S. Zheng, J. Xiamen Univ. (Natural History) **31,** 160 (1992).

23 W. Andreoni, Phys. Rev. B **45,** 4203 (1992).

24 A. Tomasulo and M. V. Ramakrishna, J. Chem. Phys. **105,** 3612 (1996).

25 M. V. Ramakrishna and R. A. Friesner, J. Chem. Phys. **95,** 8309 (1991).

26 P. Y. Feng and K. Balasubramanian, Chem. Phys. Lett. **258,** 387 (1996).

27 P. Y. Feng and K. Balasubramanian, Chem. Phys. Lett. **265,** 41 (1997).

28 P. Y. Feng and K. Balasubramanian, Chem. Phys. Lett. **265,** 547 (1997).

29 P. Y. Feng and K. Balasubramanian, Chem. Phys. Lett. **288,** 1 (1998).

30 K. R. Asmis, T. R. Taylor, and D. M. Neumark, in preparation (1998).

31 R. B. Metz, A. Weaver, S. E. Bradforth, T. N. Kitsopoulos, and D. M. Neumark, J. Phys. Chem. **94,** 1377 (1990).

32 C. Xu, G. R. Burton, T. R. Taylor, and D. M. Neumark, J. Chem. Phys. **107,** 3428 (1997).

33 B. A. Mamyrin and D. V. Shmikk, Zhurnal Eksperimental'noi i Teoreticheskoi Fiziki **76,** 1500 (1979).

34 G. Markovich, R. Giniger, M. Levin, and O. Cheshnovsky, J. Chem. Phys. **95,** 9416 (1991).

35 P. Y. Feng and K. Balasubramanian, Chem. Phys. Lett. **264,** 449 (1997).

# Chapter 6. Vibrationally Resolved Anion Photoelectron Spectra of the Low Lying Electronic States of $GaP_2^-$, $Ga_2P^-$, and $Ga_2P_3^-$


## Abstract

Anion photoelectron spectra of $GaP_2^-$, $Ga_2P^-$, and $Ga_2P_3^-$ have been taken at photodetachment wavelengths of 266 nm (4.657 eV), 355 nm (3.493 eV), 416 nm (2.977 eV), and 498 nm (2.491 eV). Using this variety of wavelengths has allowed us to vibrationally resolve the low-lying electronic states of these species. We report electron affinities, term values, and vibrational frequencies of the corresponding neutral and anion states where possible. Results are in qualitative agreement with current *ab initio* studies.


## I. Introduction

Anion photoelectron spectroscopy combines size-selectivity with reasonable spectral resolution, making it an indispensable method for investigating the spectroscopy of semiconductor clusters. In an effort to understand how the electronic and vibrational structure of semiconductor clusters changes as a function of size, we have recently completed a study of the electronic structure of $Ga_xP_y$ clusters having 18 atoms or fewer[1]. Here, we carry these studies further by obtaining higher resolution, vibrationally resolved anion photoelectron spectra of $GaP_2^-$, $Ga_2P^-$, and $Ga_2P_3^-$ clusters.

The vibrational spectroscopy of III-V semiconductor clusters has been limited to a few studies. Li *et al.*[2] used Fourier-transform infrared spectroscopy record the vibrational spectra of the diatomic and triatomic isotopomers of GaP, GaAs, and GaSb in an inert gas matrix. Arnold *et al.*[3] characterized the spectroscopy of the $In_2P^-/In_2P$ and $InP_2^-/InP_2$

systems using zero electron kinetic energy (ZEKE) spectroscopy. Lemire *et al.*[4] have studied diatomic GaAs via resonant two-photon ionization spectroscopy. Their studies afforded spectroscopic constants for the $^3\Sigma^-$ ground state and the $3^3\Pi$ spin-orbit states.

Andreoni[5] and Balasubramanian[6-9] have carried out theoretical investigations of $Ga_xP_y$ clusters. Andreoni used the Car-Parrinello molecular dynamics method to study the structures, stability, and melting of small stoichiometric GaAs, GaP, and AlAs clusters. Balasubramanian and Feng[6-9] have performed *ab initio* calculations on a series of $Ga_xP_y$ clusters with five or fewer atoms. They calculated ground and excited state geometries and energies at the complete active space self-consistent field (CASSCF) and multi-reference singles-doubles configuration interaction (MRSDCI) levels of theory with a basis set composed of relativistic effective core potentials and valence Gaussian basis sets.

Here we present vibrationally resolved photoelectron spectra of the low-lying electronic states of selected $Ga_xP_y$ clusters. Our term values are compared with Balasubramanian's *ab initio* results. Identification of the vibrational structure is made by comparison with our previous study on the $In_2P^-/In_2P$ and $InP_2^-/InP_2$ systems.

## II. Experimental

The anion photoelectron spectrometer used in this study has been described in detail previously[10,11]. Cluster anions are generated in a laser ablation/pulsed molecular beam source. A rotating and translating single crystal disc of GaP (Crystallode Inc.) is ablated with the second harmonic (532 nm) of a pulsed Nd:YAG laser. The laser pulses are typically 5.0-7.5 mJ/pulse before focussing onto the target with a 1 m lens. The resulting plasma is entrained in a supersonic beam of argon, which then passes through a

skimmer into a differentially pumped region. Negative ions in the beam are extracted perpendicular to their flow direction by a pulsed electric field and injected into a linear reflectron time-of-flight (TOF) mass spectrometer[12,13], affording a mass resolution m/Δm of 2000. The ions of interest are selectively photodetached with photons having wavelengths of 266 nm (4.657 eV), 355 nm (3.493 eV), 416 nm (2.977 eV), and 498 nm (2.491 eV). The photon wavelengths, 266 and 355 nm, were obtained by frequency quadrupling and tripling the fundamental of a pulsed Nd:YAG laser. To generate light at 416 and 498 nm the third harmonic was passed through a Raman cell filled with hydrogen at high pressure (325 psig). The electron kinetic energy (eKE) distribution is determined by TOF analysis in a 1 m field-free flight tube. The energy resolution is 8-10 meV at 0.65 eV eKE and degrades as $(eKE)^{3/2}$ at higher eKE; this is about a factor of three better than in our previous study of $Ga_xP_y$ clusters, in which a shorter (30 cm) flight tube was used. The laser polarization angle can be rotated by means of a half-wave plate. Due to the natural isotope abundance of gallium ($Ga^{69}$:$Ga^{71}$, 100.0:66.4) each cluster stoichiometry has a mass distribution. In each case the most intense mass was photodetached.

## III. Results

Photoelectron spectra have been taken of $GaP_2^-$, $Ga_2P^-$, and $Ga_2P_3^-$. While several other $Ga_xP_y^-$ clusters were investigated, these were the only clusters showing vibrational resolution apart from $GaP^-$ which will be treated in a future publication. The spectra are shown in Figures 1-3, respectively. The photoelectron spectra are reported in electron binding energy, eBE, which is defined as $eBE = h\nu - eKE$. The polarization angle, $\theta$, is

the angle between the electric vector of the photon and the axis along which the electrons are detected. Peaks having different polarization dependences generally result from transitions to different neutral electronic states, hence this is a useful means of distinguishing contributions from overlapping electronic bands. Our spectral resolution is optimal for features at low electron kinetic energy according to the relationship in the experimental section. Varying the wavelength allows us to resolve spectral features as seen for feature X in the top two panels of Figure 1.

## IV. Analysis and Discussion

In a previous study[1] we obtained low-resolution (~30 meV) anion photoelectron spectra of $Ga_xP_y^-$ ($x,y \leq 9$) at 266 nm. As a result we were able to identify the electronic states of the smaller $Ga_xP_y$ clusters based on the calculations of Balasubramanian and coworkers[6-9]. In our previous study, we were only able to compare changes in vertical detachment energies with the term energies calculated by Balasubramanian. The electronic state assignments made in our previous paper[1] are assumed here. However, the new spectra are vibrationally resolved allowing us to estimate the adiabatic electronic affinities and term values. Table 1 compares the results of the present and the previous studies. The assignment of the vibrational structure depends heavily on the previous results of the ZEKE/PES spectra taken of the $InP_2^-/InP_2$ and $In_2P^-/In_2P$ systems[3].

### A. $GaP_2$

Figure 1 shows the photoelectron spectra of $GaP_2^-$ taken at 266, 355, and 498 nm and at a polarization angle of $\theta=90^\circ$. Spectra taken at other polarization angles show no

overlapping electronic transitions, so this polarization optimally represents these electronic states. The top panel shows the entire spectrum taken at 266 nm. Three electronic states are visible labeled X, A, and B. In accordance with our previous study[1] we assign features X, A, and B to the $^2B_2$, $^2A_1$, and $^2B_1$ states. At the appropriate wavelength each electronic state shows resolved vibrational structure. Feature A is similar in appearance to feature X having a FWHM of 319 and 291 meV, respectively, indicative of a large geometry change. Feature B shows the most clearly resolved structure.

The $^2B_2$ ground state is calculated[7] to have a $C_{2v}$ geometry with an acute $\angle$ P-Ga-P bond angle of 43.9°. A preliminary Franck-Condon analysis allows us to estimate the origin to occur at 1.726 eV, yielding an electron affinity of the same value. The vibrational structure reveals a progression with an average spacing of 240 $cm^{-1}$. In analogy to the ground state we are able to estimate the vibrational frequency and the origin of the first excited $^2A_1$ state to be 329 $cm^{-1}$ and 2.976 eV, respectively. This affords a term value of 1.250 eV. Balasubramanian[7] calculates this splitting to be 1.07 eV, a difference of ~250 meV. The ZEKE spectra of $InP_2^-$ taken by Arnold *et al.*[3] show progressions in the $\tilde{X}$ and $\tilde{A}$ states having frequencies of 190 and 287 $cm^{-1}$ and they were assigned to the $\nu_2$ bending modes of each state, respectively. We make the same assignment to the observed progressions in the $\tilde{X}$ and the $\tilde{A}$ states of $GaP_2$. This gives a bending frequency of 240 and 329 $cm^{-1}$ for these states, respectively. The assignment of

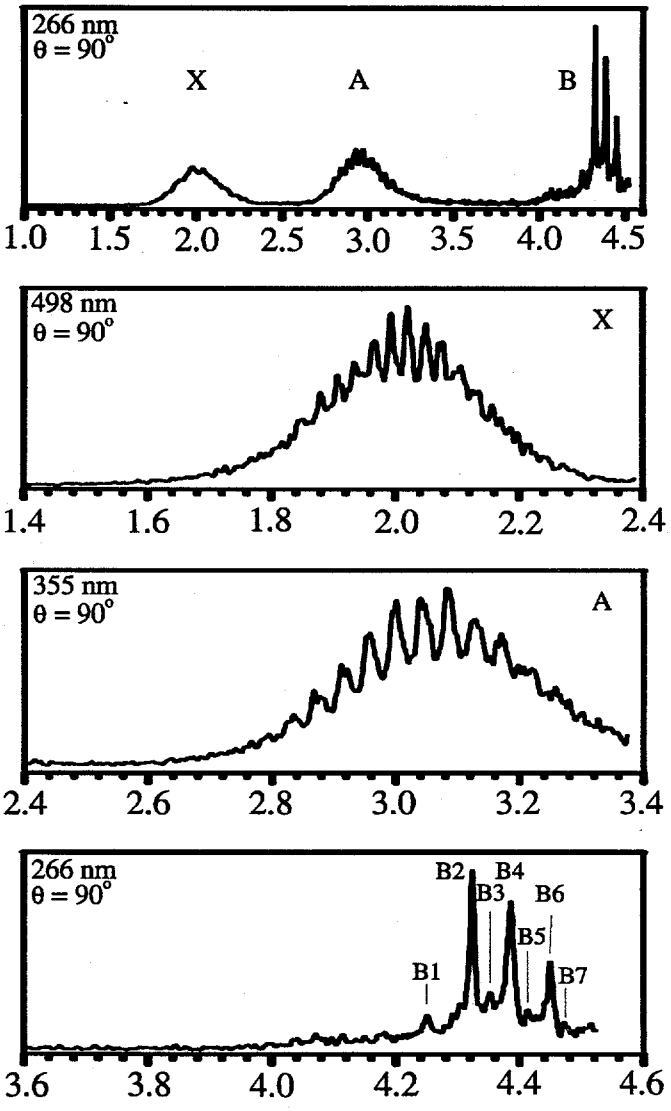


Fig. 1. Photoelectron spectra of $GaP_2^-$ taken at the photodetachment wavelengths of 266, 355, and 498 nm. Laser polarization angle is θ=90° with respect to the direction of electron collection.

the ground state frequency is also in accord with the frequency of 220.9 $cm^{-1}$ reported by Li *et al.*[2]

Feature B is much less congested than the two bands previously discussed, allowing us to see more detail. The most intense peak, B2, represents the origin of the $^2B_1$ state and is located at 4.324 eV, affording a term value of 2.598 eV. The calculated value[7], 2.33 eV, is also ~250 meV below the experimental value. The most intense progression incorporating peaks B2, B4, and B6 exhibits a comparatively large frequency of 500 $cm^{-1}$. This mode most likely corresponds to P-P motion and we assign it to $\nu_1$. Peak B1 is a hot band corresponding to the same mode in the ion with a frequency of 589 $cm^{-1}$. Combination bands with a frequency of 234 $cm^{-1}$ are indicated by peaks labeled B3, B5, and B7. This frequency is similar to the ground state $\nu_2$ mode, and we assign it to the $\nu_2$ bending mode. Electron affinities, term values, vibrational frequencies, and assignments for all species are given in Table 1.

## B. $Ga_2P$

Figure 2 shows the photoelectron spectra of $Ga_2P^-$ taken at the wavelengths of 355 and 416 nm and at the polarization angles of $\theta$ =0 and 90° for each wavelength. These spectra show two electronic states having very different polarization dependences. Feature X is an intense feature showing several barely resolved peaks in the 416 nm spectrum taken at $\theta$=90°. Both features X and A are strongly polarization dependent and are well separated. The transition to the first excited state results in an extended progression labeled A1-A6. We were previously[1] able to assign features X and A to the $^2B_1$ and $^2B_2$ states, respectively.

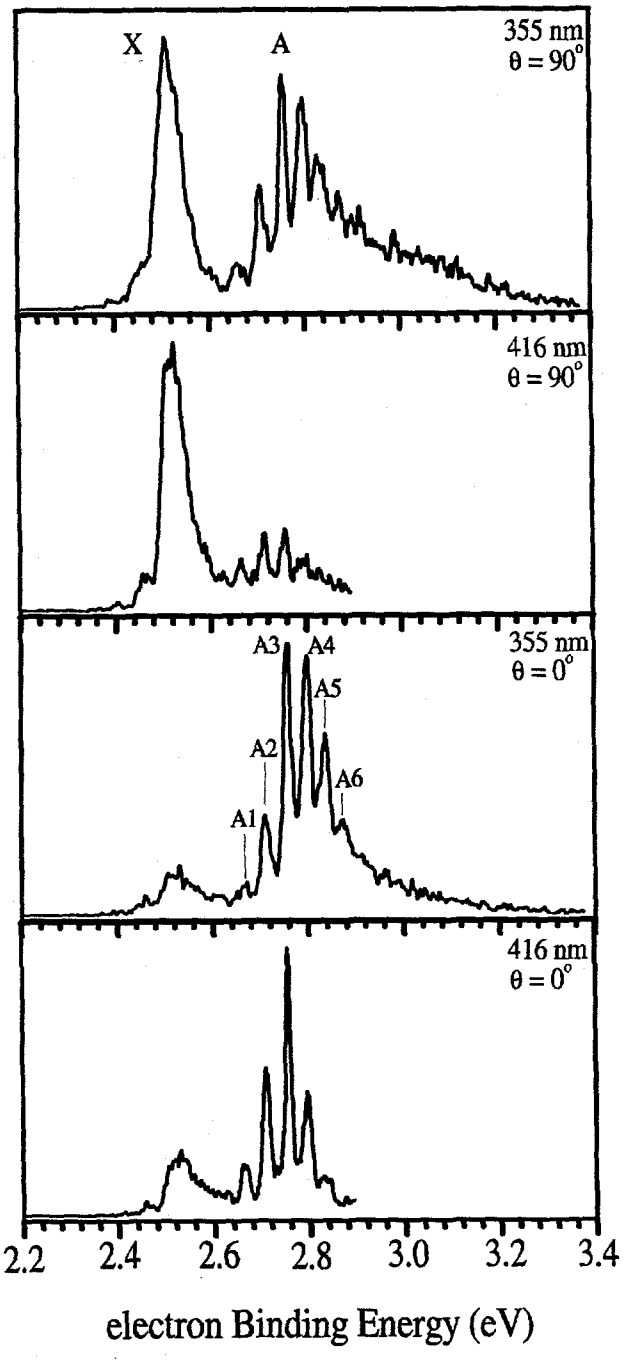


Fig. 2. Photoelectron spectra of $Ga_2P^-$ taken at the photodetachment wavelengths of 355 and 416 nm. Laser polarization angles are θ=0° and 90° with respect to the direction of electron collection.

The $^2B_1$ ground state is calculated[7] to have a $C_{2v}$ geometry with a ∠Ga-P-Ga bond angle of 111.0°. Li *et al.*[2] observe a vibrational transition of 280.5 $cm^{-1}$, assign it to the asymmetric stretch, $\nu_3$, and estimate the bond angle to be 85.7°. The higher resolution spectrum taken at 498 nm barely resolves vibrational structure spaced by 64 $cm^{-1}$. This yields an electron affinity of 2.507 eV. Again we compare our spectra with the previously studied $In_2P^-/In_2P$ system. The appearance of the 266 nm $In_2P^-$ and $Ga_2P^-$ anion photoelectron spectra are very similar[3]. Both show a single intense transition to the ground state and a broader Franck-Condon profile in the first excited state. Arnold *et al.*[3] observe two active modes in the $\tilde{X}$ state of $In_2P$. They reported the most active mode to be the $\nu_2$ bend with a frequency of 47 $cm^{-1}$. A less intense combination band involving the symmetric stretch $\nu_1$ was measured to be 204 $cm^{-1}$. By analogy, we assign the 64 $cm^{-1}$ frequency to the neutral bending mode, $\nu_2$.

Peak A3 is the most intense peak of the first excited state and is identified as the origin of the $^2B_2$ state located at 2.758 eV. This gives a term value of 0.251 eV. Balasubramanian's value[7] of 0.09 is not in accord with our measurement. Peaks A3-A6 form a progression in the neutral of 331 $cm^{-1}$. A progression of hot bands, A1 and A2 afford an anion frequency of 403 $cm^{-1}$. The transition to the $\tilde{A}$ state was not observed in the ZEKE spectrum of $In_2P^-$ because it is not allowed. The photoelectron spectrum of $In_2P^-$ does not show resolved structure either. However, peaks A3-A6 in our spectra show a progression of 331 $cm^{-1}$ in the first excited state of the neutral. The vibrational frequency of diatomic GaP is 283.6 $cm^{-1}$ as reported by Li *et al.*[2] The frequency we measure is therefore too high to be a bending mode. According to photoelectron

selection rules we expect to preferentially see activity in the totally symmetric modes.

Therefore we assign the frequency of 331 $cm^{-1}$ to the totally symmetric mode, $\nu_1$.

Table 1. Vibrational fundamentals, term values, and electron affinities of $GaP_2^-/GaP_2$ and $Ga_2P^-/Ga_2P$.[1]

| Molecule | State | $\nu_1$ ($cm^{-1}$) | $\nu_2$ ($cm^{-1}$) | $\nu_3$ ($cm^{-1}$) | Term value (eV) | Previous[2] (eV) |
|---|---|---|---|---|---|---|
| $GaP_2^-$ | $\tilde{X}\,^1A_1$ | 589 | | | -1.726 | -1.78 |
| $GaP_2$ | $\tilde{X}\,^2B_2$ | (322) | 240 (220.9) | | 0.000 | |
| | $\tilde{A}\,^2A_1$ | | 329 | | 1.250 (1.07) | 0.99 |
| | $\tilde{B}\,^2B_1$ | 500 | 234 | | 2.598 (2.33) | 2.34 |
| $Ga_2P^-$ | $\tilde{X}\,^1A_1$ | 403 | | | -2.507 | -2.42 |
| $Ga_2P$ | $\tilde{X}\,^2B_1$ | | 64 | (280.5) | 0.000 | |
| | $\tilde{A}\,^2B_2$ | 331 | | | 0.251 (0.09) | 0.27 |

[1] Frequencies and term values in parenthesis are from Ref. [2] and Ref. [7], respectively.

[2] Ref. [1].

## C. $Ga_2P_3$

The top panel of Figure 3 contains a 266 nm spectrum of $Ga_2P_3^-$ taken at a polarization angle of $\theta=0^\circ$. The lower two panels show photoelectron spectra taken at 355 nm with polarization angles of $\theta=0$ and $90^\circ$. The 266 nm spectrum clearly shows two electronic states, labeled X and A, centered at 3.14 and 3.35 eV, respectively. The 355 nm spectra show an extended vibrational progression that follows a polarization dependence. In addition, the 355 nm spectrum taken at $\theta=0^\circ$ reveals another feature labeled *a* located at 2.84 eV which is absent in the same polarization of the 266 nm spectrum.

Analysis of the final cluster, $Ga_2P_3$, is less straightforward. No experimental data is available for comparison. Current *ab initio* results[8] show a trigonal bipyramidal ($D_{3h}$) $^2A_2''$ state is calculated to lie only 0.05 eV above the distorted trigonal bipyramidal $^2B_1$ state, resulting from Jahn-Teller distortion of a $^2E''$ state. The polarization dependence indicates that feature X and A are two overlapping electronic states. In our spectra they appear to be separated by much more than the calculated value of 0.05 eV. However we can not confidently identify features X and A. Based on Franck-Condon simulations we estimate the origin of feature X to be at 3.004 eV. Vibrational analysis of feature X shows a frequency of 223 $cm^{-1}$ which most likely involves Ga-P stretching motion. The identity of feature *a* is also uncertain. It only appears in the 355 nm spectra, most dominantly at $\theta=0^\circ$. The possibility of a two-photon involving photodissociation and subsequent photodetachment of a daughter ion is unlikely.

## Acknowledgements

This research is supported by the National Science Foundation under Grant No. DMR-9814677. K. R. A. gratefully acknowledges a postdoctoral fellowship from the Swiss National Science Foundation.

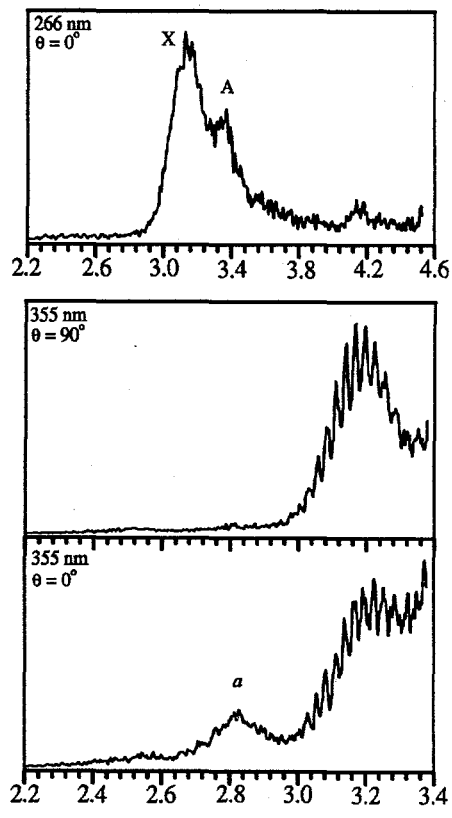


Fig. 3. Photoelectron spectra of $Ga_2P_3^-$ taken at the photodetachment wavelength of 266 and 355 nm. Laser polarization angles are θ=0° and 90° with respect to the direction of electron collection.

## References

[1] T. R. Taylor, K. R. Asmis, C. Xu, and D. M. Neumark, Chem. Phys. Lett. **297,** 133 (1998).

[2] S. Li, R. J. Van Zee, and W. Weltner, J. Phys. Chem. **97,** 11393 (1993).

[3] C. C. Arnold and D. M. Neumark, Can. J. Phys. **72,** 1322 (1994).

[4] G. W. Lemire, G. A. Bishea, S. A. Heidicke, and M. D. Morse, J. Chem. Phys. **92,** 121 (1990).

[5] W. Andreoni, Phys. Rev. B **45,** 4203 (1992).

[6] P. Y. Feng and K. Balasubramanian, Chem. Phys. Lett. **258,** 387 (1996).

[7] P. Y. Feng and K. Balasubramanian, Chem. Phys. Lett. **265,** 41 (1997).

[8] P. Y. Feng and K. Balasubramanian, Chem. Phys. Lett. **265,** 547 (1997).

[9] P. Y. Feng and K. Balasubramanian, Chem. Phys. Lett. **288,** 1 (1998).

[10] R. B. Metz, A. Weaver, S. E. Bradforth, T. N. Kitsopoulos, and D. M. Neumark, J. Phys. Chem. **94,** 1377 (1990).

[11] C. Xu, G. R. Burton, T. R. Taylor, and D. M. Neumark, J. Chem. Phys. **107,** 3428 (1997).

[12] B. A. Mamyrin and D. V. Shmikk, JETP **49,** 762 (1979).

[13] G. Markovich, R. Giniger, M. Levin, and O. Cheshnovsky, J. Chem. Phys. **95,** 9416 (1991).

# Chapter 7. Vibrationally-resolved anion photoelectron spectra of $GaX_2^-$, $Ga_2X^-$, $Ga_2X_2^-$, and $Ga_2X_3^-$ (X=P,As)


## Abstract

Vibrationally-resolved anion photoelectron spectra taken at various wavelengths have been obtained for $GaX_2^-$, $Ga_2X^-$, and $Ga_2X_3^-$ (X=P,As). In addition, we report the anion photoelectron spectra of $Ga_2X_2^-$ (X=P,As) and suggest that the lack of resolved vibrational structure is a result of extensive Franck-Condon activity. We report electron affinities, term values, and frequencies for the low-lying electronic states observed. Further, we discuss the similarities and differences between the phosphorus and arsenic containing isovalent species and compare our results to available theoretical calculations.


## I. Introduction

Since the invention of the transistor in 1947, semiconductor materials have become an essential part of the electronics industry. Group III-V materials have shown particular promise as semiconductors and have demonstrated a variety of novel characteristics. Bulk semiconductor materials have been thoroughly studied and are well understood, however small molecules made of group III-V elements have received relatively little attention despite their importance in processes such as epitaxial growth and chemical vapor deposition. It has been a goal of our research group to characterize the electronic and vibrational structure of clusters formed from bulk semiconducting materials. This study represents continued progress towards this goal by investigating the

electronic and vibrational structure of $GaX_2^-$, $Ga_2X^-$, $Ga_2X_2^-$, and $Ga_2X_3^-$ (X=P,As) clusters via anion photoelectron spectroscopy.

Several gas phase and matrix experiments have been carried out revealing the details of the electronic and vibrational structure of III-V polyatomics: BN,[1-7] GaP,[8-10] GaAs,[10,11] GaSb,[10] InP,[12-15] InAs,[12] and InSb.[12] Taylor *et al.* have carried out two studies on $Ga_xP_y^-$ clusters via anion photoelectron spectroscopy. In the first study they obtained vertical detachment energies from low-resolution spectra (30 meV) of size-selected clusters, $Ga_xP_y^-$ ($x+y \leq 18$).[9] This study showed an odd-even alternation in electron affinities consistent with the open-shell/closed-shell structure of the clusters and a size dependent trend in the electron affinity for clusters with more than 12 atoms. In a later study[8] they published preliminary results of vibrationally-resolved spectra of $GaP_2^-$, $Ga_2P^-$, and $Ga_2P_3^-$ anions and concluded that the anion ground state and the neutral states of $GaP_2$ and $Ga_2P$ are bent $C_{2v}$ structures. Comparison of the $Ga_2P^-$ spectra with *ab initio* calculations was not satisfactory, however they were able to assign the first three electronic states of $GaP_2$ to $\tilde{X}\ ^2B_2$, $\tilde{A}\ ^2A_1$, and $B\ ^2B_1$. They have also studied the diatomic GaP/$GaP^-$ and GaAs/$GaAs^-$ systems and will report on their low-lying electronic states in a forthcoming paper.[16] Li *et al.* have carried out experiments using the matrix infrared absorption technique revealing vibrational fundamentals of GaX, $GaX_2$, $Ga_2X$ (X=P,As).[10] In another paper by the same authors report the electron spin resonance spectrum of $Ga_2As_3$ in the matrix and conclude that it has a trigonal bipyramidal structure with the unpaired electron primarily located on the two-gallium atoms.[17] Jin *et al.* have taken anion photoelectron spectra of $Ga_xAs_y^-$ clusters, however low mass resolution decreased their size-selectivity and the low-resolution magnetic bottle apparatus only

allowed qualitative observation of electronic structure.[11] Electric dipole polarizabilities of gallium arsenide clusters have also been measured by Schlect *et al.*[18]

Several theoretical descriptions of polyatomic GaX (X=P,As) clusters are available. Andreoni carried out Car-Parrinello molecular dynamics calculations to study the structures, stability and melting of small stoichiometric GaP, GaAs, and AlAs clusters.[19] Feng *et al.* have performed complete active space self-consistent field (CASSCF) and multireference singles and doubles configuration interaction (MRSDCI) calculations however they only report geometries and term values for neutral and cation gallium phosphide[20-23] and gallium arsenide[24-29]clusters with up to five atoms. Recently, Balasubramanian has carried out extensive calculations including 5.5 million configurations in an effort to better describe the neutral and anion states of $GaAs_2$ and $Ga_2As$.[26]Archibong *et al.* have used coupled cluster singles and doubles (CCSD(T)) and Becke-3-parameter-Lee-Yang-Parr (B3LYP) theoretical methods to study GaP and $GaP_2$, calculating term energies and vibrational frequencies of the neutral and anion states.[30] Unpublished results by the same authors indicate that the $Ga_2P_2^-$ anion ground state has a $C_{2v}$ geometry and the two lowest lying neutral states of $C_{2v}$ symmetry are nearly degenerate.[31] Meier and coworkers investigate the $Ga_2As_2^-$ anion ground state, however they only consider the rhombic structure.[32] All other authors conclude that the neutral ground state of $Ga_2X_2$ is a rhombic structure.[22,25,27,32-34] Graves *et al.* and Al-Laham *et al.* have carried out *ab initio* calculations to determine the ground state of the 1:1 stoichiometric clusters with up to 8 atoms.[33,34] In support of the electron spin resonance experiment previously mentioned, Arratia-Perez *et al.*[35,36] have calculated the paramagnetic resonance parameters for $Ga_2As_3$ in addition to $Ga_2As$ and $GaAs_2$.[35,36]

Here we present vibrationally-resolved anion photoelectron spectra of $GaX_2^-$, $Ga_2X^-$, $Ga_2X_3^-$ (X=P,As) clusters and we also discuss the electronic structure of $Ga_2X_2$. The addition of a liquid nitrogen cooled clustering channel to our laser ablation disc source has allowed us to vibrationally cool the anion cluster precursors. This significantly improves the quality of our photoelectron spectra and allows us to more accurately report electron affinities, vibrational frequencies, and term values.

## II. Experimental

The anion photoelectron spectrometer used in this study has been described in detail previously.[37,38] Cluster anions are generated in a laser ablation/pulsed molecular beam source equipped with an additional liquid nitrogen cooled clustering channel as shown in Figure 1. The piezo electric molecular beam valve (a) releases a supersonic helium gas pulse which intercepts the resulting clusters generated by ablating a rotating and translating single crystal disc (b) of GaP or GaAs (Crystallode Inc.) with the second harmonic (532 nm) of a pulsed Nd:YAG laser (c). The laser pulses are typically 5.0-7.5 mJ/pulse before focusing onto the target with a 50 cm lens. The gas pulse continues to travel through a 1.75 inch long copper clustering channel (e). The copper channel is cooled by gravimetrically flowing liquid nitrogen through ⅛ inch diameter copper tubing in thermal contact with the channel. To prevent the valve from cooling, a ¼ inch thick insulator (d) made of Delrin is located between the copper channel and the laser ablation assembly. In addition, the laser ablation assembly is heated enough to maintain it at room temperature. Thermocouples are used to ensure that the clustering channel and molecular beam valve are maintained at the appropriate temperatures. The gas pulse

exits the clustering channel and passes through a skimmer into a differentially pumped region. Negative ions in the beam are extracted perpendicular to their flow direction by a pulsed electric field and injected into a linear reflectron time-of-flight (TOF) mass

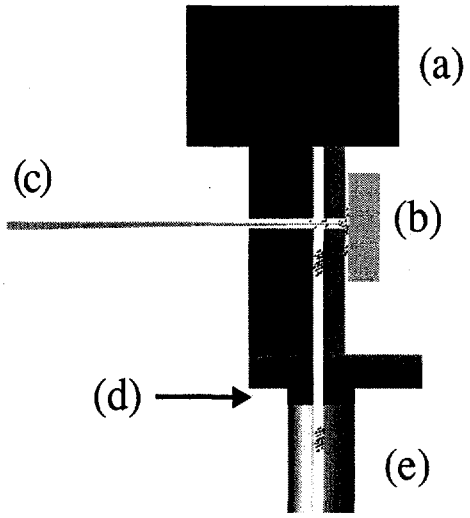


Figure 1. Diagram of the liquid nitrogen cooled clustering channel coupled with the laser ablation disc source. The diagram is labeled as follows: (a) pulsed piezo electric valve, (b) disc ablation target, (c) incident laser beam, (d) Delrin insulating disc, and (e) copper clustering channel.

spectrometer,[39,40] affording a mass resolution m/Δm of 2000. Due to the natural isotope abundance of gallium ($Ga^{69}$:$Ga^{71}$, 100.0:66.4) each cluster stoichiometry has a mass distribution. In each case the most intense mass peak was photodetached.

The ion of interest is selectively photodetached with photons having wavelengths of 355 nm (3.493 eV), 416 nm (2.977 eV), and 498 nm (2.490 eV). The 355 nm wavelength is obtained by tripling the fundamental of a pulsed Nd:YAG laser. The first

and second Stokes lines generated by passing the third harmonic (355 nm) through a high pressure Raman cell filled with hydrogen (325 psig) afford the 416 nm and 498 nm light, respectively. The electron kinetic energy (*eKE*) distribution is determined by TOF analysis in a 1 m field-free flight tube. The energy resolution is 8-10 meV at 0.65 eV *eKE* and degrades as $(eKE)^{3/2}$ at higher *eKE*. The data in electron kinetic energy is converted to electron binding energy (*eBE*) by subtracting it from the photon energy. All data are plotted in *eBE* as described by equation (1) where *EA* is the adiabatic electron affinity, $E^o$ is the internal energy of the neutral, and $E^-$ is the internal energy of the anion.

$$eBE = h\nu - eKE = EA + E^o - E^- \tag{1}$$

The angular dependence of the photodetachment intensity for polarized light and randomly oriented molecules is given by equation (2) below[41]

$$\frac{d\sigma}{d\Omega} = \frac{\sigma_{total}}{4\pi}\left[1 + \frac{\beta(eKE)}{2}(3\cos^2\theta - 1)\right] \tag{2}$$

where $\theta$ is the angle between the electric vector of the photon and the direction of electron ejection, $\sigma_{total}$ is the total photodetachment cross section and $\beta(eKE)$ is the asymmetry parameter ($-1 \le \beta \le 2$). Each electronic state typically has a characteristic asymmetry parameter and this can be used to distinguish peaks of overlapping electronic transitions. The asymmetry parameter of a peak can be calculated[42] using equation (3)

$$\beta = \frac{I_{0^o} - I_{90^o}}{\frac{1}{2} I_{0^o} + I_{90^o}} \tag{3}$$

where $I_{0^o}$ and $I_{90^o}$ are the intensities of the peak taken at the polarization angles $\theta = 0^o$ and $90^o$. The laser polarization can be rotated with respect to the direction of electron detection by using a half-wave plate.

## III. Results

Figure 2 shows the first excited ($\tilde{A}\,^2A_1$) state of $GaP_2$ taken at room temperature (HOT) and with the liquid nitrogen cooled clustering channel (COLD). These two spectra demonstrate our ability to vibrationally cool the anions prior to photodetachment allowing us to obtain a much better resolved spectrum of the neutral. Figures 3-6 show the anion photoelectron spectra of $GaX_2^-$, $Ga_2X^-$, $Ga_2X_2^-$, and $Ga_2X_3^-$ (X=P,As), respectively. For all spectra the ordinate is intensity with arbitrary units and the abscissa is in electron binding energy (*eBE*) with units of eV. Species of the same stoichiometry have similar spectra and throughout the paper descriptions apply to both species unless otherwise noted. The similarity of electronic structure can be gauged by the similarity of the asymmetry parameters for isovalent species. Where

possible $\beta$ has been determined and for $GaX_2$ these values are located in Tables 1-2. The values for $Ga_2X$ are shown graphically in Figure 4 and $Ga_2X_3$ values are discussed in the last section. The features marked with the asterisk (*) appear only in the $Ga_2X$ and $GaX_2$ spectra. They are observed in the 'cold' spectra of $Ga_2X^-$ and $GaX_2^-$ but not in the 'hot' spectra. They are most significant in the gallium arsenide species and are not significant in spectra taken at 266 nm. The nature of these features is questionable and further experiments are required to determine their origin.

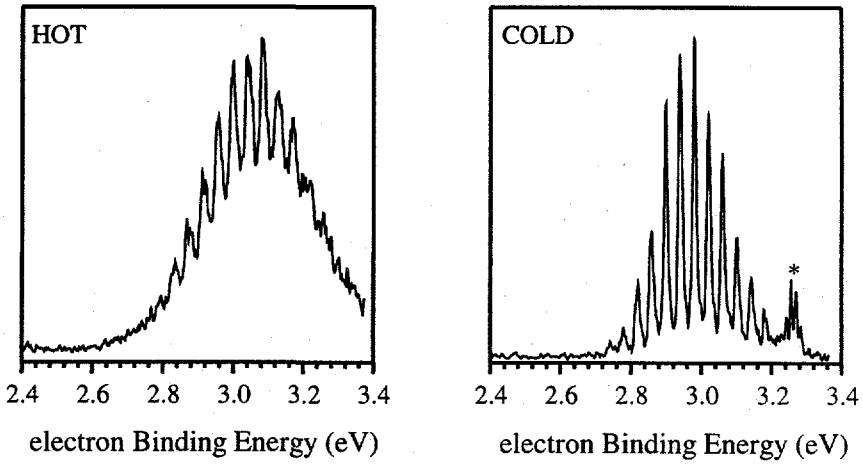


Figure 2. Comparison of 'hot' and 'cold' anion photoelectron spectra of $GaP_2^-$ taken at a wavelength of 355 nm and polarization angle of $\theta=0^\circ$. The spectrum shows only the $\tilde{A}\,^2A_1$ state of $GaP_2$.

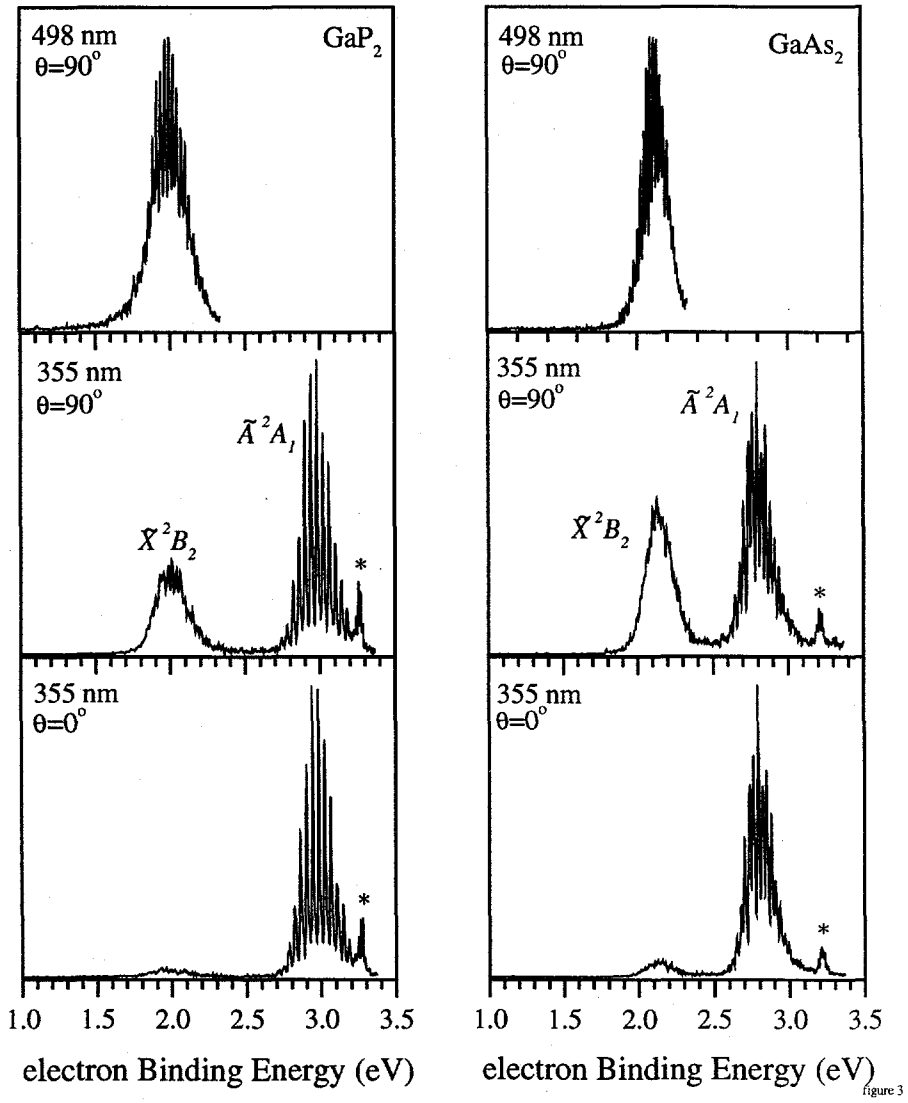


Figure 3. Anion photoelectron spectra of $GaX_2^-$ (X=P, As) taken at the wavelengths and polarization angles indicated. The features marked with an asterisk (*) are discussed in the text.

Figure 3 has six panels corresponding to the $GaX_2^-$ spectra taken at different wavelengths and polarization angles. The top panels show the spectra taken at 498 $cm^{-1}$

and θ=90°. The lower two panels show spectra taken at 355 nm and θ=90° and 0°. With the aid of *ab initio* calculations, we previously concluded that the anion ground state and neutral states of $GaP_2$ have $C_{2v}$ geometries and we assigned the ground and first excited states to the $\tilde{X}\ ^2B_2$ and $\tilde{A}\ ^2A_1$ states, respectively.[8,9,15] Given the similarities between the spectra of $GaP_2$ and $GaAs_2$ we extend these assignments to $GaAs_2$. We will further confirm this assignment in the next section. Both states of $GaX_2$ show similar extended vibrational progressions implying a large geometry change between the anion and neutral states. The $\tilde{X}\ ^2B_2$ and $\tilde{A}\ ^2A_1$ states in $GaP_2$ show Franck-Condon (FC) progressions with frequencies of 220 and 323 $cm^{-1}$, respectively. The $\tilde{X}\ ^2B_2$ state of $GaAs_2$ shows a FC progression with a frequency of 177 $cm^{-1}$ and the vibrational spacing of the $\tilde{A}\ ^2A_1$ state is regular affording a frequency of 234 $cm^{-1}$, however the intensities are irregular. The 355 nm spectra indicate that the ground state only has significant intensity at the θ=90° polarization. It is for this reason that we only report the higher resolution 498 nm spectrum at θ=90°.

Our previous studies of $Ga_2P$ and $In_2P$ have concluded that we observe photoelectron transitions from bent anion to bent neutral states.[8,9,15] Figure 4 has four panels with the photoelectron spectra of $Ga_2X^-$ taken at a wavelength of 355 nm and polarization angles of θ=0° and 90°. In addition, there are two more panels graphically showing the β parameter plotted with peak position. These spectra have three features: *X*, *A*, & *B* located at progressively higher *eBE*. Spectra were taken at a higher wavelength (416 nm)

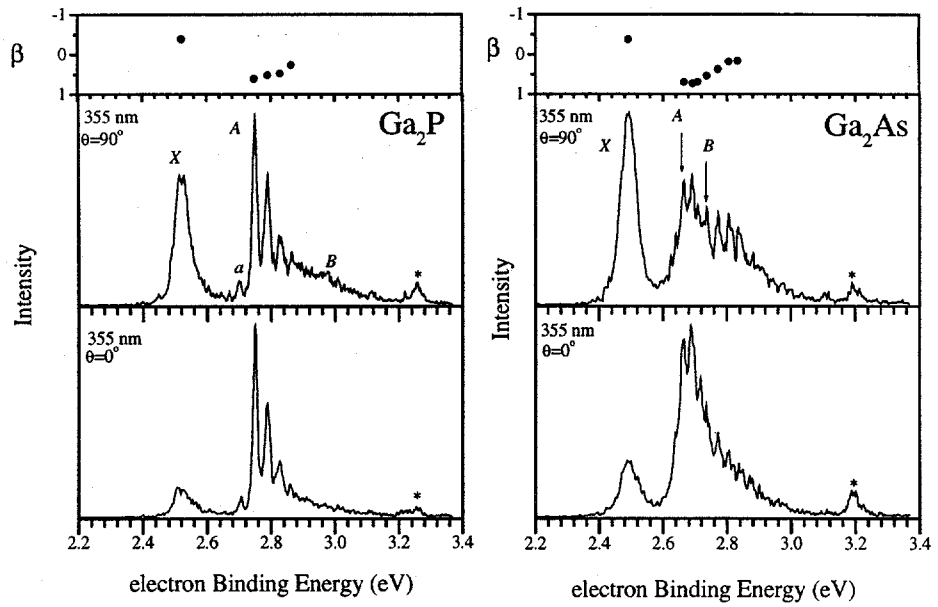


Figure 4. Anion photoelectron spectra of $Ga_2X^-$ (X=P, As) taken at a wavelength of 355 nm and polarization angles of $\theta=0^\circ$ and $90^\circ$. The plot of the $\beta$ parameters is located in the top panel. The features marked with an asterisk (*) are discussed in the text.

in an effort to vibrationally resolve feature *X* and are shown in Figure 5. Although vibrational structure was not resolved, we have a more detailed picture of feature *X*, allowing us to more accurately estimate the adiabatic electron affinity, indicated by the arrow. In Figure 4, Feature *A* of $Ga_2P$ has the best-resolved vibrational structure affording a neutral frequency of 311 $cm^{-1}$. A hot band transition, labeled as *a*, gives us an anion frequency of $375 \pm 25$ $cm^{-1}$. The vibrational structure of the analogous feature in $Ga_2As$ is obscured by feature *B* and shows no obvious pattern. In the vicinity

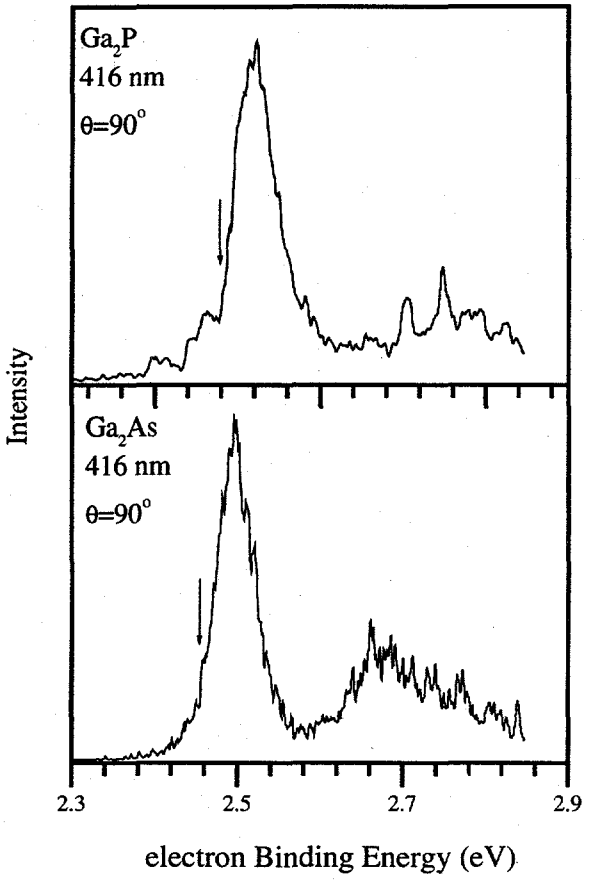


Figure 5. Anion photoelectron spectra of $Ga_2X^-$ (X=P, As) taken at a wavelength of 416 nm and $\theta=90^\circ$. Arrows indicate the origin of the transition.

of the vibrationally resolved upper state of $Ga_2P$ there is considerable intensity from a broad featureless transition having a maximum intensity in the $\theta=90^\circ$ polarization, which we label as *B*. In contrast, feature *B* of $Ga_2As$ shows vibrational structure and the origin of the transition is marked with an arrow. The $\beta$ parameters of $Ga_2X$ are constantly changing indicating we have overlapping electronic transitions. The first four peaks of

this transition yield a vibrational frequency of 250 $cm^{-1}$. The differences in the $Ga_2X^-$ spectra are the most significant of any of the isovalent species studied here.

All attempts to resolve vibrational structure in tetra-atomic stoichiometries failed. Figure 6 shows the anion photoelectron spectra of $Ga_2X_2^-$ taken at 355 nm and $\theta=0^\circ$. Spectra were taken at other polarization angles, however the $\theta=0^\circ$ spectra are optimal for showing the important spectral features. These spectra are characterized by one central dominant peak, labeled as *X*, and several low-intensity broad featureless transitions.

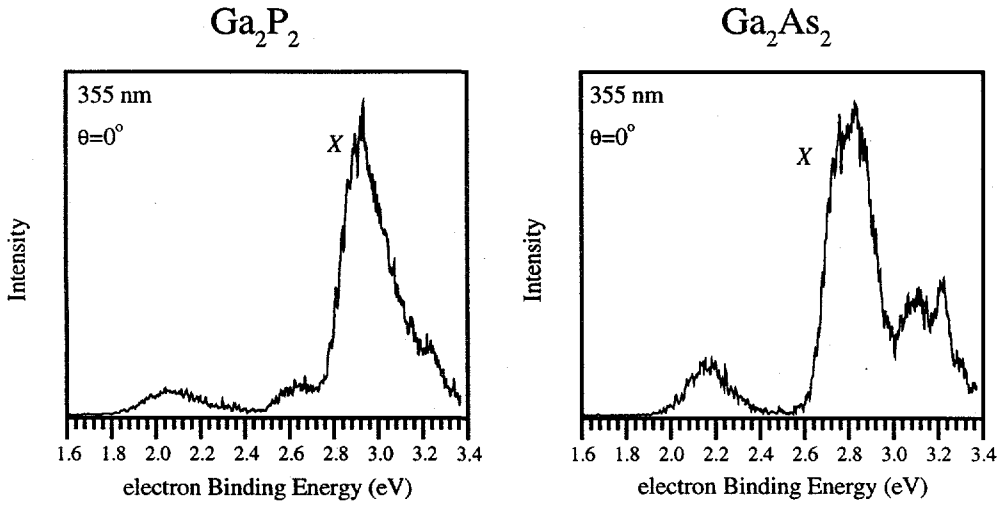


Figure 6. Anion photoelectron spectra of $Ga_2X_2^-$ (X=P, As) taken at a wavelength of 355 nm and polarization angle of $\theta=0^\circ$.

We are able to resolve vibrational structure in the photoelectron spectra of $Ga_2X_3^-$. Figure 7 shows the photoelectron spectra taken at a wavelength of 355 nm and polarization angles of $\theta=0^\circ$ and $90^\circ$. The spectra taken at $\theta=90^\circ$ (top panel) primarily shows one electronic state (labeled as *X*) with an extended progression having a frequency of 218 and 198 $cm^{-1}$ in $Ga_2P_3$ and $Ga_2As_3$, respectively. There is non-negligible intensity extending toward lower binding energy. These features are much more prominent in the $\theta=0^\circ$ spectrum (lower panel) and shows evidence of two broad

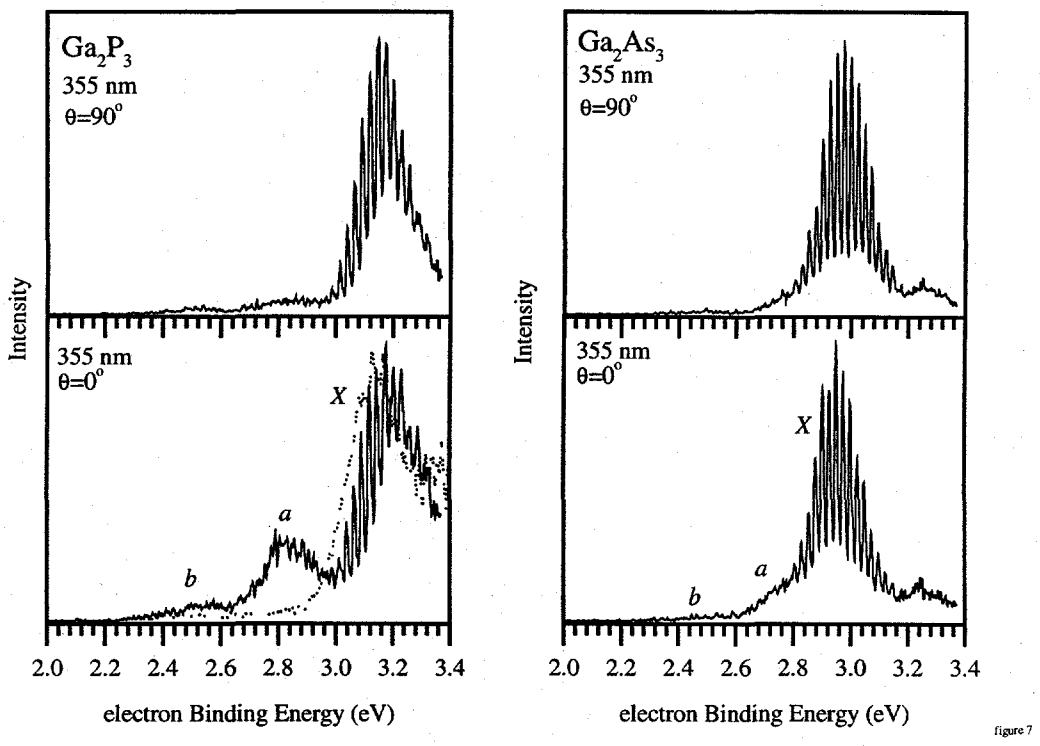


Figure 7. Anion photoelectron spectra of $Ga_2X_3^-$ (X=P, As) taken at a wavelength of 355 nm and polarization angles of $\theta=0^\circ$ and $90^\circ$. The dotted line in the lower left panel was taken at 266 nm.

featureless transitions, labeled as *a* and *b*. The 266 nm spectrum (dotted line) of $Ga_2P_3^-$ taken at $\theta=0^\circ$ is shown superimposed on the 355 nm spectra in the lower panel. Note that peaks *a* and *b* do not appear in the 266 nm spectrum of $Ga_2P_3^-$, indicating that these features are wavelength dependent.

## IV. Discussion and Analysis

In an effort to better characterize the electronic states observed, we have carried out Franck-Condon (FC) simulations. The calculations are performed within the parallel mode approximation assuming harmonic oscillator potentials. The FC simulations are carried out by iteratively optimizing the vibrational frequencies and normal coordinate change that most accurately reproduce the experimental data (a.k.a. "$\chi$ by eye"). The simulations are particularly important for extended progressions where the origin of the state is not definitively observed. When a frequency and normal coordinate change satisfactorily reproduce the spectra, the origin of the transition is shifted by $\pm 1$ quanta of the neutral frequency and the frequency and normal coordinate change are reoptimized. Under these conditions we have found that the experimental data is no longer satisfactorily reproduced and we estimate the error bars to be no larger than $\pm 1.5$ quanta of the neutral frequency. Figure 8-10 show the simulations superimposed with the experimental data. The arrows indicate the origin of the transitions as determined by the procedure above. The results of the simulations further discussed in the following sections.

## A. $GaX_2$

Calculations have shown $GaX_2^-$ to have a $^1A_1$ ground state ($\ldots 1b_1^2 4a_1^2 2b_2^2$).[26,30,32] One-electron detachment of the two highest lying orbitals results in the $^2B_2$ and $^2A_1$ neutral states. All of the available calculations on $GaX_2/GaX_2^-$ species show the same

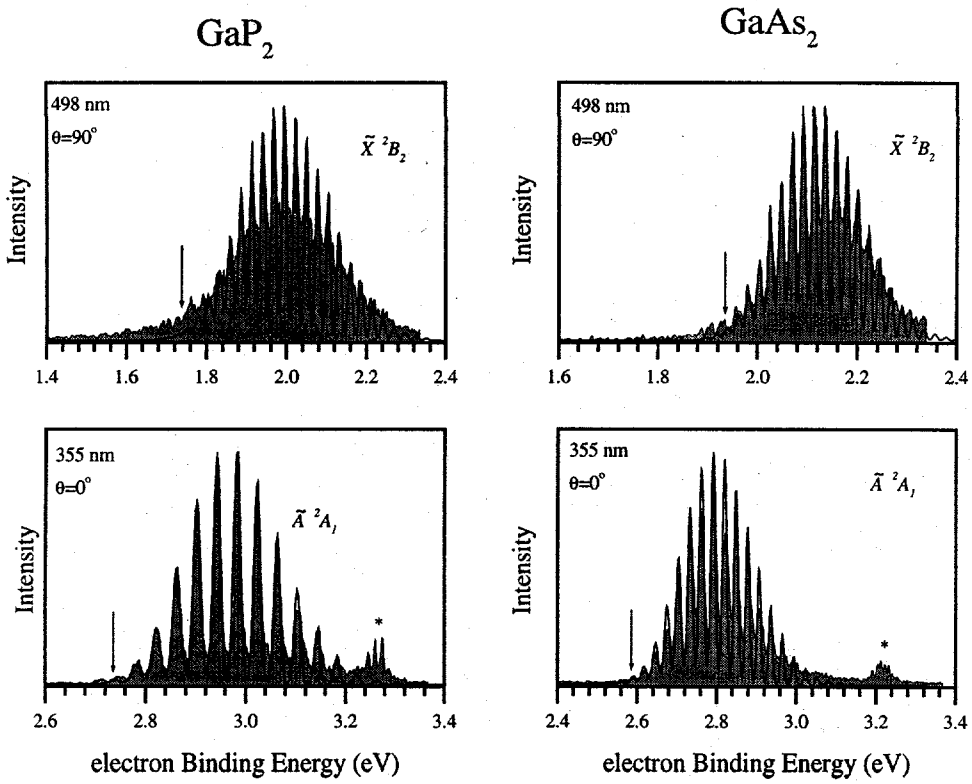


Figure 8. Anion photoelectron spectra (gray solid) superimposed with the FC simulation (black line) of $GaX_2^-$.

electronic structure and they will not be distinguished from here on out. Detachment to the neutral $\tilde{X}\ ^2B_2$ ground state shows a decrease in the X-Ga-X bond angle, which is primarily due to a large change in the Ga-$X_2$ distance.

The experimental data and the FC simulation of the $\tilde{X}\ ^2B_2$ states of $GaX_2^-$ are located in the top panels of Figure 8. The vibrational progression is very regular indicating that primarily one mode is active. The progression is extensive and we do not see a peak definitively corresponding to the origin of the transition. The arrows in the top panel indicate the adiabatic transitions according to our simulations affording an EA of $1.721 \pm 0.041$ eV and $1.937 \pm 0.033$ eV for $GaP_2$ and $GaAs_2$, respectively. The FC simulations of the ground state also afford vibrational frequencies of 220 $cm^{-1}$ and 177 $cm^{-1}$ for $GaP_2$ and $GaAs_2$, respectively.

Table 1. Comparison of geometries and energy separations of $GaP_2^-/GaP_2$.

| Reference | Species | State | Level | θ (°) | Ga-P (Å) | P-P (Å) | ΔE (eV) | $\omega_1(a_1)$ | $\omega_2(a_1)$ | $\omega_3(b_2)$ | $\beta_{355}$ |
|---|---|---|---|---|---|---|---|---|---|---|---|
| Feng *et al.*[a] | $GaP_2$ | $^2B_2$ | MRSDCI | 43.9 | 2.658 | 1.987 | 0.0 | | | | |
| | $GaP_2$ | $^2A_1$ | MRSDCI | 56.0 | 2.308 | 2.167 | 1.07 | | | | |
| | $GaP_2$ | $^2B_1$ | MRSDCI | 55.8 | 2.400 | 2.246 | 2.33 | | | | |
| | | | | | | | | | | | |
| Archibong *et al.*[b] | $GaP_2^-$ | $^1A_1$ | B3LYP | 48.9 | 2.481 | 2.056 | -1.73 (-1.75) | 590 | 260 | 240 | |
| | $GaP_2$ | $^2B_2$ | B3LYP | 43.6 | 2.657 | 1.972 | 0.0 (0.0) | 690 | 210 | 139 | |
| | $GaP_2$ | $^2A_1$ | B3LYP | 54.9 | 2.311 | 2.129 | 0.98 (.78) | 532 | 328 | 355 | |
| | $GaP_2$ | $^2B_1$ | MP2-F19[c] | 49.8 | 2.574 | 2.168 | 2.81(2.55) | 513 | 247 | 249 | |
| | | | | | | | | | | | |
| Experiment[d] | $GaP_2^-$ | $^1A_1$ | PES[d] | | | | $-1.721 \pm 0.041$ | 589 | | | |
| | $GaP_2$ | $^2B_2$ | PES[d] | | | | 0.0 | | 220 | | -0.81 |
| | $GaP_2$ | $^2B_2$ | MATRIX[e] | 52 | | | 0.0 | 322[f] | 220.9 | | |
| | $GaP_2$ | $^2A_1$ | PES[d] | | | | $1.021 \pm 0.101$ | | 323 | | +0.18 |
| | $GaP_2$ | $^2B_1$ | PES[g] | | | | $2.603 \pm 0.051$ | 500 | 234 | | |

[a] Reference [21].
[b] E. F. Archibong and A. St-Amant, In Preparation (1999). CCSD(T)-FC//B3LYP value in parentheses. Frequencies calculated with B3LYP.
[c] CCSD(T)//MP2-F19 values in parenthesis. Frequencies calculated with MP2-F19.
[d] This work.
[e] Reference [10]
[f] See discussion in text.
[g] Reference [8].

Table 2. Comparison of geometries and energy separations of $GaAs_2/GaAs_2$.

| Reference | Species | State | Level | θ (°) | Ga-As (Å) | As-As (Å) | ΔE (eV) | $\omega_1(a_1)$ | $\omega_2(a_1)$ | $\omega_3(b_2)$ | $\beta_{355}$ |
|---|---|---|---|---|---|---|---|---|---|---|---|
| Balasubramanian[a] | $GaAs_2^-$ | $^1A_1$ | MRSDCI | 52.7 | 2.586 | 2.296 | -1.50(-1.61) | 329.6 | 198.1 | 152.1 | |
| | $GaAs_2$ | $^2B_2$ | MRSDCI | 45.9 | 2.80 | 2.184 | 0.0 | 382.5 | 162.5 | 80.3 | |
| | $GaAs_2$ | $^2A_1$ | MRSDCI | 60.7 | 2.4 | 2.425 | 0.71(0.65) | 311.6 | 238.7 | 161.9 | |
| | $GaAs_2$ | $^2B_1$ | MRSDCI | | | | | | | | |
| | | | | | | | | | | | |
| Meier[b] | $GaAs_2^-$ | $^1A_1$ | FCIe | 49.6 | 2.73 | 2.29 | -1.42 | | | | |
| | $GaAs_2$ | $^2B_2$ | FCIe | 46.6 | 2.27 | 2.87 | 0.0 | | | | |
| | $GaAs_2$ | $^2A_1$ | FCIe | 58.4 | 2.44 | 2.50 | 0.65 | | | | |
| | | | | | | | | | | | |
| Experiment[c] | $GaAs_2^-$ | $^1A_1$ | PES | | | | -1.937 ± 0.033 | | | | |
| | $GaAs_2$ | $^2B_2$ | PES | | | | 0.0 | | 177 | | -0.65 |
| | $GaAs_2$ | $^2B_2$ | MATRIX[d] | 38 | | | 0.0 | | 174.1 | | |
| | $GaAs_2$ | $^2A_1$ | PES | | | | 0.651 ± 0.077 | | 234 | | +0.70 |
| | $GaAs_2$ | $^2B_1$ | PES[e] | | | | | | | | |

[a] Reference 21 values in parenthesis are MRSDCI+Q.
[b] Reference 32
[c] This work.
[d] Reference 10
[e] Reference 8.

In the photoelectron spectrum we primarily expect to see activity in the totally symmetric vibrational modes. The totally symmetric stretching mode, $\omega_1(a_1)$, of $GaP_2$ corresponds to P≡P stretching motion[30] and the P≡P bond length is calculated (1.972 Å, B3LYP)[30] to be similar to the gas phase[43] $P_2^-$ bond length of 1.979 Å. The gas phase $P_2^-$ frequency (640 $cm^{-1}$)[43] is much larger than the 220 $cm^{-1}$ progression we observe. We therefore conclude that we are observing the $\omega_2(a_1)$ symmetric stretching mode. We can make the analogous arguments for $GaAs_2$ and assign the 177 $cm^{-1}$ progression to the $\omega_2(a_1)$ symmetric stretching mode. We find our result in excellent agreement with the infrared matrix experiments of Li *et al.* where they report the $\omega_2(a_1)$ fundamentals to be 220.9 $cm^{-1}$ and 174.1 $cm^{-1}$ in $GaP_2$ and $GaAs_2$, respectively.[10] The ZEKE spectrum of $InP_2$ also indicates that the most active mode is the $\omega_2(a_1)$ mode which can best be described as symmetric stretching motion between the In atom and the $P_2$ moiety. The

theoretically calculated bond length changes for the $GaX_2^-/GaX_2$ transition, shown in Tables 1 and 2, are also in accord with this description.

In agreement with our $GaP_2$ electron affinity, Archibong *et al.* have reported the only theoretical value to be 1.73 eV (B3LYP).[30] Several calculated values of the $GaAs_2$ electron affinity are available for comparison. Lou *et al.*, Meier *et al.*, and Balasubramanian have calculated the electron affinity to be 1.9 eV (DNP), 1.57 eV (FCIe), and 1.61 eV (MRSDCI+Q), respectively.[32,44,45] The latter two values are too low, while the first more empirical calculation gives the best estimate. Archibong *et al.* also report the vibrational frequencies of the $GaP_2$ ground state modes, $\omega_1(a_1)$, $\omega_2(a_1)$, and $\omega_3(b_2)$, to be 690, 210, and 139 $cm^{-1}$ (B3LYP), respectively.[30] The calculated frequency for the $\omega_2(a_1)$ mode agrees well with our experimental value and the reported value of Li *et al.* However, Li *et al.* also observe a band in the matrix at 322 $cm^{-1}$ and assign it to the $\omega_1(a_1)$ mode. Theoretical calculations indicate that the P≡P moiety in $GaP_2$ is similar to free $P_2$ or $P_2^-$ depending on how much charge transfer is occurring.[21,30] In the most extreme case of charge transfer, the $\omega_1(a_1)$ symmetric stretch of $GaP_2$ should be similar to free $P_2^-$ which has a frequency[43] of 640 $cm^{-1}$ suggesting that the 322 $cm^{-1}$ frequency reported by Li *et al.* is too low for the $\omega_1(a_1)$ mode. Based on the results of Archibong *et al.* a reassignment of the 322 $cm^{-1}$ frequency to the $\omega_2\omega_3$ combination band seems more reasonable, if these two modes are sufficiently anharmonic and couple. The analogous arguments can be made for the 231.0 $cm^{-1}$ transition observed and assigned to $\omega_1(a_1)$ of $GaAs_2$.[10] A reassignment of this transition to the $\omega_2\omega_3$ combination band is also in agreement with recent theoretical predictions.[26]

Removal of an electron from the $4a_1$ anion molecular orbital results in the $\tilde{A}\,^2A_1$ neutral state. Calculations show that in this transition there is an increase in the X-Ga-X bond angle, which is due to a decrease in the Ga-$X_2$ distance and an increase in the X-X bond distance. The $\tilde{A}\,^2A_1$ states are simulated in the bottom panel of Figure 8 where the arrows indicate the adiabatic transition to this state according to our simulation as previously described. The well-resolved vibrational structure allows us to adequately simulate the $GaX_2$ spectra giving adiabatic detachment energies and vibrational frequencies of $2.742 \pm 0.060$ eV (323 $cm^{-1}$) and $2.588 \pm 0.044$ eV (234 $cm^{-1}$) for $GaP_2$ and $GaAs_2$, respectively. This allows us to determine the term values to be $1.02 \pm 0.10$ eV and $0.651 \pm 0.077$ eV, respectively.

The $GaP_2$ *A-X* term value determined here, is in agreement with our previously reported value[8,9] of 0.99 eV estimated by the difference in vertical detachment energies of the two states. These values are also in agreement with the theoretical values of 0.98 eV (B3LYP) and 1.07 eV (MRSDCI).[21,30] The $GaAs_2$ *A-X* term value is in good agreement with work of Meier and Balasubramanian where they calculate the term energy to be 0.65 eV at the FCIe and MRSDCI+Q levels, respectively.[32,45]

At the B3LYP level, Archibong *et al.* calculate the vibrational frequencies of the $\omega_1(a_1)$, $\omega_2(a_1)$, and $\omega_3(b_2)$ modes to be 532, 328, and 355 $cm^{-1}$, respectively.[30] The last two modes are possible candidates for the assignment, however we expect to primarily see symmetric modes active in the photoelectron spectrum and we assign the 323 $cm^{-1}$ frequency to the $\omega_2(a_1)$ bending mode. The change in geometry for the $GaAs_2$ transition is very similar to the $GaP_2$ transition and we also assign the 234 $cm^{-1}$ progression in the $GaAs_2$ *A* state to the $\omega_2(a_1)$ bending mode. These assignments are also in accord with

previously observed ZEKE spectrum of $InP_2$ where the $\omega_2(a_1)$ bending mode was the most active. Our assignment of the $\omega_2(a_1)$ bending mode is in agreement with the calculated geometry changes listed in Tables 1 and 2.

The spectrum containing the second excited $\tilde{B}\,^2B_1$ state of $GaP_2$ is not shown in the current paper, however we mention it briefly in order to reevaluate the term energy. We previously reported the adiabatic detachment energy of the *B* state origin to be 4.324 ± 0.010 eV.[8] Subtracting the new electron affinity gives us the improved $T_o(^2B_1)$=2.603 ± 0.051 eV. In addition, recent calculations by Archibong *et al.* confirm our assignments of the 500 and 589 $cm^{-1}$ frequencies to the $\omega_1(a_1)$ mode of the neutral and anion, respectively, as well as our assignment of the 234 $cm^{-1}$ frequency to the $\omega_2(a_1)$ mode of the neutral. All term values, vibrational frequencies, and assignments for $GaP_2$ and $GaAs_2$ are tabulated in Table 1 and 2, respectively.

## B. $Ga_2X$

The X $^1A_1$ anion ground states of $Ga_2X$ are calculated to have $C_{2v}$ symmetry and electron configuration of $(\ldots 3a_1^2 1b_2^2 1b_1^2 2b_2^2)$.[26,31] Removal of an electron from the anion molecular orbitals will result in $^2B_2$, $^2B_1$, and $^2A_1$ neutral states, however theoretical investigations have not definitively identified the energy ordering of these states of $Ga_2X$. The experimental data and simulation of $Ga_2P$ is shown in Figure 9. The lowest energy feature is labeled as *X* and has a narrow FC profile with a FWHM of 42 and 47 meV in $Ga_2P$ and $Ga_2As$, respectively. This FC profile is very similar to what is observed in the photodetachment spectra of $In_2P^-$.[13-15] Our inability to resolve vibrational structure suggests that the low frequency bending mode (~50 $cm^{-1}$) is the most active as is the case

with $In_2P$.[15] Feature *X* is also rather narrow consistent with the small geometry change we would expect from photodetachment from the $b_1$ molecular orbital.[15] The adiabatic electron affinities are determined from the onset of the leading edge of feature *X* for spectra taken at 416 nm and indicated with an arrow in Figure 5 giving adiabatic electron affinities of 2.481 ± 0.015 eV and 2.457 ± 0.015 eV in $Ga_2P^-$ and $Ga_2As^-$, respectively.

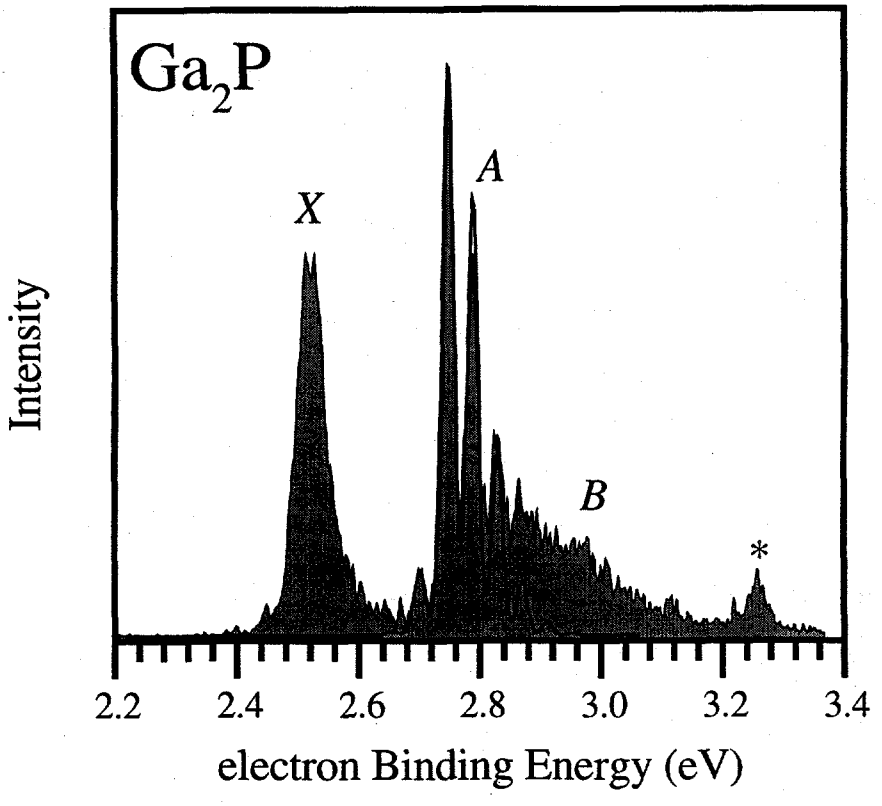


Figure 9. Anion photoelectron spectra (gray solid) superimposed with the FC simulation (black line) of $Ga_2P^-$.

The adiabatic transition for the vibrationally resolved first excited state of $Ga_2P$ (feature *A*) is unambiguously observed and shows primarily one active vibrational mode. This affords an adiabatic detachment energy of 2.749 ± 0.010 eV and a term value of 0.268 ± 0.025 eV. FC simulation of feature *A* reveals neutral and anion vibrational frequencies of 311 $cm^{-1}$ and 375 ± 25 $cm^{-1}$, respectively. Because only one vibrational mode is active we can confidently conclude that the neutral state has $C_{2v}$ symmetry since the anion is $C_{2v}$ and assign the vibrational frequencies to a totally symmetric mode. The $\omega_2(a_1)$ bending mode of $Ga_2P$ is calculated to be ~50 $cm^{-1}$ for the neutral and the anion.[26,31] The observed frequency is much larger than 50 $cm^{-1}$ and we therefore assign it to the $\omega_1(a_1)$ symmetric stretching mode.

The vibrational structure of feature *A* of $Ga_2As$ taken at 416 nm and 355 nm does not show an obvious pattern. We can however, identify the origin of the transition, marked with an arrow, and determine the adiabatic detachment energy to be 2.666 ± 0.015 eV affording a term value of 0.209 ± 0.025 eV. In analogy with $Ga_2P$ we would expect to see only the $\omega_1(a_1)$ mode active, however the unresolved structure indicates that more than one mode is active, suggesting that feature *A* of $Ga_2As$ is not the same state as feature *A* of $Ga_2P$.

The residual from subtracting the $\theta=0^\circ$ spectrum from the $\theta=90^\circ$ spectrum allows us to estimate the vertical detachment energy of feature *B* of $Ga_2P$ to be ~0.40 eV with respect to the ground state origin. This transition is featureless indicating that the neutral state has a geometry very different from the anion state. In contrast, feature *B* in $Ga_2As$ shows vibrational structure and we have indicated the origin of the transition with the arrow affording a term value of ~0.28 eV. The first three notable peaks are separated by

250 $cm^{-1}$ and must be due to a $\omega_1(a_1)$ symmetric stretching mode. Feature *B* of $Ga_2X$ exhibits further evidence that the electronic structure between these isovalent species can be different.

Current theoretical calculations are divided in their determination of the electronic symmetry of the ground and excited states.[21,26,29,46] This ambiguity makes assignments difficult, however based on our experiments and these theoretical calculations we are able to make some definitive statements. First, we have now investigated four isovalent species: $Al_2P$, $Ga_2P$, $Ga_2As$, and $In_2P$. The anion photoelectron spectra of all four of these species are very similar indicating they have qualitatively similar electronic structure in the anion and neutral states observed. The current calculations do not show this trend, however our spectra show that some continuity must exist. Second, all available calculations indicate that the anion has a bent $C_{2v}$ structure and the FC profile of both features *X* and *A* suggest that these states also have $C_{2v}$ symmetry i.e. we do not observe a prominent progression in the asymmetric stretch.

Third, simple molecular orbital arguments allow us to make an educated guess about the ground state electronic symmetry. It is well known in anion ZEKE experiments that only neutrals resulting from s-wave detachment are allowed. In the ZEKE spectra of $Ga_2As$ and $In_2P$ only feature X shows ZEKE signal.[15,47] In fact the $In_2P$ spectrum shows the strongest signal of any molecular anion studied in our laboratory. This confirms that the anion molecular orbital from which the electron is being detached must look very similar to a p-orbital. The $b_1$ orbital involving $\pi$-type bonding between the three $3p_x$ orbitals best fits this description and is also predicted to be the SOMO of $Ga_2As$ in Dirac molecular orbital calculations.[36] In addition states which result from s-wave detachment

show maximum intensity in the $\theta=90^{o}$ photoelectron spectrum. All four species, $Al_2P$, $Ga_2P$, $Ga_2As$, and $In_2P$ show this dependence. Furthermore Balasubramanian[26] calculates the most IR active mode of the $^2B_1$ state to be $\omega_3(b_1)$ 225 $cm^{-1}$ (B3LYP) which agrees nicely with the IR matrix experiment by Li *et al.*[10] where they measure a ground state frequency of 204.7 $cm^{-1}$. In the face of this evidence we conclude that the ground state for $Ga_2P$ and $Ga_2As$ is $^2B_1$. At the same time we note that preliminary studies of $Al_2P$ and $Ga_2As$ not reported here suggest that feature *X* is composed of more than one electronic state and hence the theoretical description will be far from simple.

Table 3. Comparison of geometries and energy separations of $Ga_2P/Ga_2P^-$.

| Reference | Species | State | Level | θ (°) | Ga-P (Å) | ΔE (eV) | $\omega_1(a_1)$ | $\omega_2(a_1)$ | $\omega_3(b_2)$ |
|---|---|---|---|---|---|---|---|---|---|
| Feng *et al.*[a] | $Ga_2P$ | $^2B_1$ | MRSDCI | 111.0 | 2.419 | 0.0 | | | |
| | $Ga_2P$ | $^2B_2$ | MRSDCI | 90.0 | 2.300 | 0.09 | | | |
| | $Ga_2P$ | $^2\Pi_u$ | MRSDCI | 180.0 | 2.391 | 0.16 | | | |
| | | | | | | | | | |
| Archibong *et al.*[b] | $Ga_2P^-$ | $^1A_1$ | CCSD(T)-FC | | | -2.46 (-2.46) | 319 | 56 | 397 |
| | $Ga_2P$ | $^2B_2$ | B3LYP | | | 0.0 (0.0) | 315 | 53 | 121 |
| | $Ga_2P$ | $^2B_1$ | B3LYP | | | 0.18 (.17) | 251 | 51 | 335 |
| | | | | | | | | | |
| Experiment[c] | $Ga_2P^-$ | $^1A_1$ | PES | | | -2.481 ± 0.015 | 375 ± 25 | | |
| | $Ga_2P$ | X | PES | | | 0.0 | | | |
| | $Ga_2P$ | X | MATRIX | 85.7 | | 0.0 | | | 280.5 |
| | $Ga_2P$ | A | PES | | | 0.268 ± 0.025 | 311 | | |
| | $Ga_2P$ | B | PES | | | ~0.4[d] | | | |

[a] Reference 21.

[b] Reference 31. Values in parenthesis are from CCSD(T)-FC//B3LYP. Frequencies are BP86.

[c] All work is ours except for the values in parenthesis which come from Reference 10

[d] Vertical detachment energy with respect to the neutral ground state.

Table 4. Comparison of geometries and energy separations of $Ga_2As/Ga_2As$ .

| Reference | Species | State | Level | θ (°) | Ga-As (Å) | ΔE (eV) | $\omega_1(a_1)$ | $\omega_2(a_1)$ | $\omega_3(b_2)$ |
|---|---|---|---|---|---|---|---|---|---|
| Balasubramanian [a] | $Ga_2As^-$ | $^1A_1$ | MRSDCI | 98.5 | 2.37 | -2.20(-2.17) | 240.5 | 46.5 | 275.3 |
| | $Ga_2As$ | $^2A'$ | MRSDCI | 90.3 | 2.83, 2.534 | 0.0(0.025) | 182.7 | 50.4 | 265.6 |
| | $Ga_2As$ | $^2B_2$ | MRSDCI | 79.9 | 2.407 | 0.09(0.0) | | | |
| | $Ga_2As$ | $^2B_1$ | MRSDCI | 108.2 | 2.52 | 0.16(0.22) | 194.5 | 43.0 | 225.0 |
| | | | | | | | | | |
| Experiment[b] | $Ga_2As^-$ | $^1A_1$ | PES | | | -2.457 ± 0.015 | | | |
| | $Ga_2As$ | X | PES | | | 0.0 | | | |
| | $Ga_2As$ | X | MATRIX | | | | 160 | | 204.7 |
| | $Ga_2As$ | A | PES | | | 0.209 ± 0.040 | | | |
| | $Ga_2As$ | B | PES | | | 0.28 | 250 | | |

[a] Reference 21.

[b] All work is ours except for the values in parenthesis which come from Reference 10

## C. $Ga_2X_2$

The anion photoelectron spectra of $Ga_2X_2^-$ are not vibrationally-resolved, however they merit discussion in light of the interpretation of $Ga_2X_3$ in the next section and new unpublished *ab initio* results by Archibong *et al.*[31] Figure 6 shows the anion photoelectron spectra of $Ga_2X_2^-$ taken at 355 nm and $\theta=0^\circ$. Spectra were taken at other polarization angles however for the purposes of this discussion only one polarization angle is shown. Our efforts to understand the spectroscopy of $Ga_2X_2$ have been impeded by the lack of vibrational structure. Theoretical calculations exploring only the neutral rhombic structures of this stoichiometry are inadequate to explain the spectral features we observe.[9] Preliminary calculations carried out by Archibong *et al.* have shown the anion ground state to be a distorted tetrahedron. A neutral state of the same symmetry has been found to be stable and the vertical detachment energy agrees with the most prominent feature in the spectrum. The low intensity broad featureless peaks in the spectrum correspond energetically to the neutral rhombic states. The lack of resolved vibrational structure is due a large difference between the anion and neutral geometries, which is a

result of the strong X-X bonding in the structure. This is in contrast to the vibrationally resolved anion photoelectron spectra of isovalent $Si_4$ and $Ge_4$, where both species have planar anion and neutral geometries.

## D. $Ga_2X_3$

The left and right sides of Figure 9 show the FC simulations and data for $Ga_2P_3^-$ and $Ga_2As_3^-$ taken at 355 nm and polarization angles of $\theta$=0 and 90°, respectively. The arrows indicate the adiabatic transition according to our simulation. Both species exhibit three features of which feature *X* is the most significant. Feature *X* is most clearly represented in the $\theta$=90° polarization where it appears that primarily one vibrational mode is active. The asymmetry parameter of feature *X* at 355 nm for $Ga_2P_3$ and $Ga_2As_3$ are –0.52 and –0.40, respectively, indicating their electronic structure is quite similar. Simulation for $Ga_2P_3$ afford a binding energy and vibrational frequency of 2.597 ± 0.010 eV and 218 $cm^{-1}$, respectively. The respective $Ga_2As_3$ molecular constants are 2.803 ± 0.010 eV and 198 $cm^{-1}$.

The ESR experiment of $Ga_2As_3$ by Van Zee *et al.*[48] and subsequent Dirac molecular orbital calculations by Arratia-Pérez *et al.*[36] conclude that the structure is trigonal bipyramidal with a doublet ground state. Both calculations and experiment indicate the SOMO involves pσ bonding between the arsenic atoms and pσ antibonding between the two-gallium atoms. They further conclude that the unpaired electron primarily resides on the gallium atoms. The vibrational structure we observe indicates the anion and neutral states involved in the photoelectron transition resulting in feature *X*

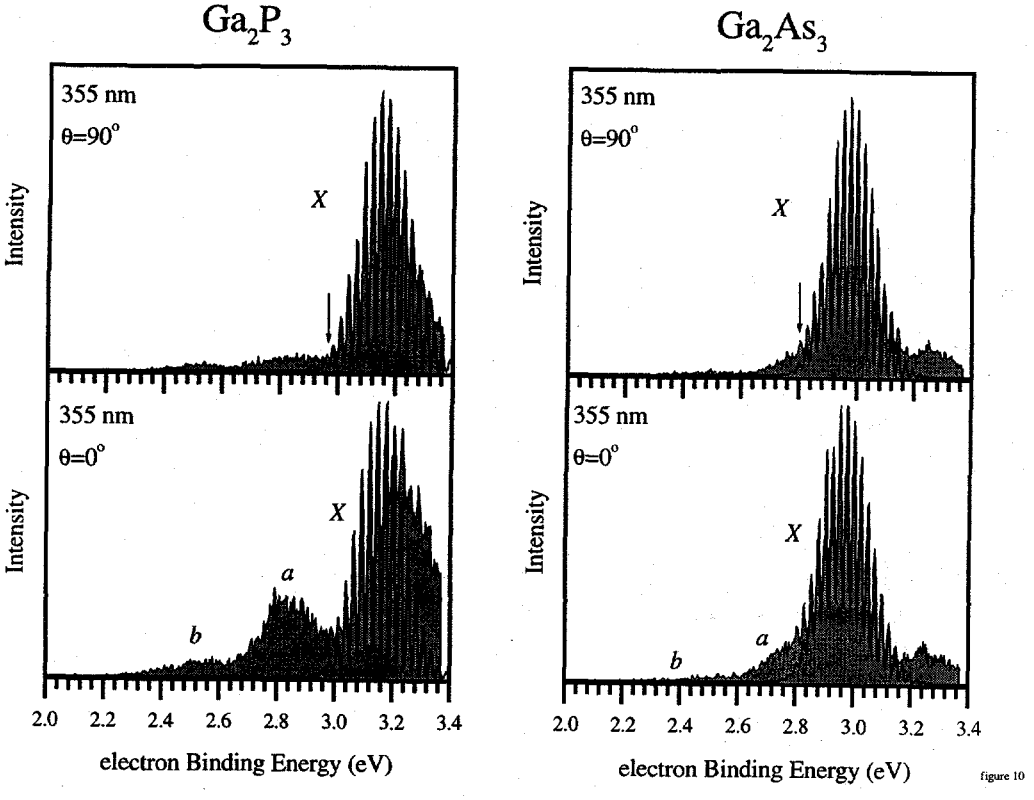


Figure 10. Anion photoelectron spectra (gray solid) superimposed with the FC simulation (black line) of $Ga_2X_3^-$.

have a high degree of symmetry. We therefore conclude that feature *X* results from a $D_{3h}$←$D_{3h}$ photoelectron transition. Balasubramanian confirms this result by finding the anion ground state to be of $D_{3h}$ symmetry.[45] Other *ab initio* calculations[20,28,44] on the neutral suggest the ground state to be $^2A$" ($D_{3h}$). The photoelectron spectrum of $Si_5$

shows similar behavior where MP2 calculations show the ground state of neutral and anion to be $D_{3h}$.[49] Photodetachment to the ground state neutral involves the removal of an electron from the antibonding orbital located between the two apical silicon atoms and the photoelectron spectrum shows a single vibrational progression in the breathing mode. We therefore assign feature *X* to the $^2A_2"(D_{3h}) \leftarrow {}^1A_1\ (D_{3h})$ transition and assign the vibrational frequency to the $\omega_2(a_1)$ symmetric breathing mode in analogy to $Si_5$.[49]

Features *a* and *b* are more difficult to assign. These features are much less prominent in $Ga_2As_3$ however the $Ga_2P_3$ spectrum indicates that they are real and significant. They do not appear to change intensity by varying source conditions and do not appear in spectra taken at 266 nm. Therefore we exclude the possibility of transitions from excited anion states. Since the appearance of these features is wavelength dependent two additional processes must be considered: autodetachment and photodissociaton followed by photodetachment of the daughter anion. It is possible that there are transitions not one electron allowed from the ground state that may be allowed by an autodetachment process. This could also account for the additional non-FC intensity of feature *X* that appears in the $\theta=0^\circ$ polarization of $Ga_2P_3$. It is also possible that $Ga_2X_3^-$ is dissociated into $Ga_2X_2^- + X$ and features *a* and *b* would arise from photodetachment of $Ga_2X_2^-$. We would expect the $Ga_2X_3^-$ dissociation to result in a bent $Ga_2X_2^-$ structure. Feature *a* in both $Ga_2X_3^-$ spectra agree very well energetically with feature *X* of $Ga_2X_2$.

## V. Conclusions

Here we have presented and discussed the anion photoelectron spectra of $GaX_2^-$, $Ga_2X^-$, $Ga_2X_2^-$, and $Ga_2X_3^-$ (X=P,As). With the aid of theoretical calculations we identify the structural and electronic symmetry of the electronic states observed and where possible have assigned the vibrational modes. The $GaX_2^-$ anion and neutral species are shown unambiguously to be of $C_{2v}$ symmetry and we assign the two neutral states observed to the $\tilde{X}\ ^2B_2$ and $\tilde{A}\ ^2A_1$ states. $Ga_2P$ and $Ga_2As$ show the first indications that the electronic structure for these isovalent III-V species maybe significantly different. The theoretical description of the electronic structure is difficult and at this time inadequate to allow definitive structural and electronic characterization. We propose that the lack of vibrationally-resolved structure in $Ga_2X_2$ is a result of extensive Franck-Condon activity consistent with recent theoretical calculations where the anion ground state is shown to be a distorted tetrahedron and the most stable neutral states are planar. The most prominent feature in the $Ga_2X_3^-$ spectra indicates that the anion and neutral are $D_{3h}$ similar to the structure of isovalent $Si_5$.

## Acknowledgements

This research is supported by the Air Force Office of Scientific Research under Grant No. F49620-97-1-0018.

# References

[1] K. R. Asmis, T. R. Taylor, and D. M. Neumark, J. Chem. Phys. **111** (1999).

[2] K. R. Asmis, T. R. Taylor, and D. M. Neumark, J. Chem. Phys. **111,** In Press (1999).

[3] K. R. Asmis, T. R. Taylor, and D. M. Neumark, The European Physical Journal D **9,** In Press (2000).

[4] L. B. Knight, D. W. Hill, T. J. Kirk, and C. A. Arrington, J. Phys. Chem. **96,** 555 (1992).

[5] L. Andrews, P. Hassanzadeh, T. R. Burkholder, and J. M. L. Martin, J. Chem. Phys. **98,** 922 (1993).

[6] C. A. Thompson, L. Andrews, J. M. L. Martin, and J. El-Yazal, J. Phys. Chem. **99,** 13839 (1995).

[7] C. A. Thompson and L. Andrews, J. Am. Chem. Soc. **117,** 10125 (1995).

[8] T. R. Taylor, K. R. Asmis, H. Gomez, and D. M. Neumark, The European Physical Journal D **9,** In Press (2000).

[9] T. R. Taylor, K. R. Asmis, C. Xu, and D. M. Neumark, Chem. Phys. Lett. **297,** 133 (1998).

[10] S. Li, R. J. Van Zee, and W. Weltner, J. Phys. Chem. **97,** 11393 (1993).

[11] C. Jin, K. J. Taylor, J. Conceicao, and R. E. Smalley, Chem. Phys. Lett. **175,** 17 (1990).

[12] S. Li, R. J. Van Zee, and W. Weltner Jr., J. Phys. Chem. **97,** 11393 (1993).

[13] C. Xu, E. Debeer, D. W. Arnold, C. C. Arnold, and D. M. Neumark, J. Chem. Phys. **101,** 5406 (1994).

[14] K. R. Asmis, T. R. Taylor, and D. M. Neumark, Chem. Phys. Lett. **308,** 347 (1999).

[15] C. C. Arnold and D. M. Neumark, Can. J. Phys. **72,** 1322 (1994).

[16] T. R. Taylor, Y. Zhao, K. R. Asmis, H. Gomez, and D. M. Neumark, J. Chem. Phys. (2000).

[17] R. J. Van Zee, S. Li, and W. Weltner Jr., J. Chem. Phys. **98,** 4335 (1993).

[18] S. Schlect, R. Schaefer, J. Woenckhaus, and J. A. Becker, Chem. Phys. Lett. **246,** 315 (1995).

[19] W. Andreoni, Phys. Rev. B **45,** 4203 (1992).

[20] P. Y. Feng and K. Balasubramanian, Chem. Phys. Lett. **265,** 547 (1997).

[21] P. Y. Feng and K. Balasubramanian, Chem. Phys. Lett. **265,** 41 (1997).

[22] P. Y. Feng and K. Balasubramanian, Chem. Phys. Lett. **258,** 387 (1996).

[23] P. Y. Feng and K. Balasubramanian, Chem. Phys. Lett. **288,** 1 (1998).

[24] K. Balasubramanian, J. Chem. Phys. **87,** 3518 (1987).

[25] K. Balasubramanian, Chem. Phys. Lett. **171,** 58 (1990).

[26] K. Balasubramanian, J. Phys. Chem. , Submitted (2000).

[27] D. W. Liao and K. Balasubramanian, J. Chem. Phys. **96,** 8938 (1992).

[28] M. Z. Liao, D. G. Dai, and K. Balasubramanian, Chem. Phys. Lett. **239,** 124 (1995).

[29] K. K. Das and K. Balasubramanian, J. Chem. Phys. **94,** 6620 (1991).

[30] E. F. Archibong and A. St-Amant, Chem. Phys. Lett. , In Press (1999).

[31] E. F. Archibong and A. St-Amant, Chem. Phys. Lett. , Submitted (1999).

[32] U. Meier, S. D. Peyerimhoff, and F. Grein, Chem. Phys. **150,** 331 (1991).

[33] R. M. Graves and G. E. Scuseria, J. Chem. Phys. **95,** 6602 (1991).

[34] M. A. Al-Laham and K. Raghavachari, Chem. Phys. Lett. **187,** 13 (1991).

[35] R. Arratia-Perez and L. Hernandez-Acevedo, J. Chem. Phys. **110,** 10882 (1999).

[36] R. Arratia-Perez and L. Hernandez-Acevedo, J. Chem. Phys. **109,** 3497 (1998).

[37] R. B. Metz, A. Weaver, S. E. Bradforth, T. N. Kitsopoulos, and D. M. Neumark, J. Phys. Chem. **94,** 1377 (1990).

[38] C. Xu, G. R. Burton, T. R. Taylor, and D. M. Neumark, J. Chem. Phys. **107,** 3428 (1997).

[39] B. A. Mamyrin and D. V. Shmikk, JETP **49,** 762 (1979).

[40] G. Markovich, R. Giniger, M. Levin, and O. Cheshnovsky, J. Chem. Phys. **95,** 9416 (1991).

[41] J. Cooper and R. N. Zare, in *Lectures in Theoretical Physics*, Vol. XI-C, edited by S. Geltman, K. T. Mahanthappa, and W. E. Brittin (Gordon and Breach, New York, 1969), pp. .

[42] K. M. Ervin and W. C. Lineberger, in *Advances in Gas Phase Ion Chemistry*, Vol. 1 (JAI Press Inc, 1992), pp. .

[43] J. T. Snodgrass, J. V. Coe, C. B. Freidhoff, K. M. McHugh, and K. H. Bowen, Chem. Phys. Lett. **122,** 352 (1985).

[44] L. Lou, L. Wang, L. P. F. Chibante, R. T. Laaksonen, P. Nordlander, and R. E. Smalley, J. Chem. Phys. **94,** 8015 (1991).

[45] K. Balasubramanian, Private Communication .

[46] P. Y. Feng and K. Balasubramanian, Chem. Phys. Lett. **284,** 313 (1998).

[47] C. C. (Arnold) Jarrold, Ph.D. Thesis, University of California, 1994.

[48] R. J. Van Zee, S. Li, and W. Weltner Jr., J. Chem. Phys. **98,** 4335 (1993).

[49] C. Xu, T. R. Taylor, G. R. Burton, and D. M. Neumark, J. Chem. Phys. **108,** 1395 (1998).

# Chapter 8. Spectroscopy of the low-lying states of the group III-V diatomics, GaP and GaAs, via anion photodetachment spectroscopies.


## Abstract

The low-lying electronic states of GaP and GaAs have been probed via zero electronic kinetic energy spectroscopy and photoelectron spectroscopy. Spin-orbit splittings, term energies, and vibrational frequencies are reported. Our experiment confirms the energy ordering of the anion and neutral states as previously calculated for these species. A comparison of electronic structure and bonding of isovalent $Si_2$, $Ge_2$, GaP, and GaAs is made. The transition from the anion ground state to the neutral ground state is not one-electron allowed, however the spectra show that the neutral ground state is accessed indirectly via an autodetachment state in both species. This allows us to accurately determine the electron affinity and compute the anion dissociation energies from literature values. The nature of the excited anion state responsible for the autodetachment process is also discussed.


## I. Introduction

In recent years, elements from groups III and V have proven very useful in the development of semiconducting devices. The bulk properties of these semiconducting systems have been well studied and their experimental properties have been satisfactorily explained by theory. The importance of these materials has spurred much interest in clusters of group III-V elements. While much of this work has focused on quantum confinement effects in very large clusters, the electronic structure of the smallest

molecular subunit, the diatomic, is not well characterized. In this paper we present the first experimental studies mapping out the low-lying electronic states of the GaP/GaP$^-$ and GaAs/GaAs$^-$ diatomic systems.

Of the III-V diatomics, the first row species, boron nitride (BN), has received the most attention experimentally.[1-8] In has been shown to have a $^3\Pi$ ground state and the triplet states have been well studied by optical spectroscopies. In a recent anion photoelectron study of BN$^-$ we were able to simultaneously observe the low-lying singlet and triplet states allowing us for the first time to relate the two manifolds energetically. Investigations of AlN and GaAs have probed their higher-lying $^3\Pi$ electronic states.[9,10] Lemire *et al.*[9] used resonant two-photon ionization spectroscopy to determine molecular constants for the spin-orbit components of the $^3\Sigma^-$ ground state of GaAs, while Ebben *et al.*[10] show AlN to have a $^3\Pi$ ground state using laser induced fluorescence. Li *et al.*[11,12] have studied several diatomic systems with matrix absorption experiments. This has yielded the vibrational fundamentals of GaX and InX (X=P, As, Sb). They have also been able to probe the low-lying electronic states of InAs and InSb determining the spin-orbit splitting of the $^3\Sigma^-$ ground state.[11] Jin *et al.* measured the first photoelectron spectrum of GaAs$^-$ from which they were able to extract an electron affinity of $2.1 \pm 0.1$ eV, however due to their low resolution they were unable to further characterize the electronic structure.

Several theoretical studies of III-V diatomics are available in the literature. Investigations of diatomic GaP have been limited to two studies. Archibong *et al.*[13] have recently looked at the electronic structure of the low-lying anion and neutral states using density functional theory (DFT) and *ab initio* methods. Manna *et al.*[14] used complete

active space self-consistent field (CASSCF) and multi-reference singles and doubles configuration interaction (MRSDCI) methods and described the GaP system incorporating spin-orbit interactions.

Diatomic GaAs has received much more theoretical attention. Meier *et al.*[15] have calculated several electronic states using MRDCI and their results agree very well with the experiment of Lemire *et al.*[9] Recent MRSDCI calculations by Manna *et al.*[16] incorporating spin-orbit effects and the MRSDCI calculations by Balasubramanian and coworkers[17-20] show general agreement with the experiment of Lemire *et al.* Both Meier and Balasubramanian study the low-lying anion states and estimate the electron affinity.[17,21] Bock *et al.*[22] have performed calculations of lower-lying electronic states at the fourth order Moller-Plesset with singles, doubles, triples and quadruple interactions (MP4(SDTQ)) level. Calculations by Graves *et al.*[23] and Smalley and coworkers[24,25] have focused on the ground states of GaAs/GaAs$^-$. These theoretical predictions[13-21,24,25] allow us to qualitatively depict the energy level diagram of GaP/GaP$^-$ and GaAs/GaAs$^-$, as shown in Figure 1. The quantitative validation of these calculations remains to be shown.

In the current paper, we use the negative ion photodetachment techniques, photoelectron spectroscopy (PES) and zero electron kinetic energy (ZEKE) spectroscopy, to study the low-lying states of the GaP/GaP$^-$ and GaAs/GaAs$^-$ systems. Using these techniques, we have previously determined the term values for the low-lying electronic states of the isovalent species, $Si_2/Si_2^-$ and $Ge_2/Ge_2^-$.[26-28] All four diatomics have a triplet manifold comprised of a $\Sigma$ and $\Pi$ states and a higher-lying singlet manifold composed of a $\Sigma$, $\Pi$, and $\Delta$ states. The electronic states in the singlet manifold of $Si_2$ and $Ge_2$ have the ordering $^1\Delta_g$, $^1\Sigma_g^+$, and $^1\Pi_u$, however the energetic ordering in GaP and GaAs is predicted

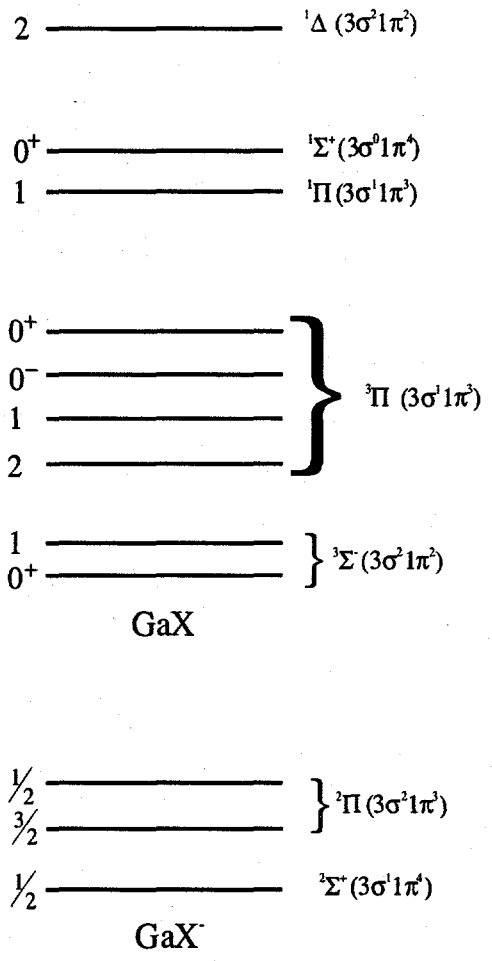


Figure 1. Energy level diagram for $GaX^-/GaX$ (X=P, As) as derived from *ab initio* calculations.

to be $^1\Pi$, $^1\Sigma^+$, and $^1\Delta$.[14-21] The anions of these species also have similar electronic structure with low-lying $^2\Sigma$ and $^2\Pi$ states. In $Si_2^-$, the $^2\Sigma^+$ state lies below the $^2\Pi$ state, but in $Ge_2^-$ the strong spin-orbit coupling pushes the $^2\Pi_{3/2}$ state below the $^2\Sigma^+$ state making it the ground state.[26,27] The relative ordering of these states in $GaP^-$ and $GaAs^-$ is experimentally unknown.

## II. Experimental

The operation of the PES and ZEKE spectrometers is similar in principle. Both experiments generate negative ions with a laser ablation/pulsed-molecular beam source, mass-select them by time-of-flight (TOF), and photodetach them with a pulsed laser. However, the electron detection schemes are very different, affording much higher resolution (2-3 $cm^{-1}$) for ZEKE than in PES (65-80 $cm^{-1}$). Although the ZEKE technique has superior resolution one can obtain photoelectron angular distributions from PES.

### A. Photoelectron spectrometer

In the anion photoelectron spectrometer,[29,30] cluster anions are generated in a laser ablation/pulsed molecular beam source. A rotating and translating single crystal disc of GaP or GaAs (Crystallode Inc.) is ablated with the second harmonic (532 nm) of a pulsed Nd:YAG laser. The laser pulses are typically 5.0-7.5 mJ/pulse before focussing onto the target with a 50 cm lens. The resulting plasma is entrained in a supersonic beam of helium and passes through a 1 ¾ inch long liquid nitrogen cooled clustering channel described elsewhere.[31] The gas pulse exits the clustering channel and passes through a skimmer into a differentially pumped region. Negative ions in the beam are extracted perpendicular to their flow direction by a pulsed electric field and injected into a linear reflectron TOF mass spectrometer,[32,33] affording a mass resolution m/Δm of 2000. Due to the natural isotope abundance of gallium ($Ga^{69}$:$Ga^{71}$, 100.0:66.4) each cluster stoichiometry has a mass distribution. In each case the most intense mass peak corresponding to $Ga^{69}As^{75}$ and $Ga^{69}P^{31}$ was studied.

## Chapter 8

Ions of desired mass are selectively photodetached with photons having wavelengths of 355 nm (3.493 eV), 416 nm (2.977 eV), and 498 nm (2.490 eV). The 355 nm wavelength is obtained by tripling the fundamental of a pulsed Nd:YAG laser. The first and second Stokes lines generated by passing the third harmonic (355 nm) through a high pressure Raman cell filled with hydrogen (325 psig) affords the 416 nm and 498 nm light, respectively. The electron kinetic energy (*eKE*) distribution is determined by TOF analysis in a 1 m field-free flight tube. The energy resolution is 8-10 meV at 0.65 eV *eKE* and degrades as $(eKE)^{3/2}$ at higher *eKE*. The data in electron kinetic energy is converted to electron binding energy (*eBE*) by subtracting it from the photon energy. All data are plotted in *eBE* as described by equation (1) where *EA* is the adiabatic electron affinity, $E^o$ is the internal energy of the neutral, and $E^-$ is the internal energy of the anion.

$$eBE = h\nu - eKE = EA + E^o - E^- \tag{1}$$

The angular dependence of the photodetachment intensity for polarized light and randomly oriented molecules is given by equation (2) below[34]

$$\frac{d\sigma}{d\Omega} = \frac{\sigma_{total}}{4\pi}\left[1 + \frac{\beta(eKE)}{2}(3\cos^2\theta - 1)\right] \tag{2}$$

where $\theta$ is the angle between the electric vector of the photon and the direction of electron ejection, $\sigma_{total}$ is the total photodetachment cross section and $\beta(eKE)$ is the asymmetry parameter ($-1 \le \beta \le 2$). Each electronic state typically has a characteristic

asymmetry parameter and can be used to distinguish peaks of overlapping electronic transitions. The asymmetry parameter of a peak can be calculated[35] using equation (3)

$$\beta(eKE) = \frac{I_{0^o} - I_{90^o}}{\frac{1}{2} I_{0^o} + I_{90^o}} \tag{3}$$

where $I_{0^o}$ and $I_{90^o}$ are the intensities of the peak taken at the polarization angles $\theta = 0^o$ and $90^o$. The laser polarization can be rotated with respect to the direction of electron detection by using a half-wave plate.

## B. ZEKE spectrometer

In the ZEKE spectrometer,[36,37] anions are generated in a similar manner to that described above, except the ablation/molecular beam source employs a rotating and translating rod instead of a disc. The anions pass through a 2 mm skimmer, are collinearly accelerated to 1 keV, and are then separated into bunches according to their masses in a 1-meter TOF tube.

After they enter the detector region, the anion of interest is photodetached by an excimer-pumped dye laser. Once the photoelectrons are produced, a time delay between 200-350 ns is applied before they are extracted coaxially by a DC electric field of approximately 3 V/cm. During this time delay, electrons with velocity components perpendicular to the molecular beam drift out of the extraction zone. Hence, only electrons with trajectories parallel to the molecular beam or zero kinetic energy are extracted. The amount of energy they acquire during the extraction depends on their

location in the extraction field, and thus their initial kinetic energies. A gated TOF detection scheme is used to selectively collect the near-zero kinetic energy electrons. The resolution of this spectrometer in the absence of rotational broadening is 2-3 $cm^{-1}$.

The electron signal is normalized to laser power and ion signal, and averaged over 1200 laser shots per point. The dyes used to obtain the ZEKE spectrum of $GaAs^-$ were Coumarin 440, Coumarin 460, Coumarin 480, Coumarin 540, Rhodamine 590, and Rhodamine 610. The dye laser wavelength is calibrated by measuring the absorption spectra of an iodine cell or a Fe-Neon cathode lamp.

## III. Results

The anion photoelectron spectra of $GaP^-$ and $GaAs^-$ taken at the laser polarization angle of $\theta=90^o$ are plotted in Figure 2. Each plot is a composite of two data sets, indicated by the break in the plot around 19,000 $cm^{-1}$, taken at the wavelengths of 498 nm and 355 nm. These two groups of peaks correspond to the triplet and singlet manifolds of neutral GaP and GaAs as discussed in the introduction and shown in Figure 1. The lower electron binding energy data (triplet manifold) was taken at a wavelength of 498 nm and the higher electron binding energy data (singlet manifold) was taken at 355 nm. In these and all other photoelectron spectra the abscissa is expressed in electron binding energy (*eBE*) and the ordinate is intensity with arbitrary units normalized to the number of laser shots.

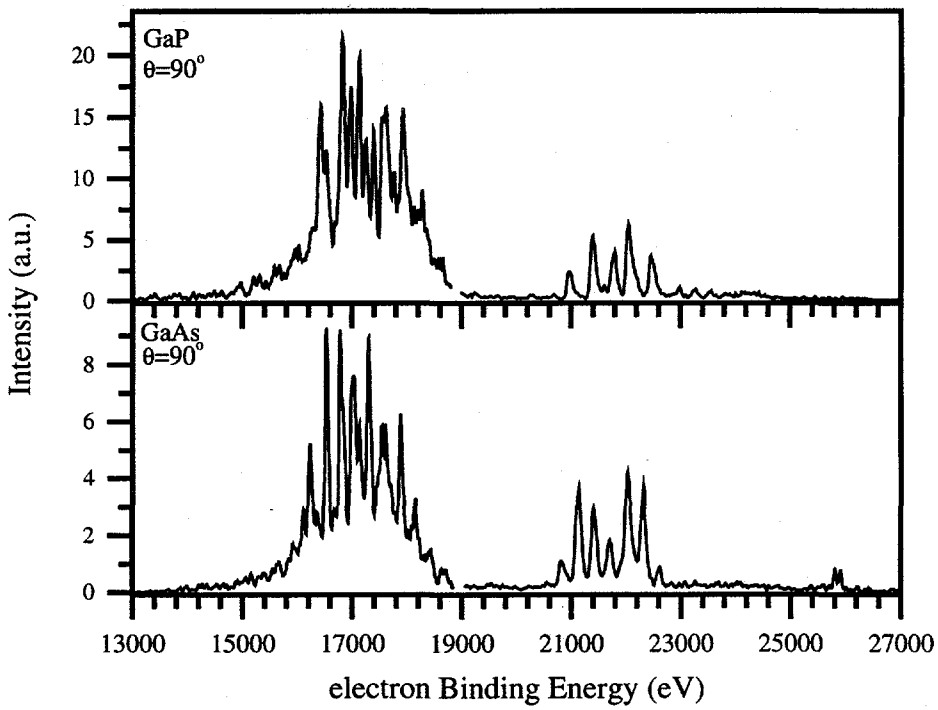


Figure 2. Composite plots of the anion photoelectron spectra of $GaP^-$ and $GaAs^-$ taken the polarization angles, $\theta=90^\circ$ and $0^\circ$. See text for further description.

The spectra of the two III-V diatomics in Figure 2 have several common features. The triplet manifolds of GaP and GaAs are congested with many transitions and show a partially resolved tail extending towards lower binding energies. The two triplet manifolds contain approximately the same number of peaks with similar intensities. The singlet manifolds for the two species also show the same number of major features, but are far less congested. Some differences between the spectra are noted. First the $GaP^-$ spectrum shows a progression of three small equally spaced peaks beginning around ~23,000 $cm^{-1}$ which are not present in the $GaAs^-$ spectrum, second, the $GaAs^-$ spectrum

shows a feature at ~26,000 $cm^{-1}$ which is not present in the $GaP^-$ spectra and third, the triplet manifold of GaP is more strongly polarization dependent than that of GaAs.

Figures 3 and 4 show expanded views of the singlet manifolds of GaP and GaAs taken at the polarization angles, $\theta=0^\circ$ and $90^\circ$, and a wavelength of 355 nm. Peaks E & F and I & K clearly dominate the $\theta=0^\circ$ spectra, while peaks A, B, & D and B, C, D, & F become major features in the $\theta=90^\circ$ spectra. This indicates that we have at least two electronic transitions in both species. The $\beta$ parameters located in the top panels quantitatively confirm our observation and further show that there are two more electronic transitions present in the GaP singlet manifold, which are absent in GaAs.

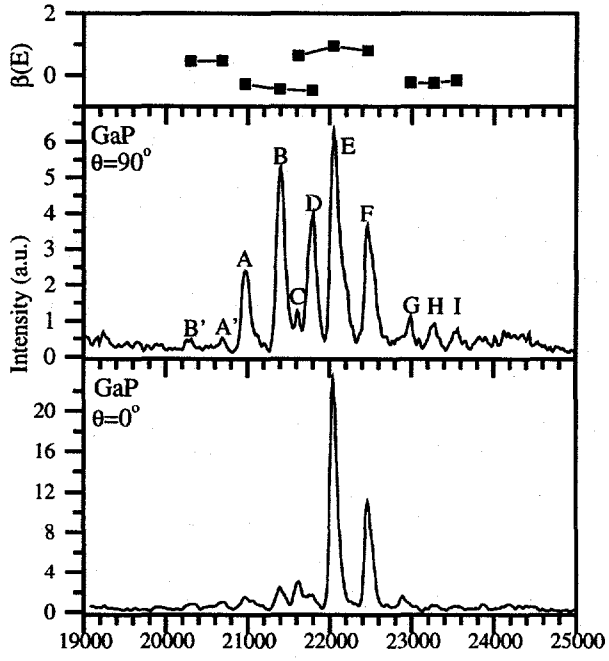


Figure 3. Anion photoelectron spectrum (bottom panel) of $GaP^-$ singlet manifold taken at 3.493 eV photon energy and $\theta=90^\circ$. Experimental $\beta$ parameters at the same photon energy are plotted in the top panel.

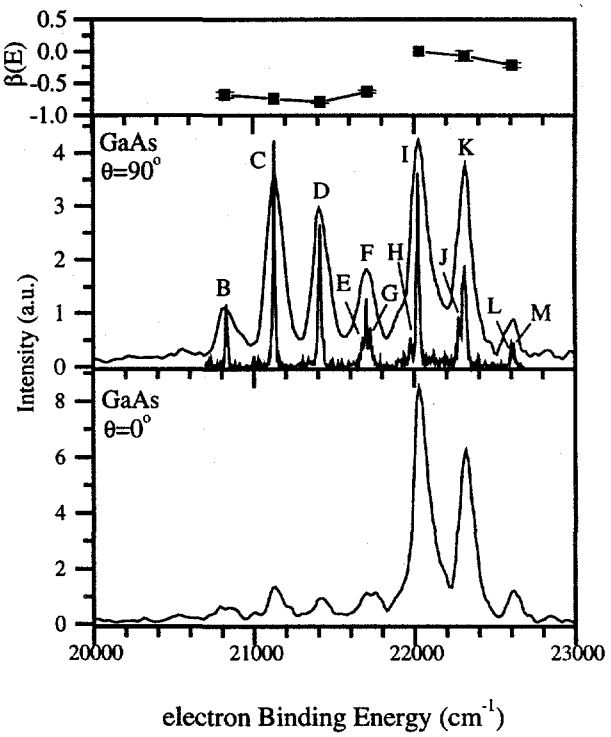


Figure 4. The bottom panel shows the ZEKE spectrum (solid gray) and anion photoelectron spectrum (black line) of $GaAs^-$ singlet manifold taken at 3.493 eV photon energy and $\theta=54.7^\circ$. Experimental $\beta$ parameters at the same photon energy (top panel).

Figures 5 and 6 show expanded views of the triplet manifolds of GaP and GaAs taken at the polarization angles, $\theta=0^\circ$ and $90^\circ$, and a wavelength of 498 nm. Each $GaAs^-$ anion photoelectron spectrum is also superimposed with the ZEKE spectrum. The peaks in the ZEKE spectra are much narrower than the photoelectron spectra and every peak in the photoelectron spectrum also appears in the ZEKE spectrum with similar intensities except for peaks A and C in the triplet manifold. The $\theta=0^\circ$ spectra of both species show a peak that clearly dominates the spectrum labeled as A. The majority of the transitions lie towards higher electron binding energy and are quite congested. The $\beta$ parameters for

the triplet manifold of $GaP^-$ can be arranged in three groups: E'-$B_2$', $B_1$'-B, and D-S. The triplet manifold of $GaAs^-$ is similar, but seems to have diminished intensity of the lowest binding energy group of transitions as observed for GaP.

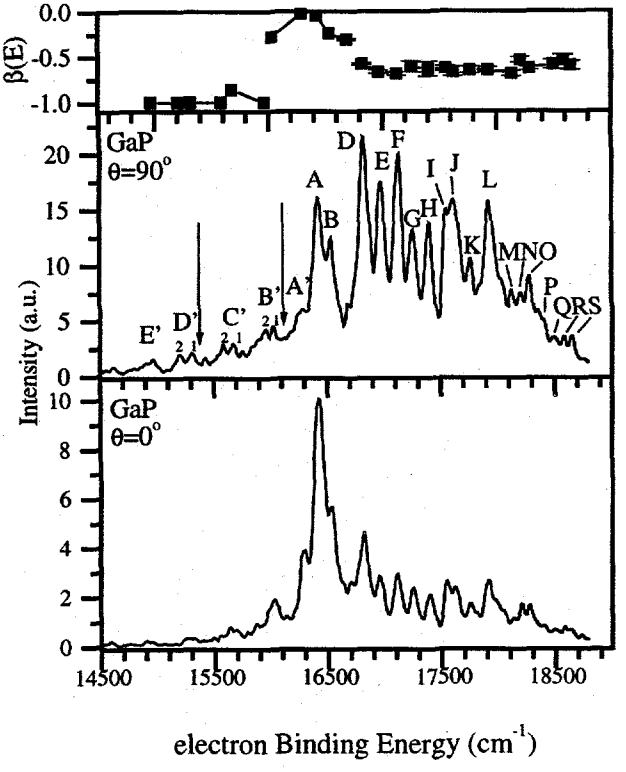


Figure 5. Anion photoelectron spectrum (bottom panel) of $GaP^-$ triplet manifold taken at 2.490 eV photon energy and θ=90°. Experimental β parameters at the same photon energy are plotted in the top panel.

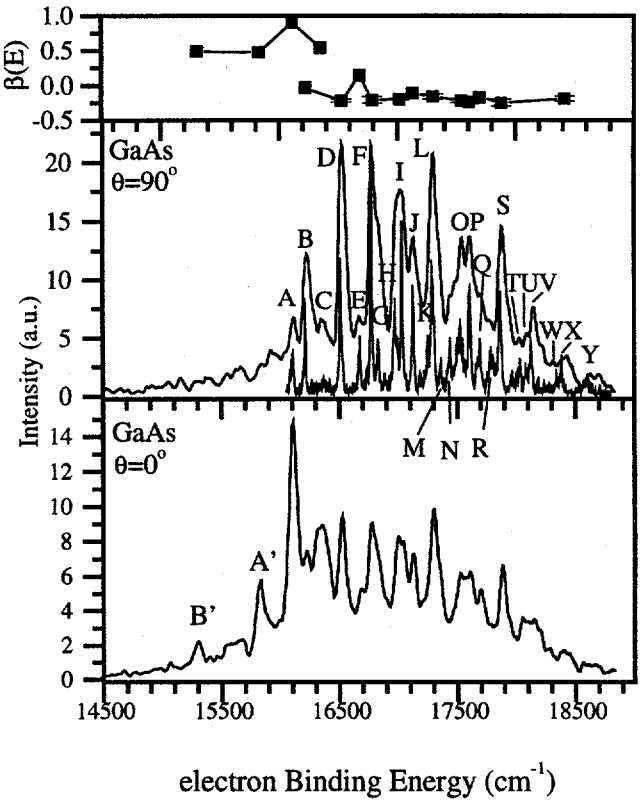


Figure 6. The bottom panel shows the ZEKE spectrum (solid gray) and anion photoelectron spectrum (black line) of $GaAs^-$ triplet manifold taken at 2.490 eV photon energy and $\theta$=54.7°. The top panel shows a plot of the experimental $\beta$ parameters at the same photon energy.

## IV. Analysis

### A. General

Both of the III-V diatomics are calculated to have the same energy ordering of electronic states as shown in Figure 1.[13-21,24,25] On the right side of the diagram we have the electronic state and the orbital occupancy. On the left is the total angular momentum

quantum number, Ω, for Hund's case (c) defined as the sum of the spin (Σ) and orbital angular momentum(Λ). The neutral ground $^3\Sigma^-$ ($...3\sigma^2 1\pi^2$) and excited $^3\Pi$ ($...3\sigma^1 1\pi^3$) states comprise the triplet manifold. Lying higher in energy are several singlet states, which define the singlet manifold. Here we have the $^1\Pi$ ($...3\sigma^1 1\pi^3$), $^1\Sigma^+$ ($...3\sigma^0 1\pi^4$), $^1\Delta$ ($...3\sigma^2 1\pi^2$) states. Based on our previous work on the silicon and germanium dimers, we will describe GaP in terms of Hund's case (a) and GaAs as Hund's case (c), the main difference being that we observe a splitting of $^3\Pi_0$ in GaAs but not in GaP.

From the anion ground state $^2\Sigma^+$ ($...3\sigma^1 1\pi^4$), transitions to neutral states with the electronic configuration of ($...3\sigma^2 1\pi^2$) are not one-electron transitions and therefore should be weak or absent. Neutral states with this configuration include the ground $^3\Sigma^-$ and excited $^1\Delta$ and 2 $^1\Sigma^+$ states. From the excited anion state $^2\Pi$ ($...3\sigma^2 1\pi^3$), only the transition to the $^1\Sigma^+$ ($...3\sigma^0 1\pi^4$) state is forbidden by the one-electron selection rule. We begin our discussion with the singlet manifolds of GaX because they are the least congested and afford information about the anion that is valuable for the assignment of the peaks in the triplet manifold.

In an effort to better characterize the electronic states observed, we have carried out Franck-Condon (FC) simulations. The calculations are performed assuming harmonic oscillator potentials. The FC simulations are carried out by iteratively optimizing the vibrational frequencies and bond length changes that most accurately reproduce the experimental data (a.k.a. "χ by eye"). In many instances the results of these simulations are given but the graphical simulation is not shown.

## B. Singlet Manifolds

### GaP

The β parameters plotted in the top panel of Figure 3 show that the peaks can be divided into four groups. The most intense features arise from two groups formed from peaks A, B, & D and C, E, & F. The spacing between A,B and C,E is the same (436 $cm^{-1}$) and different from the splitting of B,D (390 $cm^{-1}$) and E,F (428 $cm^{-1}$). The spacing and intensities of the peaks A and C indicate they are vibrational hot bands coming from the same anion state. Peaks B and E are the origins, and D and F are the first quanta of vibration spaced 390 ± 10 $cm^{-1}$ and 428 ± 8 $cm^{-1}$ from their respective origins.

Assuming that only one-electron transitions are allowed, according to Figure 1 there are two possibilities for the assignment of the two states we observe. If the anion ground state is $^2\Sigma^+$, transitions to the $^1\Pi$ and $^1\Sigma^+$ states are allowed, and if the ground state is $^2\Pi$ we should observe transitions to the $^1\Pi$ and $^1\Delta$ states. Manna *et al.*[14] predict the $^1\Pi$ and $^1\Sigma^+$ states to be separated by 401 $cm^{-1}$ (MRSDCI), while the $^1\Pi$ and $^1\Delta$ states are separated by 3225 $cm^{-1}$ (MRSDCI). Additionally, Archibong *et al.*[13] calculate the $^2\Sigma^+$ and $^2\Pi$ anion frequencies to be 420 $cm^{-1}$ and 371 $cm^{-1}$ (B3LYP), respectively. The two states we observe are separated by 653 $cm^{-1}$ and originate from the same anion electronic state with a vibrational frequency of 436 $cm^{-1}$. We therefore conclude that the anion ground state is $^2\Sigma^+$ and we assign peaks B and E to the origins of the $^1\Pi \leftarrow ^2\Sigma^+$ and $^1\Sigma^+ \leftarrow ^2\Sigma^+$ photoelectron transitions, respectively.

Because we have significant intensity from vibrational hotbands, we might expect to see contributions from electronic hotbands. Peaks B' and A' are located at an electron binding energy of 20,301 $cm^{-1}$ and 20,688 $cm^{-1}$, respectively and are separated by 387

Table 1. GaP singlet manifold peak positions and assignments.

| Peak | Position | Assignment |
|---|---|---|
| B' | 20301 | $^1\Pi \leftarrow {}^2\Pi_{3/2}$ origin |
| A' | 20688 | $^1\Pi(v=1) \leftarrow {}^2\Pi_{3/2}$ |
| A | 20970 | $^1\Pi \leftarrow {}^2\Sigma^+(v=1)$ |
| B | 21394 | $^1\Pi \leftarrow {}^2\Sigma^+$ origin |
| C | 21616 | $^1\Sigma^+ \leftarrow {}^2\Sigma^+(v=1)$ |
| D | 21789 | $^1\Pi\ (v=1) \leftarrow {}^2\Sigma^+$ |
| E | 22047 | $^1\Sigma^+ \leftarrow {}^2\Sigma^+$ origin |
| F | 22463 | $^1\Sigma^+\ (v=1) \leftarrow {}^2\Sigma^+$ |
| G | 22987 | $^1\Delta \leftarrow {}^2\Pi_{3/2}$ origin |
| H | 23269 | $^1\Delta(v=1) \leftarrow {}^2\Pi_{3/2}$ |
| I | 23543 | $^1\Delta(v=2) \leftarrow {}^2\Pi_{3/2}$ |

$cm^{-1}$. This spacing matches the frequency of the $^1\Pi$ state, however Figure 3 shows that these low intensity features have a $\beta$ parameter different from the previously assigned $^1\Pi \leftarrow {}^2\Sigma^+$ photoelectron transition indicating that they arise from a different anion state. The $^1\Pi$ state is also one-electron accessible from the $^2\Pi$ excited anion state and we assign peak B' to the origin of the $^1\Pi \leftarrow {}^2\Pi_{3/2}$ transition. This affords a $^2\Sigma^+ - {}^2\Pi_{3/2}$ anion splitting of 1093 $cm^{-1}$, which is comparable to the $^2\Sigma^+ - {}^2\Pi$ splitting of 805 $cm^{-1}$ (CCSD(T)) calculated by Archibong *et al.* [13] Peaks G, H, and I are spaced by 285 $cm^{-1}$. The only electronic state calculated to have a similar frequency is the $^1\Delta$ state (278 $cm^{-1}$).[14] This state is also one-electron accessible from the $^2\Pi$ excited anion state and we assign peaks G, H, and I to the $^1\Delta \leftarrow {}^2\Pi_{3/2}$ transition. Peak assignments and positions are located in Table 1.

## GaAs

We can analyze the ZEKE spectrum of the GaAs singlet manifold in an analogous manner to our analysis of the GaP singlet manifold. The β parameters plotted in Figure 4 indicate that we have at least two electronic states. The ZEKE spectrum shows that peaks C, D, F, and H form a progression with a frequency of 288 $cm^{-1}$ and peak B is a hotband transition giving an anion frequency of 297 $cm^{-1}$. Peaks I, K, and L form another progression with a frequency of 290 $cm^{-1}$, where peak G is a hotband transition with the same anion frequency of 299 $cm^{-1}$ hence, the two transitions originate from the same anion state. We therefore have two progressions with apparent origins at C and I, separated by 898 $cm^{-1}$. We see no significant contributions of transitions from excited anion electronic states.

Based on similarity with GaP, we assign peaks C and I to the origins of the $^1\Pi \leftarrow {}^2\Sigma^+$ and $^1\Sigma^+ \leftarrow {}^2\Sigma^+$ photoelectron transitions, respectively. Balasubramanian's calculation of the $^2\Sigma^+$ ground state frequency of 303 $cm^{-1}$ (SOCI) is in closer agreement with our measurement than Meier's value of the 248 $cm^{-1}$ (MRDCI). Our experiment affords a $^1\Pi - {}^1\Sigma^+$ energy separation of 898 $cm^{-1}$. Manna *et al.*[16] have the closest calculated energy separation of 664 $cm^{-1}$. All other calculations over-estimate this splitting by a factor of two.[15,17,21] Table 2 summarizes the GaAs singlet manifold assignments.

Table 2. GaAs singlet manifold peak positions and assignments.

| Peak | ZEKE Position | PES Position | Assignment |
|---|---|---|---|
| | | 20567 | |
| A | 20722 | | |
| B | 20829 | 20827 | $^1\Pi(v=0) \leftarrow {}^2\Sigma^+(v=1)$ |
| | | 21026 | |
| C | 21126 | 21130 | $^1\Pi \leftarrow {}^2\Sigma^+$ origin |
| | 21404? | | |
| D | 21413 | 21418 | $^1\Pi(v=1) \leftarrow {}^2\Sigma^+$ |
| E | 21678 | | $^1\Pi(v=3) \leftarrow {}^2\Sigma^+(v=1)$ |
| F | 21702 | | $^1\Pi(v=2) \leftarrow {}^2\Sigma^+$ |
| G | 21725 | 21711 | $^1\Sigma^+(v=1) \leftarrow {}^2\Sigma^+(v=1)$ |
| H | 21976 | | $^1\Pi(v=4) \leftarrow {}^2\Sigma^+(v=1)$ |
| | 21901? | 21906 | small |
| I | 22024 | 22034 | $^1\Sigma^+ \leftarrow {}^2\Sigma^+$ origin |
| N1? | 22107? | | small |
| J | 22278 | | |
| K | 22315 | 22314 | $^1\Sigma^+(v=1) \leftarrow {}^2\Sigma^+$ |
| L | 22602 | 22610 | $^1\Sigma^+(v=2) \leftarrow {}^2\Sigma^+$ |
| M | 22617 | | |
| Z0 | | 25705 | |
| Z1 | | 25810 | |
| Z2 | | 25903 | |
| Z3 | | 25939 | |

## C. Triplet Manifolds

### GaP

In the singlet manifold we have shown transitions resulting from the two anion electronic states, $^2\Sigma^+$ and $^2\Pi_{3/2}$. Figure 1 indicates that three photoelectron transitions are one-electron allowed from these two anion states. The $^3\Pi$ spin-orbit states can be

accessed through a one-electron transition from either of the $^2\Sigma^+$ and $^2\Pi$ anion states, while the $^3\Sigma^-$ neutral ground state can only be accessed from the $^2\Pi$ anion excited states. The $\beta$ parameters in Figure 5 also show evidence of three different photoelectron transitions.

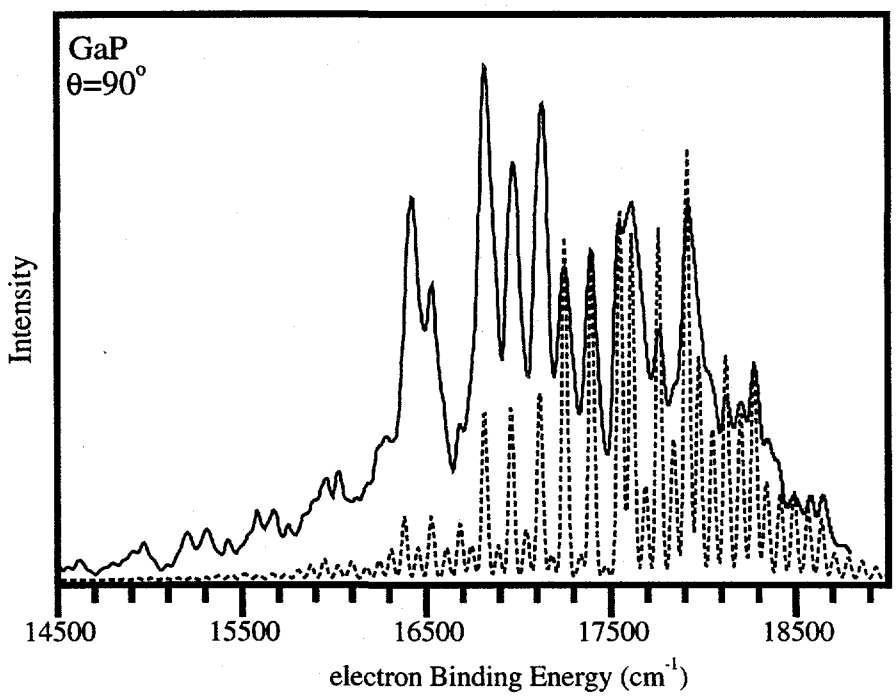


Figure 7. The photoelectron spectrum of GaP taken at $\theta$=90° and a wavelength of 498 nm (solid line). The spectrum is superimposed with a FC simulation as discussed in the text (dashed line).

We expect the highest energy transition to be the $^3\Pi \leftarrow ^2\Sigma^+$ transition and this should correspond to peaks D-S. Within the Hund's case (a) framework and in analogy to $Si_2$ we expect to see the $^3\Pi$ state split into three spin-orbit states: $^3\Pi_2$, $^3\Pi_1$, and $^3\Pi_0$. Thus among peaks D-S we must look for a repeating pattern of three equally spaced

peaks corresponding to these spin-orbit states. Peaks D, E, & F and G, H, & I fit this pattern. The spacing within each triplet of peaks is ~150 $cm^{-1}$, giving a $^3\Pi_2$–$^3\Pi_0$ separation to be ~300 $cm^{-1}$. Using peaks G, H, and I as the origins of the $^3\Pi$ transitions, we are able to adequately simulate peaks D-S shown in Figure 7. As expected, calculations show the $^3\Pi$ spin-orbit states to have the same bond distances and vibrational frequencies,[14] hence the simulation, shown in Figure 7, is performed using the same bond length changes and anion and neutral frequencies of 436 $cm^{-1}$ and 363 $cm^{-1}$, respectively, for all three spin-orbit states. The anion frequency is in agreement with the vibrational hotband transitions we assigned to the $^2\Sigma^+$ anion state in our analysis of the singlet manifold. Hence, we assign peaks D, E, and F to the v=1 vibrational hotbands of the $^2\Sigma^+$ anion ground state. In good agreement with our results, Archibong *et al.* and Manna *et al.* report the $^3\Pi$ neutral frequency to be 351 $cm^{-1}$ (B3LYP) and 357 $cm^{-1}$ (MRSDCI), respectively.[13,14] However the calculated $^3\Pi_2$–$^3\Pi_0$ spin-orbit splitting is only 128 $cm^{-1}$ (MRSDCI)[14] compared to our value of ~300 $cm^{-1}$.

Now we consider peaks $B_1$'–B. Possible one-electron transitions are the $^3\Sigma^-$ $\leftarrow{}^2\Pi_{3/2}$ and $^3\Pi$ $\leftarrow{}^2\Pi_{3/2}$ transitions. However, neither is likely based on the intensities of the electronic hotbands observed in the singlet manifold. Another possibility is the $^3\Sigma^-$ $\leftarrow{}^2\Sigma^+$ transition, which we would expect to be a weak or absent transition because it is a two-electron process. In addition the calculated bond lengths[13] of these two states are significantly different and we would expect to see an extended vibrational progression instead of the observed narrow profile, which does not show a progression with the known ground state vibrational frequency of 283.6 $cm^{-1}$.[12] Another possibility for the

appearance of features $B_1$'-B is an autodetachment process. Autodetachment involves fan optical transition to a short-lived anion state, which further decays to states of the corresponding neutral through the loss of an electron. Wavelength dependent intensities of spectral features are the signature of an autodetachment process since the optical transition must be resonant. Figure 8 shows the $\theta=0^{\circ}$ and $90^{\circ}$ spectra of the GaP triplet

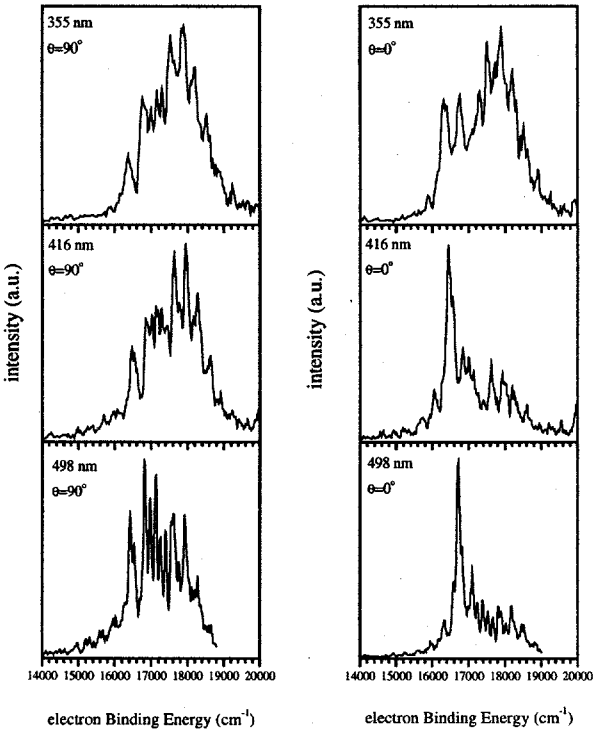


Figure 8. Photoelectron spectra of the GaP triplet manifold taken at the polarizations of $\theta=0$, $90^{\circ}$ and wavelengths of 355 nm, 416 nm, and 498 nm. Note the dramatic change between the 416 nm and 355 nm spectra at the polarization $\theta=0^{\circ}$.

manifold taken at wavelengths of 355, 416, and 498 nm. The biggest intensity contrast is between the $\theta=0^{\circ}$ spectra taken at 355 and 416 nm, where peak A changes dramatically with respect to the rest of the spectrum. This indicates that the anion absorption must be broad, covering at least 498-416 nm. Since we have already observed the $^3\Pi$ state the only energetically possible state that could correspond to peaks $B_1$'–B is the $^3\Sigma^-$ ground state. We assign peak A to the $^3\Sigma^-(v=0) \leftarrow ^2\Sigma^+(v=0)$ transition, affording an electron affinity of $2.036 \pm 0.008$ eV. The theoretical prediction of 1.96 eV (B3LYP) by Archibong *et al.* is in good agreement with our result.[13] This yields a $^3\Pi$-$^3\Sigma^-$ neutral splitting of 831 $cm^{-1}$. Manna *et al.* and Archibong *et al.* calculate the splitting to be 782 $cm^{-1}$ (MRSDCI) and 734 $cm^{-1}$ (CCSD(T)), respectively.[13,14] The energy separation of peaks A and A' is 134 $cm^{-1}$. We have determined the anion frequency to be 436 $cm^{-1}$ and the neutral frequency[12] has been measured to be 283.6 $cm^{-1}$ affording a frequency difference of 152 $cm^{-1}$. The assignment of A' to the, $^3\Sigma^-(v=1) \leftarrow ^2\Sigma^+(v=1)$ sequence band is reasonable with in the error of our experiment. We find no satisfactory assignment for peaks B1' and B at this time. The analogous arguments apply to peaks A', A and C of the GaAs triplet manifold and will be discussed later.

This leaves us with peaks E'-B1' which we assign to the overlapping $^3\Sigma^- \leftarrow ^2\Pi_{3/2}$ and $^3\Pi \leftarrow ^2\Pi_{3/2}$ transitions. Peaks B2', C2', and D2' have a spacing of 379 $cm^{-1}$ and peaks D1' and C1' are ~100 $cm^{-1}$ to the blue of C2' and D2'. However, the ~100 cm-1 splitting is similar to the $Si_2^-$ $^2\Pi$ spin-orbit splitting of 115 $cm^{-1}$ and the 369 $cm^{-1}$ is in agreement with Archibong's $^2\Pi$ frequency of 371 $cm^{-1}$ (B3LYP). These peaks do show a pattern

Table 3. GaP triplet manifold peak positions and assignments.

| Peak | Position | Assignment |
|---|---|---|
| E' | 14966 | $^3\Pi, ^3\Sigma^- \leftarrow ^2\Pi_{3/2}$ |
| D2' | 15204 | $^3\Pi, ^3\Sigma^- \leftarrow ^2\Pi_{3/2}$ |
| D1' | 15312 | $^3\Pi, ^3\Sigma^- \leftarrow ^2\Pi_{3/2}$ |
| C2' | 15583 | $^3\Pi, ^3\Sigma^- \leftarrow ^2\Pi_{3/2}$ |
| C1' | 15675 | $^3\Pi, ^3\Sigma^- \leftarrow ^2\Pi_{3/2}$ |
| B2' | 15962 | $^3\Pi, ^3\Sigma^- \leftarrow ^2\Pi_{3/2}$ |
| B1' | 16029 | $^3\Pi_2 \leftarrow ^2\Pi_{3/2}$ (v=1) |
| A' | 16287 | $^3\Sigma^-$(v=1) $\leftarrow ^2\Sigma^+$(v=1) |
| A | 16421 | $^3\Sigma^- \leftarrow ^2\Sigma^+$ origin |
| B | 16532 | ? $^3\Pi_1 \leftarrow ^2\Sigma^+$(v=2)? |
| C | 16688 | ? $^3\Pi_0 \leftarrow ^2\Sigma^+$(v=2)? |
| D | 16817 | $^3\Pi_2 \leftarrow ^2\Sigma^+$(v=1) |
| E | 16962 | $^3\Pi_1 \leftarrow ^2\Sigma^+$(v=1) |
| F | 17123 | $^3\Pi_0 \leftarrow ^2\Sigma^+$(v=1) |
| G | 17252 | $^3\Pi_2 \leftarrow ^2\Sigma^+$ origin |
| H | 17400 | $^3\Pi_1 \leftarrow ^2\Sigma^+$ origin |
| I | 17551 | $^3\Pi_0 \leftarrow ^2\Sigma^+$ origin |
| J | 17618 | $^3\Pi_2$(v=1) $\leftarrow ^2\Sigma^+$ |
| K | 17766 | $^3\Pi_1$(v=1) $\leftarrow ^2\Sigma^+$ |
| L | 17922 | $^3\Pi_0$(v=1) $\leftarrow ^2\Sigma^+$ |
| M | 18131 | $^3\Pi_1$(v=2) $\leftarrow ^2\Sigma^+$ |
| N | 18205 | $^3\Pi_0$(v=3) $\leftarrow ^2\Sigma^+$(v=1) |
| O | 18285 | $^3\Pi_0$(v=2) $\leftarrow ^2\Sigma^+$ |
| P | 18349 | $^3\Pi_2$(v=3) $\leftarrow ^2\Sigma^+$ |
| Q | 18494 | $^3\Pi_1$(v=3) $\leftarrow ^2\Sigma^+$ |
| R | 18580 | $^3\Pi_0$(v=4) $\leftarrow ^2\Sigma^+$(v=1) |
| S | 18642 | $^3\Pi_0$(v=3) $\leftarrow ^2\Sigma^+$ |

however, no assignments are clear. With the energetics we have determined so far, the origins of the $^3\Sigma^- \leftarrow ^2\Pi_{3/2}$ and $^3\Pi \leftarrow ^2\Pi_{3/2}$ transitions are calculated to be at binding energies of 15,328 $cm^{-1}$ and 16,159 $cm^{-1}$, respectively. These energies are indicated by the arrows in Figure 5, however they do not seem to correlate to any of the spectral

features. All assignments and peak positions are located in Table 3. The summarized molecular constants for GaP/GaP$^-$ are located in Table 5.

Table 5. Comparison of experimental and theoretical molecular constants of GaP.[a]

| Ref. | Method | $X\,^2\Sigma^+$ | $A\,^2\Pi_{3/2}$ | $X\,^3\Sigma_1^-$ | $X\,^3\Sigma_{0+}^-$ | $A\,^3\Pi_2$ | $B\,^3\Pi_1$ | $C\,^3\Pi_{0+}$ | $^3\Pi_{0-}$ | $D\,^1\Pi$ | $E\,^1\Sigma^+$ | $F\,^1\Delta$ | EA |
|---|---|---|---|---|---|---|---|---|---|---|---|---|---|
| 13[b] | CCSD(T) | 0 | 805 | 0 | | 734 | | | | | 5585 | | |
| | | 458 | 371[‡] | 302 | | 351[‡] | | | | | 445[‡] | | |
| | | 2.139 | 2.268 | 2.447 | | 2.447 | | | | | 2.238 | | |
| 14 | MRSDCI | | | 5 | 0 | 716 | 788 | 834 | 844 | 5605 | 6006 | 8830 | |
| | | | | 265 | 266 | 358 | 357 | 359 | 358 | 387 | 439 | 278 | |
| | | | | 2.496 | 2.498 | 2.260 | 2.258 | 2.257 | 2.260 | 2.229 | 2.105 | 2.478 | |
| | | | | | | | | | | | | | |
| Experiment | | 0 | 1093 | 0 | | 831 | 979 | 1130 | | 4973 | 5626 | 7659 | 2.036 ± 0.008 |
| | | 436 | | 283.6[c] | | 363 | 363 | 363 | | 390 ± 10 | 428 ± 8 | 285 | |

[a] For each calculation the first row gives the splitting, the second row gives the vibrational frequency, and the third row gives the bond length.
[b] Reference [13] calcuations carried out at CCSD(T)-F14/6-311+G(2df).
[‡] Carried out at B3LYP/6-311+G(2df).
[c] Reference [12], infrared matrix absorption experiment.

## GaAs

The higher resolution ZEKE spectrum, shown in Figure 6, allows us to easily pick out underlying vibrational structure. Peaks D, F, I, and L form a progression with a frequency of 260 cm$^{-1}$. Peaks P, S, V, X, and Y form the progression having a frequency of 258 cm$^{-1}$. In addition, peak B is assigned as a vibrational hot band, giving an anion frequency of 302 cm$^{-1}$ in agreement with the previously observed vibrational hotband transitions in the single manifold. Balasubramanian, Meier, and Manna *et al.* calculate the $^3\Pi$ frequency to be 236, 260, and 234 cm$^{-1}$, respectively.[15-17]

The absence of electronic hot band assignments in the singlet state suggests that in the triplet manifold of GaAs we are primarily going to see the $^3\Pi \leftarrow\!- {}^2\Sigma^+$ transition. The two progressions observed in the ZEKE spectrum having their origins with peak D and P are separated by 1093 cm$^{-1}$. The calculated energy separation[16] of the $^3\Pi_2$ and $^3\Pi_{0-}$ states

is ~900 $cm^{-1}$ and the experimental energy separation in isoelectronic $Ge_2$ is 968 $cm^{-1}$.[27] We assign peaks D and P to the $^3\Pi_2 \leftarrow ^2\Sigma^+$ and $^3\Pi_{0^-} \leftarrow ^2\Sigma^+$ transitions, respectively.

Transitions to all four possible $^3\Pi_i$ spin-orbit states are possible and it is curious that we see only two pronounced progressions in the spectrum. The calculations of Manna *et al.* suggest a possible explanation.[16] They indicate that the $^3\Pi_1$ and $^3\Pi_{0^+}$ states are mixed with the $^3\Sigma^-_1$ and $^3\Sigma^-_{0^+}$ states, respectively. To the degree these states are mixed we would expect them to differ in electronic character from the $^3\Pi_2$ and $^3\Pi_{0^-}$ states. This mixing could account for the difference in the calculated ground state ($^3\Sigma^-_{0^+}$)[9,16] and the experimentally observed ground state ($^3\Sigma^-_1$).[9,16]

Peaks O, R, and T are separated by ~270 $cm^{-1}$ in agreement with what we expect for the frequency of a $^3\Pi$ spin-orbit state. Peak O is assigned as the origin of the $^3\Pi_{0^+}$ state and is separated from the $^3\Pi_{0^-}$ state by 83 $cm^{-1}$. The splitting of the $^3\Pi_0$ states is calculated[16] to be 32 $cm^{-1}$, however the splitting measured[27] for isoelectronic $Ge_2$ is 112 $cm^{-1}$. The assignment of the $^3\Pi_1$ state is less obvious. The calculations by Manna *et al.*[16] predict that the $\Omega$=2, 1, 0 states of GaAs are equally separated in energy by ~500 $cm^{-1}$. Possible candidates for the assignment of this state are peaks H and J.

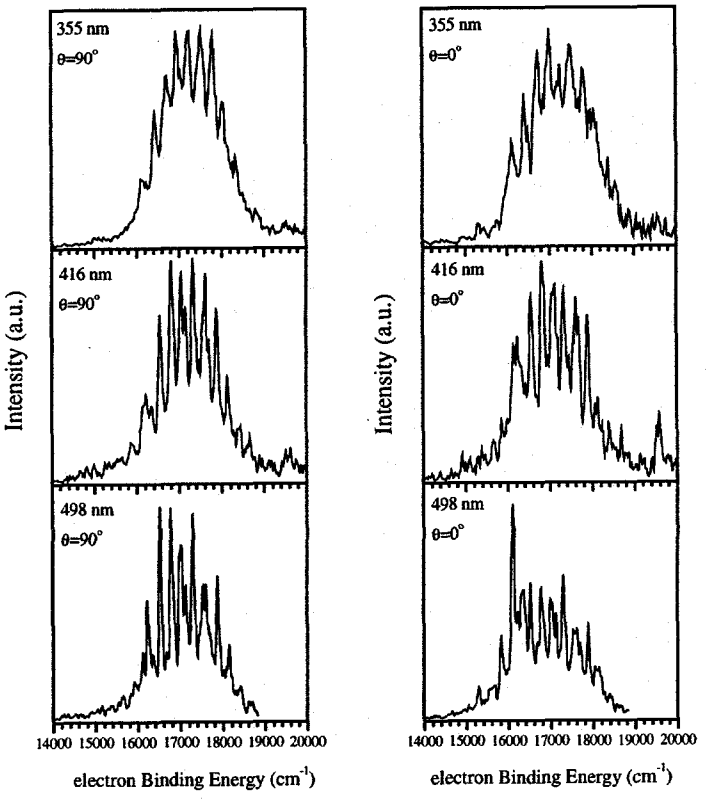


Figure 9. Photoelectron spectra of the GaAs triplet manifold taken at the polarizations of θ=0, 90° and wavelengths of 355 nm, 416 nm, and 498 nm. Note the dramatic change between the 416 nm and 355 nm spectra at the polarization θ=0°.

The anion photoelectron spectra of Figure 9 show that the intensities of peaks A', A, and C are wavelength dependent and in analogy to features A', A, and B of the GaP triplet manifold, we assign these features to an autodetachment process. We do not expect to see intensity due to autodetachment in the ZEKE spectrum. Peak A in the ZEKE spectrum shows only minor intensity while no signal is observed for peaks A' and

C. We assign peak A' and A to the indirect $^3\Sigma^-(v=0) \leftarrow ^2\Sigma^+(v=1)$ and $^3\Sigma^-(v=0) \leftarrow ^2\Sigma^+(v=0)$ transitions, respectively. The energy separation between these peaks is 284 $cm^{-1}$, which is reasonably close to the previously determined anion ground state frequency of 298 $cm^{-1}$. The assignment of peak A gives us an adiabatic electron affinity of 2.047 ± 0.001 eV. This is certainly with in the error bars of the Smalley measurement, 2.1 ± 0.1 eV.[38] The electron affinities calculated by Balasubramanian and Meier *et al.*, 1.4 ± 0.02 eV (SOCI) and 1.51 eV (MRDCI), respectively, are clearly too low. However, Lou *et al.* report a much closer value of 1.82 eV employing the more empirical DFT method using the local density functional (LDF).[24]

The patternless non-negligible intensity extending towards lower electron binding energy from peak A is attributed to electronic hotband transitions, $^3\Sigma^- \leftarrow ^2\Pi_{3/2}$ and $^3\Pi \leftarrow ^2\Pi_{3/2}$. Several other peaks shown in Figure 6 and listed in Table 4 remain to be assigned. With the experimental and theoretical information available so far, we are not able to gain further insight into their identity. Table 4 shows the proposed assignments and peak positions for the triplet manifold and Table 6 summarizes the molecular constants and compares them with *ab initio* calculations and other experimental results.

Table 4. GaAs triplet manifold peak positions and assignments.

| Peak | ZEKE Position | PES Position | Assignment |
|---|---|---|---|
| B' | | 15304 | |
| A' | | 15827 | |
| A | 16109 | 16111 | $^3\Sigma^- \leftarrow {}^2\Sigma^+$ origin |
| B | 16211 | 16224 | $^3\Pi_2(v=0) \leftarrow {}^2\Sigma^+(v=1)$ |
| C | | 16353 | |
| D | 16511 | 16528 | $^3\Pi_2 \leftarrow {}^2\Sigma^+$ origin |
| E | 16677 | 16682 | ??? |
| | 16736 | | $^3\Pi_2(v=2) \leftarrow {}^2\Sigma^+(v=1)$ |
| F | 16775 | 16792 | $^3\Pi_2(v=1) \leftarrow {}^2\Sigma^+(v=0)$ |
| G | 16832 | | $^3\Pi_1(v=0) \leftarrow {}^2\Sigma^+(v=1)$ |
| | 16886 | | |
| H | 16975 | | $?^3\Pi_1 \leftarrow {}^2\Sigma^+$origin? |
| | 16992 | | $^3\Pi_2(v=3) \leftarrow {}^2\Sigma^+(v=1)$ |
| I | 17033 | 17019 | $^3\Pi_2(v=2) \leftarrow {}^2\Sigma^+(v=0)$ |
| J | 17126 | 17130 | $?^3\Pi_1 \leftarrow {}^2\Sigma^+$origin? |
| | 17191 | | |
| K | 17250 | | $^3\Pi_2(v=4) \leftarrow {}^2\Sigma^+(v=1)$ |
| L | 17286 | 17301 | $^3\Pi_2(v=3) \leftarrow {}^2\Sigma^+(v=0)$ |
| M | 17364 | | |
| N | 17440 | 17430 | |
| | 17501 | | $^3\Pi_2(v=5) \leftarrow {}^2\Sigma^+(v=1)$ |
| O | 17529 | 17540 | $^3\Pi_{0+} \leftarrow {}^2\Sigma^+$ origin |
| | 17547 | | $^3\Pi_2(v=4) \leftarrow {}^2\Sigma^+(v=0)$ |
| P | 17609 | 17607 | $^3\Pi_{0-} \leftarrow {}^2\Sigma^+$ origin |
| | 17672 | | |
| Q | 17694 | 17696 | ???? |
| R | 17782 | | $^3\Pi_{0+}(v=1) \leftarrow {}^2\Sigma^+(v=0)$ |
| S | 17865 | 17882 | $^3\Pi_{0-}(v=1) \leftarrow {}^2\Sigma^+(v=0)$ |
| | 17968 | | $^3\Pi_{0+}(v=4) \leftarrow {}^2\Sigma^+(v=2)$ |
| | 18010 | | $^3\Pi_{0+}(v=3) \leftarrow {}^2\Sigma^+(v=1)$ |
| T | 18029 | 18050 | $^3\Pi_{0+}(v=2) \leftarrow {}^2\Sigma^+(v=0)$ |
| U | 18081 | | $^3\Pi_{0-}(v=3) \leftarrow {}^2\Sigma^+(v=1)$ |
| V | 18124 | 18148 | $^3\Pi_{0-}(v=2) \leftarrow {}^2\Sigma^+(v=0)$ |
| W | 18340 | | $^3\Pi_{0-}(v=4) \leftarrow {}^2\Sigma^+(v=1)$ |
| X | 18384 | 18416 | $^3\Pi_{0-}(v=3) \leftarrow {}^2\Sigma^+(v=0)$ |
| Y | | 18636 | $^3\Pi_{0-}(v=4) \leftarrow {}^2\Sigma^+(v=0)$ |

Table 6. Comparison of experimental and theoretical molecular constants of GaAs.[a]

| Ref. | Method | $X\,^2\Sigma^+$ | $A\,^2\Pi_{3/2}$ | $X\,^3\Sigma_1^-$ | $X\,^3\Sigma_{0+}^-$ | $A\,^3\Pi_2$ | $B\,^3\Pi_1$ | $C\,^3\Pi_{0+}$ | $^3\Pi_{0-}$ | $D\,^1\Pi$ | $E\,^1\Sigma^+$ | $F\,^1\Delta$ | EA |
|---|---|---|---|---|---|---|---|---|---|---|---|---|---|
| 17 | SOCI | 0 | 797 | 0 | | 1830 | | | | 6440 | 7768 | 7874 | 1.4 ± 0.02 |
| | | 303 | 216 | 215 | | 236 | | | | 277 | 279 | 214 | |
| | | 2.268 | 2.426 | 2.60 | | 2.38 | | | | 2.34 | 2.23 | 2.58 | |
| 15,21 | MRDCI | 0 | 160 | 0 | | 1400 | | | | 6000 | 7300 | 7600 | 1.51 |
| | | 248 | 212 | 202 | | 260 | | | | 278 | 277 | 210 | |
| | | 2.33 | 2.47 | 2.60 | | 2.38 | | | | 2.35 | 2.25 | 2.59 | |
| 16 | MRSDCI | | | 76 | 0 | 736 | 1215 | 1751 | 1783 | 6283 | 6947 | 8771 | |
| | | | | 181 | 180 | 234 | 240 | 234 | 231 | 265 | 297 | 189 | |
| | | | | 2.667 | 2.673 | 2.396 | 2.338 | 2.389 | 2.401 | 2.356 | 2.218 | 2.649 | |
| | | | | | | | | | | | | | |
| Experiment | | 0 | | -402[b] | | 0 | | 1010 | 1093 | 4615 | 5513 | | 2.047 ± 0.001 |
| | | 298 | | | | 260 | | 258 | 260 | 288 | 290 | | |

[a] For each calculation the first row gives the splitting, the second row gives the vibrational frequency, and the third row gives the bond length.

[b] The following molecular constants are from Reference 9. $^3\Sigma_1^-$ $T_o$=0 cm$^{-1}$, w=215 cm$^{-1}$, $r_e$=2.53 Å and $^3\Sigma_{0+}^-$ $T_o$=43 cm$^{-1}$, w=209 cm$^{-1}$, $r_e$=2.55 Å.

# V. Discussion

## A. Dissociation Energies

The dissociation energies of the anions of GaX, $Si_2$, and $Ge_2$ have been calculated according to the relation

$$D_o(AB^-) = EA(AB) + D_o(AB) - EA(B)$$

In this expression we calculate $D_o(AB^-)$, the dissociation energy of the diatomic anion, from the experimental values of $D_o(AB)$, the dissociation energy of the neutral ground state, and the electron affinities, $EA(AB)$ and $EA(B)$. In the case of the heteronuclear diatomics $B$ is either P or As. All of the values are tabulated in Table 7. In each case the anion dissociation energy is larger than the corresponding neutral, consistent with a shorter anion bond length and higher anion vibrational frequency indicating the anion HOMO is bonding.

Table 7. Tabulated electron affinities and dissociation energies of isovalent species.

| | $Si_2$ | $Ge_2$ | GaP | GaAs |
|---|---|---|---|---|
| *EA(B)* | 1.385 ± 0.005[a] | 1.233 ± 0.003 Error! Bookmark not defined. | 0.7465 ± 0.0003 Error! Bookmark not defined. | 0.81 ± 0.03 Error! Bookmark not defined. |
| *EA(AB)* | 2.202 ± 0.010[b] | 2.035 ± 0.001 Error! Bookmark not defined. | 2.036 ± 0.008 Error! Bookmark not defined. | 2.047 ± 0.001 Error! Bookmark not defined. |
| $D_o(AB)$ | 3.31 ± 0.07[c] | 2.70 ± 0.07[d] | 2.38 ± 0.11[e] | 2.06 ± 0.05[f] |
| $D_o(AB^-)$ | 4.13 ± 0.07[g] | 3.50 ± 0.074 Error! Bookmark not defined. | 3.67 ± 0.11 Error! Bookmark not defined. | 3.29 ± 0.081 Error! Bookmark not defined. |

## B. Isovalent Species

Now that we have interpreted the photodetachment spectra of $GaX^-$, it is useful to compare their electronic structure with that of the isovalent group IV dimers, $Si_2$ and $Ge_2$. Table 8 compares the term energies and vibrational frequencies of the four diatomics. The anions $Si_2^-$, $GaP^-$, and $GaAs^-$ all show a $^2\Sigma^+$ ground state with a low-lying $^2\Pi$ state. In $GaP^-$ and $GaAs^-$ only the lower spin-orbit component, $^2\Pi_{3/2}$ is observed. Both $^2\Pi$ spin-orbit states are observed in $Si_2^-$ and are split by 115 $cm^{-1}$.[39] The spin-orbit interaction is strong enough in $Ge_2^-$ to push the $^2\Pi_{3/2}$ state lower in energy than the $^2\Sigma^+$ making it the ground state. The electron affinities of GaX and $Ge_2$ are ~2.0 eV, however

[aa] Reference [40].
[b] Reference [26].
[c] Reference [41].
[d] Reference [42].
[e] Reference [43].
[f] Reference [9].
[g] This Work.

$Si_2$ is about 200 meV larger. This is due to the stability of the corresponding anion, which has a larger dissociation energy than the other species.

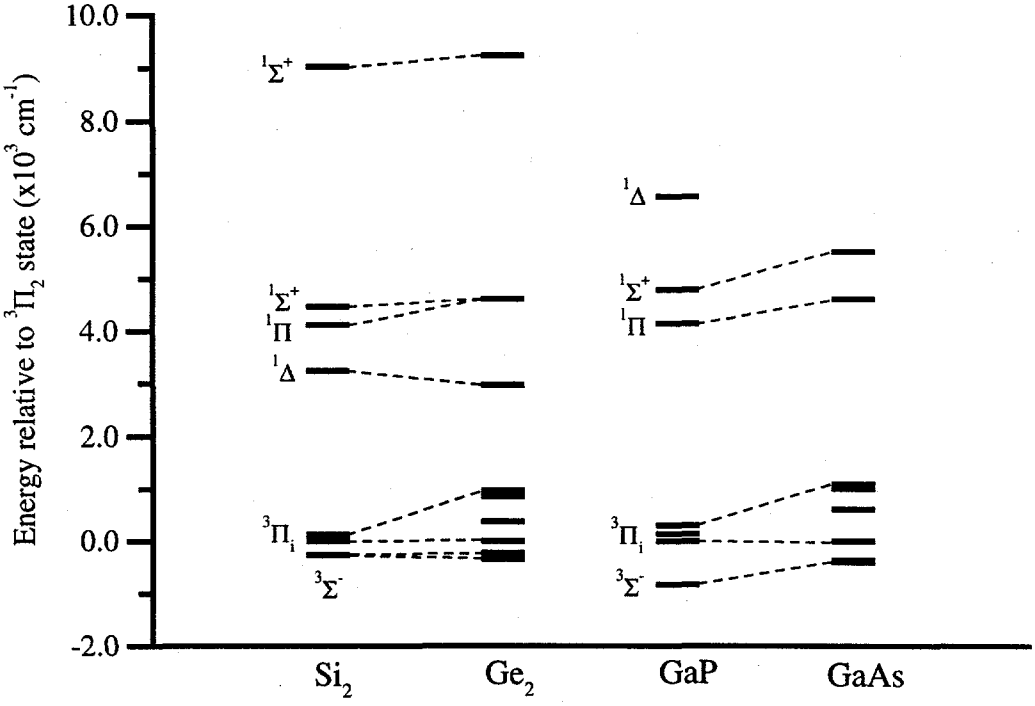


Figure 10. Energy level diagram showing the electronic structure of the neutral states of the isoelectronic species, $Si_2$, $Ge_2$, GaP, and GaAs. The energy is referenced with respect to the $^3\Pi_2$ state for each species.

Figure 10 shows the energy levels of the neutral states of the four diatomics referenced with respect to the $^3\Pi_2$ state. The $^3\Sigma^-$ state is the ground state in all four diatomics. In $Ge_2$ and GaAs the $^3\Sigma^-$ splits into the $\Omega = 0+$, 1 spin-orbit components within Hund's case (c). In $Ge_2$, the $\Omega = 0+$ state is the lowest followed by the $\Omega = 1$ state however in GaAs the order is reversed. In addition, the splitting in $Ge_2$ is larger (114 cm$^-$

$^1$) than GaAs (43 $cm^{-1}$). This trend was rationalized by Manna *et al.* to be a result of strong mixing with nearby states with the same $\Omega$.[16] In general, the vibrational frequencies for all spin-orbit components with the same $\Lambda$ have the same vibrational frequency.

It appears that the $^3\Pi$ spin-orbit states fall into the same energetic ordering of $\Omega = 2<1<0$ for all four diatomics. As expected, the magnitude of the $^3\Pi_i$ spin-orbit splitting decreases with decreasing mass. Transitions from the anion ground state appear to be equivalent in intensity and bond length change except for the $^3\Pi_1 \leftarrow {}^2\Sigma^+$ transition in GaAs. This transition does not show the same bond length change as the other three $^3\Pi_i$ spin-orbit states.

The ordering of states in the singlet manifold of the homonuclear diatomics is quite different from the heteronuclear diatomics. The figure shows that the state ordering for $Si_2$ is $^1\Delta < {}^1\Pi \leq {}^1\Sigma^+$ and in $Ge_2$ the $^1\Pi$ and $^1\Sigma^+$ states are nearly degenerate. In contrast, in GaX the ordering is $^1\Pi < {}^1\Sigma^+ < {}^1\Delta$. The magnitude of the vibrational frequencies of these states is also unique. The homonuclear species show the following trend $^1\Pi > {}^1\Delta > {}^1\Sigma^+$ while GaX show $^1\Sigma^+ > {}^1\Pi > {}^1\Delta$. The differences in electronic structure of the singlet manifolds is most likely due to the polar nature of the bond in the heteronuclear diatomics.

Table 8. Summary of spectroscopic constants for the isovalent species.

| Species | $X\ ^2\Sigma^+$ | $A\ ^2\Pi_{3/2}$ | $X\ ^3\Sigma_1^-$ | $X\ ^3\Sigma_{0+}^-$ | $A\ ^3\Pi_2$ | $B\ ^3\Pi_1$ | $C\ ^3\Pi_{0+}$ | $^3\Pi_{0-}$ | $D\ ^1\Pi$ | $E\ ^1\Sigma^+$ | $F\ ^1\Delta$ |
|---|---|---|---|---|---|---|---|---|---|---|---|
| $Si_2$[a] | 0 | 216.5[b] | 0 | | 266 | 331 | 395 | | 4387 | 4726 | 3508 |
| | 557 | 542.2[b] | 508 | | 557 | 540 | 532 | | 532 | | 484 |
| $Ge_2$[c] | 279 ± 10 | 0 | 114 | 0 | 337 | 711 | 1193 | 1305 | 4943 | 4941 | 3308 |
| | 326 ± 10 | 309 ± 5 | 286 ± 5 | | | | | 308 | 303 ± 5 | 204 ± 7 | 276 ± 3 |
| GaP | 0 | 1093 | 0 | | 831 | 979 | 1130 | | 4973 | 5626 | 7659 |
| | 436 | | 283.6[d] | | 363 | 363 | 363 | | 390 ± 10 | 428 ± 8 | 285 |
| GaAs | 0 | | 0[e] | 43[e] | 402 | 1017 | 1420 | 1500 | 5017 | 5915 | |
| | 298 | | 215[e] | 209[e] | 260 | 302 | 258 | 260 | 288 | 290 | |

[a] Reference 26.
[b] Reference 39
[c] Reference 27.
[d] Reference 12, infrared matrix absorption experiment.
[e] Reference 9.

## C. Autodetachment state

We can not derive much information about the autodetachment state, however we know that it must satisfy the criteria for an optically allowed electronic transition from the anion ground state ($^2\Sigma^+$) and have good FC overlap with the final neutral state ($^3\Sigma^-$).

# VI. Conclusions

The simultaneous study of GaP and GaAs combined with the resolution of vibrational structure have proven invaluable to our ability to confidently make spectral assignments. For these two diatomics we have been able to report term energies and vibrational frequencies for seven neutral spin-orbit states and two anion states. We have confirmed the energy ordering of these states as predicted by theory. An autodetachment process allows us to observe the $^3\Sigma^-$ ground state of both diatomics, affording accurate

electron affinities, and allowing us to determine the anion ground state dissociation energies.

## Acknowledgements

This research is supported by the National Science Foundation under Grant No. DMR-9814677. T.R.T. would also like to thank Prof. Edet F. Archibong and Prof. K. Balasubramanian for their prepublication results and instructive conversations.

# References

[1] A. E. Douglas and G. Herzberg, Canadian Journal of Research A **18,** 179 (1940).

[2] O. A. Mosher and R. P. Frosch, J. Chem. Phys. **52,** 5781 (1970).

[3] H. Bredohl, I. Dubois, Y. Houbrechts, and P. Nzohabonayo, J. Mol. Spectrosc. **112,** 430 (1985).

[4] H. Bredohl, I. Dubois, Y. Houbrechts, and P. Nzohabonayo. J. Phys. B: At. Mol. Phys. **17,** 95 (1984).

[5] C. J. Reid, Int. J. Mass Spec. Ion Proc. **127,** 147 (1993).

[6] R. R. Reddy, A. S. R. Reddy, and T. V. R. Rao, Physica C **132,** 373 (1985).

[7] K. R. Asmis, T. R. Taylor, and D. M. Neumark, Chem. Phys. Lett. , in press (1998).

[8] M. Lorenz, J. Agreiter, A. M. Smith, and V. E. Bondybey, J. Chem. Phys. **104,** 3143 (1996).

[9] G. W. Lemire, G. A. Bishea, S. A. Heidecke, and M. D. Morse, J. Chem. Phys. **92,** 121 (1990).

[10] M. Ebben and J. J. ter Meulen, Chem. Phys. Lett. **177,** 229 (1991).

[11] S. Li, R. J. Van Zee, and W. Weltner Jr., J. Phys. Chem. **98,** 2275 (1994).

[12] S. Li, R. J. Van Zee, and W. Weltner Jr., J. Phys. Chem. **97,** 11393 (1993).

[13] E. F. Archibong and A. St-Amant, Chem. Phys. Lett. , In Press (1999).

[14] B. Manna and K. K. Das, Journal of Molecular Structure (Theochem) **467,** 135 (1999).

[15] U. Meier, S. D. Peyerimhoff, P. J. Bruna, and F. Grein, J. Mol. Spectrosc. **134,** 259 (1989).

[16] B. Manna and K. K. Das, J. Phys. Chem. A **102,** 9876 (1999).

[17] K. Balasubramanian, J. Mol. Spectrosc. **139,** 405 (1990).

[18] K. Balasubramanian, J. Chem. Phys. **86,** 3410 (1987).

[19] K. Balasubramanian, J. Chem. Phys. **92,** 2123 (1990).

[20] K. Balasubramanian, Chemical Reviews **90,** 93 (1990).

[21] U. Meier, S. D. Peyerimhoff, and F. Grein, Chem. Phys. **150,** 331 (1991).

[22] C. W. Bock, K. D. Dobbs, G. J. Mains, and M. Trachtman, J. Phys. Chem. **95,** 7668 (1991).

[23] R. M. Graves and G. E. Scuseria, J. Chem. Phys. **95,** 6602 (1991).

[24] L. Lou, L. Wang, L. P. F. Chibante, R. T. Laaksonen, P. Nordlander, and R. E. Smalley, J. Chem. Phys. **94,** 8015 (1991).

[25] L. Lou, P. Nordlander, and R. E. Smalley, J. Chem. Phys. **97,** 1858 (1992).

[26] C. C. Arnold, T. N. Kitsopoulos, and D. M. Neumark, J. Chem. Phys. **99,** 766 (1993).

[27] C. C. Arnold, C. S. Xu, G. R. Burton, and D. M. Neumark, J. Chem. Phys. **102,** 6982 (1995).

[28] T. N. Kitsopoulos, C. J. Chick, Y. Zhao, and D. M. Neumark, J. Chem. Phys. **95,** 1441 (1991).

[29] R. B. Metz, A. Weaver, S. E. Bradforth, T. N. Kitsopoulos, and D. M. Neumark, J. Phys. Chem. **94,** 1377 (1990).

[30] C. Xu, G. R. Burton, T. R. Taylor, and D. M. Neumark, J. Chem. Phys. **107,** 3428 (1997).

[31] T. R. Taylor, K. R. Asmis, H. Gomez, and D. M. Neumark, J. Chem. Phys. , In preparation (2000).

[32] B. A. Mamyrin and D. V. Shmikk, Sov. Phys. JETP **49,** 762 (1979).

[33] G. Markovich, R. Giniger, M. Levin, and O. Cheshnovsky, J. Chem. Phys. **95,** 9416 (1991).

[34] J. Cooper and R. N. Zare, in *Lectures in Theoretical Physics*, Vol. XI-C, edited by S. Geltman, K. T. Mahanthappa, and W. E. Brittin (Gordon and Breach, New York, 1969), pp. .

[35] K. M. Ervin and W. C. Lineberger, in *Advances in Gas Phase Ion Chemistry*, Vol. 1 (JAI Press Inc, 1992), pp. .

[36] C. C. Arnold, Y. X. Zhao, T. N. Kitsopoulos, and D. M. Neumark, J. Chem. Phys. **97,** 6121 (1992).

[37] T. N. Kitsopoulos, I. M. Waller, J. G. Loeser, and D. M. Neumark, Chem. Phys. Lett. **159,** 300 (1989).

[38] C. Jin, K. J. Taylor, J. Conceicao, and R. E. Smalley, Chem. Phys. Lett. **175,** 17 (1990).

[39] Z. Liu and P. B. Davies, J. Chem. Phys. **105,** 3443 (1996).

[40] T. M. Miller, in *CRC Handbook of Chemistry and Physics*, 79 ed., edited by D. R. Lide (CRC Press, Boca Raton, FL, 1999), pp. .

[41] R. W. Schmude Jr., Q. Ran, K. A. Gingerich, and J. E. Kingcade Jr., J. Chem. Phys. **102,** 2574 (1995).

[42] J. E. Kingcade, H. M. Nagaratha-Naik, I. Shim, and K. A. Gingerich, J. Chem. Phys. **90,** 2830 (1986).

[43] V. Piacente and K. A. Gingerich, High Temp. Sci. **3,** 219 (1971).

# Epilogue

## Moral of the story

Folks who throw dirt on you aren't always trying to hurt you and folks who pull you out of a jam aren't always trying to help you. But the main point is when you are neck deep in shit, keep your mouth shut.